Antisymmetrisation in a Jacobi coordinate based no-core shell model approach

Dissertation
zur
Erlangung des Doktorgrades (Dr. rer. nat.)
der Mathematisch-Naturwissenschaftlichen Fakultät
der
Rheinischen Friedrich-Wilhelms-Universität Bonn

vorgelegt von
Susanna Liebig
aus
Köln

Bonn 2013

Angefertigt mit Genehmigung der Mathematisch-Naturwissenschaftlichen Fakultät
der Rheinischen Friedrich-Wilhelms-Universität Bonn

1. Gutachter: Prof. Dr. Ulf-G. Meißner

2. Gutachter: Prof. Dr. Hans-Werner Hammer

Tag der Promotion: 14.05.2013

Erscheinungsjahr: 2013

Summary:

The theory of the strong interaction, Quantum Chromodynamics (QCD), provides the generally accepted description of strongly interacting processes. Due to the confinement of the fundamental degrees of freedom of QCD, the quarks and gluons, the objects that are observable in experiments are their bound states, the hadrons. Since QCD cannot be analysed within perturbation theory in the low-energy domain relevant here, different approaches are necessary. One of these, an effective field theory (EFT) approach, has been very successful for the description of low-energy reactions. Especially, systems of few nucleons, which are the subject of this work, require a systematic scheme for the formulation of the interactions of the nucleons involved to be able to predict their low-energy observables with controlled accuracy. Here, a brief summary of the content of this thesis is given:

In Chapter 1, we constitute the problem that we want to advance, namely the calculation of bound and excited states of few-nucleon systems by solving the non-relativisic Schrödinger equation. We motivate, why a systematic derivation of the nuclear interactions is needed, and review the theoretical framework of chiral EFT. The expansion of the chiral nuclear potential and the appearance of few-nucleon forces up to fourth order is discussed. Additionally, a decoupling of high- and low-momenta contributions is desirable for the potential, realised by renormalisation group methods that are introduced briefly. At the end of this chapter, we give an overview of existing techniques for the numerical calculation of light nuclei, their fields of applicability and strengths and failures. Special emphasis lies on the no-core shell model (NCSM) approach since it is the aim of this thesis to develop a Jacobi coordinate based formalism within this method. Jacobi or relative coordinates are more advisable for calculations that explicitly take higher order contributions to the nuclear potential into account.
In the NCSM, the few-nucleon basis states are given in a harmonic oscillator basis.Due to the Pauli principle, the basis states of bound few-nucleon systems have to be antisymmetric. An algorithm for the antisymmetrisation of the Jacobi coordinate based states is derived in Chapter 2 which forms a matrix eigenvalue problem. We describe this formalism in detail for three-nucleon states and generalise the explicit evaluation of the required matrix elements to systems with A nucleons. To solve the Schrödinger equation, new basis states are derived which make it possible to consider three- and few-nucleon contributions explicitly. With this, the solution of the Schrödinger equation, also a matrix eigenvalue equation, takes a similar form as the antisymmetrisation of basis states.
In Chapter 3, numerical aspects of the calculations are discussed including tests of the parallelisation. The parallelisation is strongly required due to the large dimensions of the matrices for the antisymmetrisation and the Schrödinger equation likewise. Additionally, we specify the evaluation of the matrix elements of

the two-nucleon contribution to the nuclear potential and the method with which we analyse the results.
The results for the binding energies of ^{3}H and ^{4}He as well as for the ground state, the lowest excited state and of the excitation energy of ^{6}Li considering NN forces are presented in Chapter 4. We also discuss first results of the binding energy of ^{7}Li and our expectations for larger model spaces that are in progress. Furthermore, we analyse these results with regard to their convergence and their cutoff dependence.
Finally, a summary and an outlook on future work is given in Chapter 5.
The Appendices contain technical details and explicit calculations.

Contents

Chapter 1

Introduction

Within the Standard Model, the theory of the strong interaction is Quantum Chromodynamics (QCD). Due to the so-called confinement, the fundamental degrees of freedom of QCD, the quarks and gluons, can not be observed as free particles. However, their bound states, the hadrons, are observable in experiments. At high energies, the running coupling constant of QCD, α_s, is small [1,2], so that QCD has been confirmed for high energy processes. For low energy reactions, a perturbative treatment of QCD is not feasible. One possibility to approach this area are numerical solutions based on lattice field theory. Though further algorithmic and technical progress is demanding, hadron masses for QCD have been predicted [3]. However, investigations of systems consisting of more than one baryon have not yet advanced to be comparable to experiments [4]. In this work we are specifically interested in systems of few nucleons. It is conceivable that quark and gluon degrees of freedom cannot be resolved for a description of few-nucleon systems at low energies since first excitations of the nucleons themselves are much higher in energy than excitations of few-nucleon systems. To make predictions for this area of QCD a formulation in terms of nucleon degrees of freedom is more efficient. In the energy regime we work in, even relativistic effects are not important, therefore we describe the system with the non-relativistic Schrödinger equation, involving the interactions between the nucleons.
There are several approaches to derive the nucleon-nucleon (NN) interaction, for example NN interaction models that are based on meson exchange or on phenomenology alone, such as Nijmegen I and II, CD–Bonn and the Argonne V18 (AV18) [5–7]. These NN interaction models describe existing NN data very successfully and are therefore generally called "realistic interactions". Although their prediction of many low energy few-nucleon observables is model independent and in good agreement with experiments, scattering observables at higher energies and binding energies are not well described and model dependent which is interpreted in general as an indication for a significant contribution of three-nucleon forces (3NF) [8]. Especially the aspect that few-nucleon observables like binding and excitation energies are strongly dependent on the chosen NN model indicates

that the 3NF are not uniquely defined but depend on the representation of the NN forces [9, 10]. In the context of these models, the 3NF are usually tuned to reproduce the ^{3}H binding energy, however, this does not remove all discrepancies concerning the 3N data. For such calculations, 3NF based on a two-pion exchange are implemented in general, such as the Tucson–Melbourne [11], Urbana–IX [12] or Illinois [13] model. Although it is known that these models need to be consistent with the employed NN interaction, such a consistency is not inherent in this approach. In many modern studies of NN and 3N forces, a different approach has therefore been used. Here the nuclear interaction has been derived from the symmetries of QCD by the formulation of an effective field theory (EFT). Separating the energy scales of the problem, an effective Lagrangian is devised that describes the interaction of the relevant degrees of freedom: pions and nucleons. The derivation of both the NN and the 3N forces from the same effective Lagrangian ensures that the formulation of NN, 3N and higher body forces is consistent. It is also possible to give a systematic estimate of the importance of the few-nucleon forces and their contribution to the nuclear potential within a model-independent framework. An overview of this approach is given in Sec. 1.1. With the nuclear potential resulting from this formulation, predictions for nuclear systems can be made by solving the Schrödinger equation. Unfortunately, this becomes technically difficult for systems larger than 4 nucleons. A considerable problem is the rather strong short-range interaction in combination with a much longer ranged one-pion exchange force. However, it turns out that this short-range interaction can be systematically reduced by renormalisation group (RG) methods, as outlined in Sec. 1.2. Interestingly, this is again strongly related to multi-body forces. Finally, we briefly summarise the techniques available for the solution of the few- and many-nucleon problem in Sec. 1.3.

1.1 Chiral nuclear forces

The nucleon is primarily composed of u and d quarks which are much lighter than the mass of the nucleon itself, $m_{\mathrm{N}} = 938.92$ MeV, whereas the u- and d-quark masses at reasonable renormalisation scales of 1-2 GeV are smaller than 10 MeV [14]. Therefore, the quark masses can be neglected in first approximation when studying QCD. In this limit, the Lagrangian of QCD is symmetric under so-called chiral $\mathrm{SU}(2)_L \times \mathrm{SU}(2)_R$ transformation, i.e. under independent rotations in flavour space of left- and right-handed quarks. Experimentally, only simultaneous flavour rotations seem to be a symmetry of QCD, the well-known isospin symmetry. This is now understood as the spontaneous breakdown of chiral symmetry to isospin $\mathrm{SU}(2)_V$ symmetry. According to Goldstone's theorem [15], this gives rise to one massless scalar particle for every generator of the broken symmetry group. The group SU(2) is generated by the three Pauli matrices, hence the spontaneous breaking of $\mathrm{SU}(2)_L \times \mathrm{SU}(2)_R$ to $\mathrm{SU}(2)_V$ results in three Goldstone bosons. In case

of the spontaneous chiral symmetry breakdown they can be identified with the three charge states of the pion. Due to the explicit symmetry breaking by the non-vanishing quark masses, these pseudo-Goldstone bosons acquire a non-zero mass. However, the pion mass $m_\pi \approx 140$ MeV is still much smaller than other hadronic masses.

Based on chiral symmetry, an EFT can be formulated in terms of pions and nucleons, chiral perturbation theory (χPT) [16]. Since the pion fields decouple for low momenta due to the $\mathrm{SU}(2)_L \times \mathrm{SU}(2)_R$ symmetry, a perturbative expansion of the chiral Lagrangian in terms of (Q/Λ_χ) is possible, where Q is a typical momentum, usually assumed to be of the order of the pion mass m_π, and Λ_χ the so-called chiral symmetry breaking scale. Since terms that are induced by the explicit chiral symmetry breaking are proportional to m_π, the chiral Lagrangian is expanded simultaneously in both low momenta and pion masses. With this expansion, a systematic estimate of the importance of diagrams contributing to a specific process scaling as $\left(Q/\Lambda_\chi\right)^\nu$ can be given, the so-called power counting. The counting index ν is determined using naive dimensional analysis by

$$\nu = -4 + 2N + 2L + \sum_i V_i \Delta_i \quad \text{with} \quad \Delta_i = d_i + \frac{1}{2} n_i - 2 \,, \tag{1.1}$$

for a diagram with N nucleons involved, L pion loops, V_i vertices of type i, d_i derivatives and n_i nucleon lines at vertex i. Since $\Delta_i \geq 0$ due to chiral symmetry, a finite number of diagrams that contribute to a given order can be identified, classifying the diagrams with lowest ν as leading order (LO) contributions, those with the second smallest ν as next-to-leading (NLO) order and so on. Thus, the pion-nucleon (πN) interaction is described in a systematic way.

Although $\pi\pi$ and πN interactions are well-described by χPT, perturbation theory is obviously not applicable for the NN interaction. The NN interaction is too strong which is reflected e.g. by the existence of bound states of nucleons. Weinberg [17–19] realised that the large mass of the nucleon implies an enhancement of certain contributions that destroy the naive dimensional analysis leading to Eq. (1.1). This is most easily seen within time-ordered perturbation theory. It becomes evident that the so-called reducible diagrams with an intermediate state that involves only nucleons destroy the naive power counting. This is exemplified in Fig. 1.1, where the Feynman box diagram of the two-pion exchange is shown as the sum of all possible time-ordered graphs. The first two time-ordered diagrams do not contain a purely nucleonic intermediate state (irreducible diagrams) and scale as expected. The other time-ordered diagrams are reducible which leads to an unnatural enhancement proportional to m_N/m_π. However, the reducible diagrams can be taken into account to infinite order by the iterations of the Lippmann–Schwinger (LS) equation with the kernel that contains the irreducible diagrams. With this modification of the original power counting one derives a nuclear potential that includes all irreducible diagrams up to a certain order in

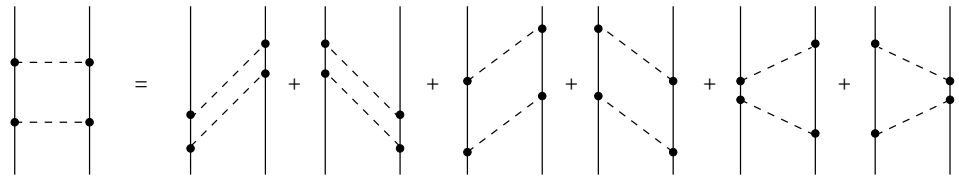

Figure 1.1: Feynman diagram of the two-pion exchange and its time-ordered representation; solid lines denote nucleons and dashed lines denote pions. The last four diagrams contain intermediate states involving only nucleons and are therefore called reducible.

a systematic way which also allows for a derivation of 3NF and higher-body interactions within the same framework. The bound states are naturally generated by this procedure. For details we refer to [20] and references therein.
With each order of the expansion new terms appear in the chiral Lagrangian that are not fixed by symmetry aspects and that parameterise the short range physics. These parameters are generally called low-energy constants, LEC's. While πNN coupling constants can be extracted from πN data, the new LEC's for NN and 3N (or other) contributions require NN and 3N (or other) data to be determined. With this the chiral power counting exhibits the very natural hierarchy that NN forces are the most dominant ones while few-N forces are suppressed, illustrated in Fig. 1.2 from [21]:
The LO contributions with $\nu = 0$ result from two-nucleon tree diagrams (Eq. (1.1): $N = 2$ and $L = 0$) with vertices of the type $\Delta_i = 0$, i.e. with two nucleon lines ($n_i = 2$) and one derivative ($d_i = 1$) or four nucleon lines and no derivative. These are the one-pion exchange and the NN contact interactions, parameterised by two LEC's C_S and C_T, as pictured in Fig. 1.2.
As the diagrams for $\nu = 1$ vanish due to parity conservation, the NLO contributions are those with $\nu = 2$: two-nucleon one-loop diagrams with LO vertices and the NN contact interaction involving two derivatives, determined by seven new LEC's C_1-C_7.
At N^{2}LO ($\nu = 3$), additional two-pion exchange diagrams contribute to the NN potential. There are no new NN contact interactions but first 3NF contributions with three topologies: a two-pion exchange contribution which also is the basis of most 3NF models, a one-pion contact diagram (D-term) and a pure contact diagram (E-term). While the strength of the 3NF two-pion exchange diagram is given by the same πNN and $\pi\pi$NN couplings already determined for the NN forces, the contact diagrams have a priori unknown strength, parameterised by the LEC's c_D and c_E respectively. In current studies including 3NF, they are adjusted to correctly reproduce the binding energy of ^{3}H. For a unique determination of these LEC's, at least one additional few-body datum is required, such as e.g. the neutron–deuteron doublet scattering length $^2a_{nd}$ [22], the binding energy of ^{4}He [23], the radius of ^{4}He [24] or even the ^{3}H beta decay [25]. With this, the

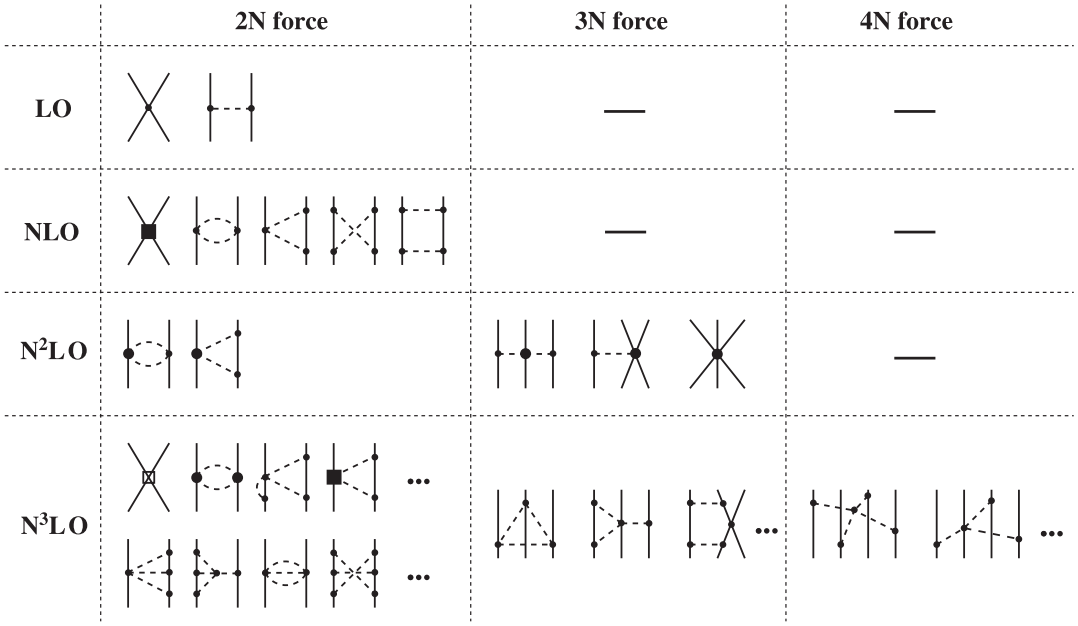

Figure 1.2: Chiral expansion of the contributions of few-nucleon forces to the nuclear potential [21].

determination of the chiral nuclear forces is complete up to N^2LO which allows for a qualitative description of low-energy observables. However, for a quantitative analyse with today's applications higher accuracies are required. Proceeding to N^3LO, NN observables show the desired accuracy [26, 27]. The here appearing 3NF [28,29] and 4NF [30,31] have also been formulated. Fortunately, their LEC's are those related to the NN forces. Thus, no new unknown parameters are implicated. Since first investigations indicate that their contribution is quantitatively significant [32, 33], further studies are required. The preparation of such studies is the major motivation for this work.

In practice it is important to regularise the nuclear forces. The LS equation generates a series of loop diagrams that are divergent. Since these divergencies cannot be removed analytically, the most practical way for the regularisation of this problem is a cutoff function to remove momenta larger than a parameter Λ from the integrals. Predictions of the observables therefore depend on this parameter Λ. This variation is used as an estimate for contributions of higher orders of the chiral expansion. In this thesis, we employ realisations of the chiral potential where $\Lambda \sim 500 - 600$ MeV.

1.2 Low–momentum potentials

Most nuclear interactions induce a strong correlation of nucleons due to their strongly repulsive short-distance behaviour which is a long standing problem for the calculation of few- and many-body problems. Though this behaviour is much softer for standard chiral interactions with $\Lambda \sim 500$ MeV than for phenomenological ones, these correlations cannot be handled in today's many-body applications. In recent years, RG techniques that derive low–momentum potentials, the so-called $V_{\mathrm{low}\,k}$ and V_{SRG}, were developed to further soften the interactions.
To obtain $V_{\mathrm{low}\,k}$ the high–momentum modes are integrated out under the condition that the on-shell t-matrix is not changed for the initial NN potential, V_{NN}, in all NN partial waves. Therefore, the binding energy of the deuteron and the phase shifts remain the same for momenta below the momentum cutoff of this technique, i.e. below the scale that separates high and low momenta of the initial potential [34,35]. Yet the numerous evaluations of the t-matrix slow the numerical calculation of the potential considerably and complicate the formalism if 3NF are included.
The Similarity Renormalisation Group (SRG) offers a more efficient method that evolves the low–momentum potential, V_{SRG}, with a continous sequence of unitary transformations U of an initial NN potential. This potential is energy-independent like $V_{\mathrm{low}\,k}$. In addition, due to the nature of the unitary transformations, not only the low–energy phase shifts are preserved but also those at high energies and other high–energy observables [35]. Instead, the application of the so-called flow equation formalism renders the nuclear Hamiltonian close to a band-diagonal form in the full momentum range considered. The initial Hamiltonian $H = T_{\mathrm{rel}} + V_{\mathrm{NN}}$ (with T_{rel} the relative kinetic energy) is transformed as $H_s = U_s H U_s^\dagger$, where s is the so-called flow parameter. Since T_{rel} is assumed to be independent of s, the evolved potential V_s is given by $H_s = T_{\mathrm{rel}} + V_s$. With a suitable specification of the transformation the evolution of V_s is defined as

$$\frac{\mathrm{d}\,V_s}{\mathrm{d}s} = \Big[\big[G_s, H_s\big], H_s\Big] \,. \tag{1.2}$$

Among others, the simplest choice for the operator G_s is T_{rel}. This leads to an exponential suppression of matrix elements that are far from the diagonal with increasing s, hence:

$$V_{\mathrm{SRG}}\,(p', p) \approx V_{s=0}\,(p', p)\; e^{-s\left(p'^{\,2} - p^2\right)^2} \,. \tag{1.3}$$

With this the variable $\lambda = s^{-1/4}$ is a measure of the diagonal width of V_{SRG} in momentum space and is regarded as the momentum cutoff for this low–momentum potential [35]. A more detailed derivation of the flow equation formalism is given in [36] and references therein.
The transformation of the NN interaction to an equivalent one leads to corresponding changes of 3N and higher-body forces in both techniques. Though in

principle possible, it is not feasible to calculate these additional 3NF for $V_{\text{low } k}$ at this point, but only for V_{SRG}. A study of corresponding terms for the chiral interactions is useful for a quantitative understanding of these higher-body interactions. To this aim, it is assumed that in first approximation changes of pure 3N and 4N contact interactions in the chiral approach correspond to the change of the induced 3N and higher-body forces if the cutoff parameter Λ or the variable λ, respectively, is varied in the range of $300 - 500$ MeV. Explicit calculations are consistent with this assumption:
For ^{3}H (^{4}He) it has been shown that the 3NF contribution to the binding energy is approximately 700 keV (4 MeV). This agrees to the observed cutoff dependence of predictions of these energies for a variation of Λ or λ, respectively, in the above mentioned range. It is conceivable though not strictly proven that this cutoff dependence estimates the contributions of the 3N contact term that is part of the leading 3NF.
Furthermore, the cutoff dependence decreases to ~ 50 keV for the binding energy of ^{4}He if the SRG method is also applied to the 3NF. In contrast, first estimates of the 4NF contribution give ~ 500 keV here [33]. Since a 4N contact interaction is not expected for the leading 4NF, this also indicates that the cutoff variation is a good estimate for the contribution of multi-nucleon contact interactions.
Hence, at least for Λ or $\lambda \geq 300$ MeV, the multi-nucleon force contributions seem to be compatible with the expectations based on chiral interactions, and the SRG method does not induce unnaturally large multi-nucleon forces. On the other hand, it becomes clear that for quantitative studies of binding and excitation energies the inclusion of at least 3NF and probably 4NF is required.
With this in mind, we now discuss state-of-the-art few- and many-body techniques to solve the quantum mechanical bound state problem.

1.3 Numerical techniques

The aim of this thesis is an implementation of the no-core shell model (NCSM) approach for the solution of a nuclear bound state problem. Therefore, we want to summarise techniques available to study light nuclear systems and motivate our formalism.
In general, the Schrödinger equation can also be solved exactly for scattering problems of systems up to $A \leq 4$ [37–40] which has been used extensively to study 3NF [8]. Low-energy observables do not seem to be largely influenced by 3NF in 3N systems which do not show any resonances. Scattering reactions only become sensitive to 3NF at high energies, $E_{\text{lab}} \sim 100$ MeV [8]. The models cannot describe these data correctly due to the absence of consistently defined 3NF. Since the accuracy of predictions based on chiral interactions at the order Q^3 is too low in this energy regime, reasonable conclusions on chiral 3NF cannot be drawn from 3N scattering. For 4N scattering, calculations are restricted to

energies below three-body breakup. Due to the existence of resonances in this regime still some sensitivity to 3NF is expected [37].
For the 3N- and 4N-system, very precise results have been achieved within the Faddeev–Yakubovsky scheme (FY) e.g. by Nogga *et al.* [41] for bound states, by Witala *et al.* [42] for scattering and breakup reactions including relativistic effects, and most recently by Deltuva *et al.* [43] for three–cluster nuclear reactions. The Yakubovsky components of the wave function are decomposed into partial waves and defined iteratively by the Faddeev–Yakubovsky equations, for four nucleons as:

$$\begin{aligned} \psi_1 &= G_0 t_{12} P \big[(1 - P_{34})\, \psi_1 + \psi_2 \big] \\ \psi_2 &= G_0 t_{12} \tilde{P} \big[(1 - P_{34})\, \psi_1 + \psi_2 \big] \,. \end{aligned} \tag{1.4}$$

The two-nucleon transition matrix t_{12} is determined by a two-nucleon LS equation, and P and $\tilde{P}$ are permutation operators that can be expressed in terms of transposition operators P_{ij} that interchanges the particles i and j:

$$\begin{aligned} P &= P_{12} P_{23} + P_{13} P_{23} \\ \tilde{P} &= P_{13} P_{24} \end{aligned} \quad . \tag{1.5}$$

The fully antisymmetrised wave function Ψ, which is required because the nucleons are identical particles, is obtained as:

$$\Psi = \big[1 - (1 + P)\, P_{34} \big]\, (1 + P)\, \psi_1 + (1 + P) \left(1 + \tilde{P} \right) \psi_2 \,. \tag{1.6}$$

The set of FY equations is usually presented in a momentum space basis leading to a set of coupled integral equations. After discretisation a high dimensional eigenvalue equation is obtained that can be solved iteratively [44]. This is feasible only for ^{3}H, ^{3}He and ^{4}He. The results are very accurate and can be obtained for a large class of NN potentials, i.e. non-local interactions. We remark that 3NF can also be incorporated in such calculations. Therefore, we will use the results of FY calculations of ^{3}H and ^{4}He binding energies as a test of the formalism developed in this work.
A different technique to calculate 3N and 4N observables very accurately is the Hyperspherical Harmonics (HH) Variational Method, applied e.g. by Viviani *et al.* [45]. The calculations are performed in a basis of fully antisymmetrised HH, and the coefficients for the expansion of the wave functions are determined with a variational principle. Like the FY formalism, this is also applicable to non-local potentials. An extension to larger A is in progress, very recently formulated for $A = 5$ and 6 in [46, 47], including test calculations with not fully realistic potentials.
A similar method is the Effective Interaction HH method where, in addition to the expansion in HH, projectors are used that divide the Hilbert space of the

Hamiltonian into a model space and a residual space with corresponding effective interaction operators [48, 49]. This improves the numerical aspect of the calculations since the number of required basis states is decreased significantly and short–distance contributions are described more efficiently, which results in a better convergence [50]. Calculations for few-nucleon systems up to $A = 6$ are possible and more complicated potentials can be included already, yet only NN forces have been considered so far for $A = 6$, 3NF have been included for calculations of ^{3}H and ^{3}He [51]. Since calculations for larger A have started only recently, it remains to be seen wether converged results for ground and excited states become possible in future.

Within the Stochastic Variational Method (SVM) the wave functions are approximated by Gaussian trial functions, including the orbital part by a successively coupled product of spherical harmonics. This results in a large number of variational parameters that are determined by a stochastic optimisation procedure. Trial functions that yield the lowest energies ar chosen as basis states [52]. Thus the SVM is applicable to larger systems, e.g. $A = 10$ [53], since the number of basis states is small when employing an efficient optimisation procedure. However, for such large systems only semi-realistic interactions and no 3NF have been used. Due to technical difficulties this limitation has not been overcome yet to our knowledge.

For nuclei with $A = 6 - 10$, the Argonne–Los Alamos collaboration developed the so-called Green's Function Monte Carlo Method (GFMC). Within this method, the calculation is done in two steps. First, a trial wave function is obtained using a variational method. In the second step, thir trial wave function is improved by an imaginary time evolution that projects on the trial ground state for a specific total angular momentum, parity and isospin [54]. By orthogonalisation, it has also been possible to extract first excited states [55]. Since the time evolution is performed stochastically, wave functions cannot be obtained by this method. The main technical problem is that this method is limited to the class of local potentials with the operator structure of the AV18 family of interactions. Calculations with these phenomenological AV18 NN potential and the Illinois 7 (IL7) 3NF yield by construction the energies of ground states and excited states close to the experimental values. Yet the restriction to this class of interactions does not allow to study any model dependence within this scheme. Thus, especially predictions for systems that are not or not yet experimentally determined are not comparable to results from other methods which is usually a useful error estimate. However, the existing results [54, 56, 57] may well serve as benchmark for calculations within a different scheme. Remarkably the current limit of the calculations is not set by the spatial coordinates of the nucleons which can be handled by the stochastic methods used. Instead, the limit is given by the number of spin-isospin channels that grows exponentially for large A. Here, a recently developed formalism to calculate the properties of light nuclei based on lattice calculations in combination with the theoretical framework of chiral EFT is more

efficient [58–60]. It turns out that a direct implementation of the effective Lagrangian, the perturbative treatment of higher order terms and the use of the approximate Wigner symmetry lead to a linear scaling of the computation times with the number of nucleons A. Even states that have a cluster structure like the ^{12}C Hoyle state [61, 62] can be obtained with high accuracy. For this system $\sim 3\%$ were estimated in [63, 64], calculations for heavier systems can be expected in near future [65].
In this thesis, we want to advance the NCSM. This is a highly efficient technique for light nuclei which is formulated in the harmonic oscillator (HO) basis. A finite model space is accomplished by truncating the basis at a finite oscillator energy $\mathcal{N} = 2n + l$, where n is the HO quantum number and l the orbital momentum of the state. Originally, the truncation of the HO basis was realised such that the center-of-mass (CM) motion can be exactly separated from the internal motion even for a formulation in single-particle coordinates, the so-called m–scheme. Recently, it was proposed to drop this constraint in favour of an importance truncation algorithm (IT-NCSM) where the basis states are accepted if a test shows their significance. In this way, very large model spaces can be accessed [66], however, there is an ongoing discussion whether this induces uncontrolled errors due to spurious CM admixtures [67]. In the m–scheme, antisymmetric basis states can be realised with the Slater determinant. Unfortunately, it turns out that calculations including 3NF are extraordinarily more computationally demanding than those using NN interactions due to the large size of 3NF matrices. Therefore, an extension to 4NF does not seem to be in reach.
To obtain the antisymmetric basis states in relative or Jacobi coordinates, a matrix eigenvalue problem has to be solved that is defined by an explicit application of the antisymmetrisation operator (for details see 2.1). So far, only very light systems have been described in Jacobi coordinates [68–71] since the antisymmetrisation is difficult to implement. We want to overcome this limitation mainly due to the fact that 3NF are much better to handle in this scheme. Employing relative coordinates, the large size of the 3NF matrices is considerably reduced since the they allow an easy implementation of angular momentum and isospin conservation. In view of these constraints a further development of a Jacobi coordinate based NCSM formalism appears to be timely.
Very sophisticated calculations have been performed for systems up to $A = 13$ within the m–scheme but using 3NF. The results show good convergence of the binding energies. The strength of this method is the possibility to extract excitation energies with good accuracy since it turns out that for many excitation energies only small model spaces are required. Unfortunately, there are exceptions, e.g. the Hoyle state is not easily reproduced in a NCSM formulation. On the other hand, the energies of narrow resonances can be well obtained.
The NCSM has been used in several studies involving chiral 3NF [23, 24]. The results show that the description of light nuclei is improved by considering the leading chiral forces, still some dicrepancies remain that imply significant contri-

butions at higher orders. For a complete higher order calculation, also 4NF need to be taken into account. This work is therefore a prerequisite for investigations of extended chiral studies within the NCSM.
There are approaches to heavier nuclei, such as the Coupled Cluster (CC) and the Density Functional Theory (DFT). The Coupled Cluster method is used for $A < 100$ [35] systems which works best for closed shell nuclei like ^{16}O [72] and those close by with ongoing progress towards open–shell nuclei [73,74]. Developed for nuclear systems [75,76], it was mostly applied in quantum chemistry [77] since typical nuclear interactions were difficult to handle within this scheme. With the upcoming of low–momentum interactions this has changed. 3NF have been implemented [78].
$A > 100$ nuclei are object of DFT. Because of the large number of nucleons predictions for those nuclei are not based on microscopic forces which are the subject of this work. We still note that there is an ongoing research on the implementation of realistic interactions [79–83].
Due to the observed significance of higher order contributions to the nuclear potential it is demanding to analyse light nuclei thoroughly, of which the p–shell nuclei are of special interest. They are the first systems of bound states where all combinations of neutrons and protons appear in a three– and four–nucleon subsystem which leads to various possible spin–isospin configurations Thus, several bound states of the individual nuclei exist which are largely influenced by 3NF. Within the NCSM approach, not only very precise results of ground-state energies but also these excited states can be calculated without difficulty. Moreover, the excitation energies show a considerably faster convergence than the binding energies. Therefore, a realisation of the NCSM approach in Jacobi coordinates is a promising endeavour on the way to gain more insight into the nature of few–nucleon forces.

This thesis is organised as follows:
In Chapter 2 we introduce the formalism of the antisymmetrisation of the HO basis states for three- and A-nucleon systems. The transposition operator $\widehat{P}_{23}$ is evaluated explicitly followed by a generalised extension to $\widehat{P}_{A(A-1)}$ and the required recoupling of the related basis states. In order to solve the Schrödinger equation, new basis states are derived which makes it possible to take three- and few-nucleon forces into account explicitly.
In Chapter 3, the parallelisation of the calculations is described including tests of the numerical performance with regard to the runtime behaviour and the memory capacity that is required for an exemplary model space. Additionally, the evaluation of the two-nucleon contribution to the binding energy is described. We specify the nuclear potential that is used for the calculations and introduce a method to extrapolate converged results.
In Chapter 4, we present the results for the binding energies of ^{3}H, ^{4}He, the

ground state and the lowest excited state of ^{6}Li and the excitation energy in the model space of $\mathcal{N}_6 = 8$, and of the ground state of ^{7}Li in the model space of $\mathcal{N}_7 = 7$ including NN forces. The convergence with increasing model spaces and the cutoff dependence is discussed.
Chapter 5 summarises the present achievements and gives an outlook on the possibilities of improvement and on the extension of our formalism to other sectors of nuclear physics.
Technical details and explicit calculations are deferred to the Appendices.

Chapter 2

Formalism

As motivated in Chapter 1 we want to study binding and excitation energies of few-nucleon systems by solving the Schrödinger equation. The Schrödinger equation describes few-nucleon systems at low energies, for which relativistic effects do not play an important role. This forms an eigenvalue problem assuming a finite basis of antisymmetric states since the nucleons are considered to be identical. The NCSM describes many-body systems containing A point-like non-relativistic nucleons in the HO basis where all A nucleons of the system are considered to be active [84]. In order to do practical calculations, the HO basis is truncated at a maximal total oscillator energy $\mathcal{N}_A$ with

$$\mathcal{N}_A \;=\; \sum_{i=1}^{A} 2n_i + l_i \;\;, \tag{2.1}$$

where $n_i = 0, 1, 2, \ldots$ is the HO quantum number and l_i the orbital momentum of the i-th nucleon. For our calculations we choose Jacobi coordinates, expressed in single-nucleon coordinates as defined in Eq. (2.10), since they separate the relative motion from the CM motion and ensure translational symmetry of the system if the space is constrained according to (2.1). The CM contribution can simply be omitted, and with this the Hamiltonian only contains the nuclear potential and the intrinsic kinetic energy that depend on relative coordinates which renders the Hamiltonian spherically symmetric. Therefore, the permutation operator $\widehat{\mathcal{P}}$ not only preserves the total oscillator energy $\mathcal{N}_A$ but also the total angular momentum J_A and the total isospin T_A, which allows for an exact antisymmetrisation within a given model space. The formalism of antisymmetrisation is discussed in detail in the following section.

2.1 Generation of antisymmetrised basis states

Bound few-nucleon states are restricted by the Pauli principle to antisymmetric states. The antisymmetrisation of any complete set of basis states is realised in

general for A nucleons as follows:
The antisymmetrisation operator $\widehat{\mathcal{A}}$ is the sum of all $A!$ possible permutations $\widehat{\mathcal{P}}$ of the A nucleons. Accordingly, for $A-1$ nucleons the antisymmetrisation operator contains all $(A-1)!$ permutations $\widehat{\tilde{\mathcal{P}}}$ of the $A-1$ nucleons. Considering that every permutation can be decomposed in a number of transpositions $\widehat{\mathcal{P}}_{ij}$ with definite signum $\varepsilon_{\widehat{\mathcal{P}}}$, the set of permutations of A nucleons, which is the symmetric group with A objects ($\mathcal{S}_A$), can be written as :

$$\left\{\widehat{\mathcal{P}}\right\} \;=\; \left\{\widehat{\tilde{\mathcal{P}}}\,\mathbb{1},\, \widehat{\tilde{\mathcal{P}}}\widehat{\mathcal{P}}_{A1},\, \widehat{\tilde{\mathcal{P}}}\widehat{\mathcal{P}}_{A2},\, \ldots,\, \widehat{\tilde{\mathcal{P}}}\widehat{\mathcal{P}}_{A(A-1)} \,|\widehat{\tilde{\mathcal{P}}} \in \mathcal{S}_{A-1}\right\} = \mathcal{S}_A. \qquad (2.2)$$

Useful properties of the transposition operator $\widehat{\mathcal{P}}_{ij}$ are specified in App. A.3.
With this the general expression for $\widehat{\mathcal{A}}$ reads

$$\begin{aligned}
\widehat{\mathcal{A}} \;&=\; \frac{1}{A!}\sum_{\widehat{\mathcal{P}}\in\mathcal{S}_A} \varepsilon_{\widehat{\mathcal{P}}}\,\widehat{\mathcal{P}} \\
&=\; \frac{1}{A!}\sum_{\widehat{\tilde{\mathcal{P}}}\in\mathcal{S}_{A-1}} \varepsilon_{\widehat{\mathcal{P}}}\left(\widehat{\tilde{\mathcal{P}}} + \sum_{i=1}^{A-1}\widehat{\tilde{\mathcal{P}}}\,\widehat{\mathcal{P}}_{Ai}\right) \\
&=\; \frac{1}{A!}\sum_{\widehat{\tilde{\mathcal{P}}}\in\mathcal{S}_{A-1}} \varepsilon_{\widehat{\tilde{\mathcal{P}}}}\left(\widehat{\tilde{\mathcal{P}}} - \sum_{i=1}^{A-1}\widehat{\tilde{\mathcal{P}}}\,\widehat{\mathcal{P}}_{Ai}\right) \\
&=\; \frac{1}{A!}\sum_{\widehat{\tilde{\mathcal{P}}}\in\mathcal{S}_{A-1}} \varepsilon_{\widehat{\tilde{\mathcal{P}}}}\widehat{\tilde{\mathcal{P}}}\left(\mathbb{1} - \sum_{i=1}^{A-1}\widehat{\mathcal{P}}_{Ai}\right). \qquad (2.3)
\end{aligned}$$

A convenient choice for the complete basis is the set of antisymmetric $(A-1)$-nucleon states coupling to a single nucleon, i.e. the states are antisymmetric with respect to all $(A-1)!$ permutations of the $A-1$ nucleons. In this work, we denote such HO–states by $|\,\beta_{AN}\rangle$. To find the antisymmetric A-nucleon HO-basis states, which we will refer to as $|\,\Gamma_{AN}\rangle$, the matrix $\langle\,\beta'_{AN}|\,\widehat{\mathcal{A}}\,|\,\beta_{AN}\rangle$ is diagonalised to solve the matrix eigenvalue equation

$$\sum_{\beta_{AN}}\langle\,\beta'_{AN}|\,\widehat{\mathcal{A}}\,|\,\beta_{AN}\rangle\langle\,\beta_{AN}\,|\,\Gamma\rangle = \lambda\,\langle\,\beta'_{AN}|\,\Gamma\rangle\,. \qquad (2.4)$$

Since the antisymmetrisation operator $\widehat{\mathcal{A}}$ is hermitean and $\widehat{\mathcal{A}}^2 = \widehat{\mathcal{A}}$, which indicates that $\widehat{\mathcal{A}}$ is a projector, Eq. (2.4) has solutions for $\lambda = 0$ and $\lambda = 1$ only. The physical eigenstates $|\,\Gamma_{AN}\rangle$ are those with $\lambda = 1$. It turns out that this reduces the number of Γ_{AN}–states approximately by a factor of $\frac{1}{A}$ relative to the number of β_{AN}–states. While the β_{AN} are a complete basis for the space of antisymmetric $(A-1)$-nucleon states, the Γ_{AN}–states span the space of antisymmetric A-nucleon

states, which is why we can express the Γ_{AN}–states completely in terms of β_{AN}–states. This results in one orthogonality relation for the overlap $\langle\, \beta_{AN}|\, \Gamma_{AN}\rangle$:

$$\sum_{\beta_{AN}} \langle\, \Gamma'_{AN}|\, \beta_{AN}\rangle\langle\, \beta_{AN}|\, \Gamma_{AN}\rangle = \delta_{\Gamma'_{AN}\,\Gamma_{AN}}\,. \tag{2.5}$$

Additionally, the antisymmetry of the $(A-1)$-nucleon states of $|\, \beta_{AN}\rangle$ can be used to further simplify the antisymmetrisation operator:

$$\begin{aligned}
\langle\, \beta'_{AN}|\, \frac{1}{A!} \sum_{\hat{\widehat{\mathcal{P}}}\in\mathcal{S}_{A-1}} \varepsilon_{\hat{\widehat{\mathcal{P}}}}\hat{\widehat{\mathcal{P}}} \left(\mathbb{1} - \sum_{i=1}^{A-1} \widehat{\mathcal{P}}_{Ai} \right) |\, \beta_{AN}\rangle \\
&= \frac{1}{A!}\, \langle\, \beta'_{AN}|\, \sum_{\hat{\widehat{\mathcal{P}}}\in\mathcal{S}_{A-1}} \varepsilon^2_{\hat{\widehat{\mathcal{P}}}} \left(\mathbb{1} - \sum_{i=1}^{A-1} \widehat{\mathcal{P}}_{Ai} \right) |\, \beta_{AN}\rangle \\
&\qquad \text{with } \widehat{\mathcal{P}}_{Ai} \overset{\text{Eq. (A.18)}}{=} \widehat{\mathcal{P}}_{Ai}\widehat{\mathcal{P}}_{(A-1)i}\widehat{\mathcal{P}}_{(A-1)i} \\
&\qquad\qquad \overset{\text{Eq. (A.21)}}{=} \widehat{\mathcal{P}}_{(A-1)i}\widehat{\mathcal{P}}_{A(A-1)}\widehat{\mathcal{P}}_{(A-1)i} \\
&= \frac{1}{A!}\, \langle\, \beta'_{AN}|\, \sum_{\hat{\widehat{\mathcal{P}}}\in\mathcal{S}_{A-1}} \left(\mathbb{1} - (A-1)\, \widehat{\mathcal{P}}_{A(A-1)} \right) |\, \beta_{AN}\rangle \\
&= \frac{1}{A}\, \langle\, \beta'_{AN}|\, \left(\mathbb{1} - (A-1)\, \widehat{\mathcal{P}}_{A(A-1)} \right) |\, \beta_{AN}\rangle\,,
\end{aligned} \tag{2.6}$$

where $\widehat{\mathcal{P}}_{A(A-1)}$ performs a coordinate transformation corresponding to an interchange of the nucleons A and $A-1$.
As mentioned above, the antisymmetrisation operator $\widehat{\mathcal{A}}$ conserves the total oscillator energy $\mathcal{N}_A$ in addition to J_A and T_A, which will be demonstrated later in this section. Therefore, the antisymmetrisation can be done $(\mathcal{N}_A\,, J_A\,, T_A)$-blockwise, which decreases the dimensionality of the problem and makes the antisymmetrisation feasible in fact. With this, the Γ_{AN}–states are uniquely numerated by the block-internal index $|\, \gamma_{AN}\rangle$ and its $(\mathcal{N}_A\,, J_A\,, T_A)$-block, $|\, (\mathcal{N}_A\,, J_A\,, T_A)\ \gamma_{AN}\rangle$, and the complete set of antisymmetric A-nucleon states is:

$$\big\{|\, \Gamma_{AN}\,\rangle\big\} \;=\; \bigcup_{\mathcal{N}_n\,\leq\,\mathcal{N}_A} \big\{|\, (\mathcal{N}_n\,, J_A\,, T_A)\, \gamma_{AN}\,\rangle\big\}. \tag{2.7}$$

A step-by-step antisymmetrisation of systems with $A = 2, 3, \ldots, A$ is therefore required to find the antisymmetric A-nucleon states. This successive application of the formalism starts with $A = 3$ since antisymmetric 2N–states are selected by the Pauli principle in a trivial way:

$$|\Gamma_{2N}\rangle = |(\mathcal{N}_{12}\,, J_{12}\,, T_{12}) \;\; n_{12}\,(\,l_{12}\; s_{12})\, J_{12}\; T_{12}; (s_1\; s_2)\, s_{12}\;\; (t_1\; t_2)\, T_{12}\,\rangle$$

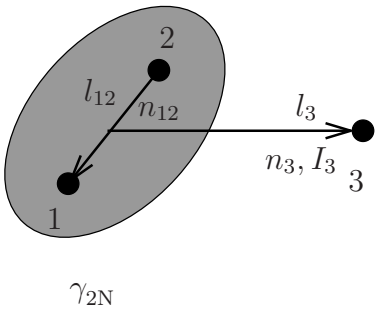

Figure 2.1: β_{3N}–state

(2.8)

with the condition $(-1)^{l_{12}+s_{12}+T_{12}} = -1$. The subscripts 1 and 2 distinguish the single nucleons with spin s_i and isospin t_i ($s_i = t_i = \frac{1}{2}$ for single nucleons), l_{12} is their relative orbital momentum and n_{12} the HO quantum number of this oscillator. As throughout this work, the explicit coupling is specified after the semicolon. These Γ_{2N}–states are the antisymmetric $(A-1)$-nucleon subsystems coupling to a single nucleon to form the $|\,\beta_{3N}\rangle$ as shown in Fig. 2.1.
We define them as

$$|\,(\mathcal{N}_3\,,J_3\,,T_3\,)\,\beta_{3N}\rangle = |\,(\mathcal{N}_3\,,J_3\,,T_3\,)\;\;\Gamma_{2N}\;\;n_3\,(l_3\,s_3)\,I_3\;t_3\,;\,(J_{12}\;I_3)J_3\;\;(T_{12}\;t_3)T_3\,\rangle,$$

(2.9)

where n_3 is the HO quantum number of nucleon 3, l_3 its relative orbital momentum with respect to the antisymmetric subsystem, spin and isospin $s_3 = t_3 = \frac{1}{2}$ and I_3 its angular momentum. Again, the explicit coupling scheme is pointed out after the semicolon.
We start with a system where nucleon 1 and nucleon 2 are coupled in an antisymmetric subsystem while nucleon 3 is a spectator (Fig. 2.2 i)). For these assignments the Jacobi coordinates are defined as follows:

$$\begin{aligned}\vec{\rho}_{12} &= \frac{\vec{r}_1 - \vec{r}_2}{b_{12}} \\ \vec{\rho}_3 &= \frac{\vec{r}_3 - \frac{1}{m_1+m_2}\,(m_1\,\vec{r}_1 + m_2\,\vec{r}_2)}{b_3}\,,\end{aligned} \tag{2.10}$$

where $\vec{r}_i$ and m_i are the single particle coordinate and the mass of particle i, respectively. These coordinates are dimensionless since we express them in terms

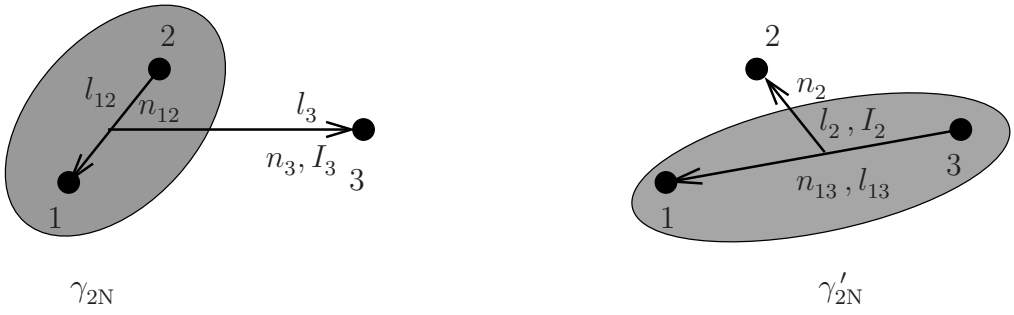

$\gamma_{2\mathrm{N}}$ $\gamma'_{2\mathrm{N}}$

i) **ii)**

Figure 2.2: **i)** $\beta_{3\mathrm{N}}$– and **ii)** $\beta'_{3\mathrm{N}}$–state

of the characteristic HO lengths b_i given by[1]

$$b_{12} = \sqrt{\frac{1}{\mu_{12}\,\omega}}$$

$$\text{and} \qquad b_3 = \sqrt{\frac{1}{\mu_3\,\omega}}\,, \tag{2.11}$$

$$\text{where} \qquad \mu_{12} = \frac{m_1\,m_2}{m_1+m_2}$$

$$\text{and} \qquad \mu_3 = \frac{m_3\,(m_1+m_2)}{m_1+m_2+m_3}\,. \tag{2.12}$$

Here, ω is the angular frequency of the oscillator, and μ_{12} and μ_3 are the reduced masses of the subsystem (12) and of the third particle with respect to the the cluster m_1+m_2, respectively. We assume the i particles to be identical (nucleons), therefore $m_i = m_{\mathrm{N}}$.

A possible choice for the antisymmetrisation operator is $\widehat{\mathcal{A}} = \frac{1}{3}\,\left(\mathbb{1} - 2\,\widehat{\mathcal{P}}_{23}\right)$. The transposition operator $\widehat{\mathcal{P}}_{23}$ interchanges nucleon 2 and nucleon 3, which corresponds to a transformation of their coordinates, as illustrated in Fig. 2.2 ii). The antisymmetric subsystem is now (13), nucleon 2 is a spectator, and the set of Jacobi coordinates is defined analogously to Eq.s (2.10)-(2.12), e.g.:

$$\vec{\rho}_{13} = \frac{\vec{r}_1 - \vec{r}_3}{b_{13}}$$

[1] As throughout this work we use natural units where $\hbar = 1 = c$.

$$\vec{\rho}_2 \;=\; \frac{\vec{r}_2 - \frac{1}{m_1+m_3}\,(m_1\,\vec{r}_1 + m_3\,\vec{r}_3)}{b_2} \quad \text{etc.} \tag{2.13}$$

For the transition from (12)3 to (13)2 one finds:

$$\begin{aligned}
&\langle\, \beta'_{3\mathrm{N}} | \widehat{\mathcal{P}}_{23} |\, \beta_{3\mathrm{N}} \rangle \\
&= \langle (\mathcal{N}'_3\,, J'_3\,, T'_3) \quad (\mathcal{N}_{13}\,, J_{13}\,, T_{13})\,\gamma'_{2\mathrm{N}} \;\; n_2\,(l_2\,s_2)\,I_2\,;(J_{13}\;I_2)\,J'_3 \;\; (T_{13}\;t_2)\,T'_3| \\
&\qquad |\,(\mathcal{N}_3\,, J_3\,, T_3) \quad (\mathcal{N}_{12}\,, J_{12}\,, T_{12})\,\gamma_{2\mathrm{N}} \;\; n_3\;(l_3\,s_3)\,I_3\,;(J_{12}\;I_3)\,J_3 \;\; (T_{12}\;t_3)\,T_3\rangle \\
&= \delta_{\mathcal{N}'_3\mathcal{N}_3}\,\delta_{J'_3J_3}\,\delta_{T'_3T_3} \\
&\quad \times (-1)^{s_{13}+s_2+s_{12}+s_3+T_{13}+t_2+T_{12}+t_3+l_2+l_3} \\
&\quad \times \hat{J}_{13}\,\hat{I}_2\,\hat{J}_{12}\,\hat{I}_3\,\hat{s}_{13}\,\hat{s}_{12}\,\hat{T}_{13}\,\hat{T}_{12} \\
&\quad \times \sum_{LS} \hat{L}^2\,\hat{S}^2 \begin{Bmatrix} s_2 & s_1 & s_{12} \\ s_3 & S & s_{13} \end{Bmatrix} \begin{Bmatrix} t_2 & t_1 & T_{12} \\ t_3 & T_3 & T_{13} \end{Bmatrix} \\
&\qquad \times \begin{Bmatrix} l_{13} & s_{13} & J_{13} \\ l_2 & s_2 & I_2 \\ L & S & J_3 \end{Bmatrix} \begin{Bmatrix} l_{12} & s_{12} & J_{12} \\ l_3 & s_3 & I_3 \\ L & S & J_3 \end{Bmatrix} \\
&\qquad \times \langle n_{13}\,l_{13}\,,\; n_2\,l_2 \;:\; L\,|\,n_{12}\,l_{12}\,,\; n_3\,l_3 \;:\; L\rangle\,,
\end{aligned} \tag{2.14}$$

where $\mathcal{N}'_3 = \mathcal{N}_{13} + 2n_2 + l_2$, as usual $s_i = \frac{1}{2} = t_i$ for single nucleons, $\hat{x} = \sqrt{2x+1}$, and $\langle n_{13}\;l_{13}\,,\;n_2\;l_2\;:\;L\,|\,n_{12}\;l_{12}\,,\;n_3\,l_3\;:\;L\rangle$ is the general HO bracket for the transition (12)3 $\rightarrow$ (13)2 in configuration space as defined e.g. in [85].

This relation is found in three steps:

a) $\underline{JJ\textbf{-coupling} \rightarrow\; LS\textbf{-coupling :}}$

First, it is useful to disentangle the orbital matrix elements from the spin part. A standard recoupling gives the desired result:

$$\begin{aligned}
&\big\langle \big[\,(l_{13}\;s_{13})\,J_{13}\;\;(l_2\;s_2)\,I_2\big]\,J'_3\,\big|\,\big[\,(l_{12}\;s_{12})\,J_{12}\;\;(l_3\;s_3)\,I_3\big]\,J_3\big\rangle \\
&\qquad = \delta_{L'L}\,\delta_{S'S}\,\delta_{J'_3J_3}\;\;\hat{J}_{13}\,\hat{I}_2\,\hat{J}_{12}\,\hat{I}_3 \\
&\qquad\quad \times \sum_{LS,L'S'} \hat{L}'\,\hat{S}'\,\hat{L}\,\hat{S} \begin{Bmatrix} l_{13} & s_{13} & J_{13} \\ l_2 & s_2 & I_2 \\ L' & S' & J'_3 \end{Bmatrix} \begin{Bmatrix} l_{12} & s_{12} & J_{12} \\ l_3 & s_3 & I_3 \\ L & S & J_3 \end{Bmatrix}
\end{aligned}$$

$$\times \left\langle \left[\left(l_{13}\, l_2 \right) L' \;\; \left(s_{13}\, s_2 \right) S' \right] J_3 \,\middle|\, \left[\left(l_{12}\, l_3 \right) L \;\; \left(s_{12}\, s_2 \right) S \right] J_3 \right\rangle$$

$$= \hat{J}_{13}\, \hat{I}_2\, \hat{J}_{12}\, \hat{I}_3 \sum_{LS} \hat{L}^2\, \hat{S}^2 \left\{ \begin{array}{ccc} l_{13} & s_{13} & J_{13} \\ l_2 & s_2 & I_2 \\ L & S & J_3 \end{array} \right\} \left\{ \begin{array}{ccc} l_{12} & s_{12} & J_{12} \\ l_3 & s_3 & I_3 \\ L & S & J_3 \end{array} \right\}$$

$$\times \left\langle \left[\left(l_{13}\, l_2 \right) L \;\; \left(s_{13}\, s_2 \right) S \right] J_3 \,\middle|\, \left[\left(l_{12}\, l_3 \right) L \;\; \left(s_{12}\, s_3 \right) S \right] J_3 \right\rangle \tag{2.15}$$

b) spin S/isospin T matrix elements:

The spin part of the coordinate transformation is simply given by a $6j$–symbol:

$$\begin{aligned} \left\langle \left[\left(s_1\, s_3 \right) s_{13}\; s_2 \right] S' \,\middle|\, \left[\left(s_1\, s_2 \right) s_{12}\; s_3 \right] S \right\rangle &= \delta_{S'S}\, (-1)^{s_{13}+s_2-S'-s_1-s_2+s_{12}} \\ &\quad \times \left\langle \left[s_2 \;\; \left(s_1\, s_3 \right) s_{13} \right] S' \,\middle|\, \left[\left(s_2\, s_1 \right) s_{12}\; s_3 \right] S \right\rangle \\ &= (-1)^{s_{13}-S-s_1+s_{12}+s_1+s_2+s_3+S} \\ &\quad \times \hat{s}_{13}\, \hat{s}_{12} \left\{ \begin{array}{ccc} s_2 & s_1 & s_{12} \\ s_3 & S & s_{13} \end{array} \right\} \\ &= (-1)^{s_{13}+s_{12}+s_2+s_3} \\ &\quad \times \hat{s}_{13}\, \hat{s}_{12} \left\{ \begin{array}{ccc} s_3 & s_1 & s_{13} \\ s_2 & S & s_{12} \end{array} \right\} \end{aligned} \tag{2.16}$$

The same calculations can be done analogously for the isospin T showing the conservation of the total isospin.

c) configuration space:

The probably most complicated step is the transformation of the orbital part. We want to rewrite this in such a way that HO brackets of [85] can be used. There, the matrix elements $\langle n_{13}\, l_{13}\,,\; n_2\, l_2 \;:\; L \,|\, n_{12}\, l_{12}\,,\; n_3\, l_3 \;:\; L \rangle$ for the HO brackets are introduced corresponding to a transformation $\mathcal{T}$ for the coordinate transformation $(12)3 \rightarrow (13)2$ of the form

$$\mathcal{T} \;=\; \left(\begin{array}{cc} \sqrt{\frac{d}{1+d}} & \sqrt{\frac{1}{1+d}} \\ \sqrt{\frac{1}{1+d}} & -\sqrt{\frac{d}{1+d}} \end{array} \right). \tag{2.17}$$

For our definition of the Jacobi coordinates (Eq. (2.10)) this requires additional phases:

$$\begin{pmatrix} \vec{\rho}_{13} \\ \vec{\rho}_{2} \end{pmatrix} = \begin{pmatrix} \sqrt{\frac{d}{1+d}} & -\sqrt{\frac{1}{1+d}} \\ -\sqrt{\frac{1}{1+d}} & -\sqrt{\frac{d}{1+d}} \end{pmatrix} \begin{pmatrix} \vec{\rho}_{12} \\ \vec{\rho}_{3} \end{pmatrix}$$

$$\text{or} \qquad \begin{pmatrix} \vec{\rho}_{13} \\ -\vec{\rho}_{2} \end{pmatrix} = \begin{pmatrix} \sqrt{\frac{d}{1+d}} & \sqrt{\frac{1}{1+d}} \\ \sqrt{\frac{1}{1+d}} & -\sqrt{\frac{d}{1+d}} \end{pmatrix} \begin{pmatrix} \vec{\rho}_{12} \\ -\vec{\rho}_{3} \end{pmatrix} \tag{2.18}$$

with $d = \dfrac{m_2\, m_3}{m_1\,(m_1+m_2+m_3)} = \dfrac{1}{3}$ for three nucleons. The transformation is therefore given by:

$$(-1)^{l_2+l_3}\ \langle n_{13}\ l_{13}\,,\ n_2\ l_2\ :\ L\,|\,n_{12}\ l_{12}\,,\ n_3\, l_3\ :\ L\rangle_{d=\frac{1}{3}}\,. \tag{2.19}$$

We remark that the required sign changes for $\vec{\rho}_2$ and $\vec{\rho}_3$ lead to an additional phase factor. The complete expression Eq.(2.14) easily follows from a) – c). We will show that the antisymmetrisation for A-nucleon states can be traced back to these expressions which demonstrates the conservation of $\mathcal{N}_A$, J_A and T_A. Therefore, we will drop the 'prefix' $(\mathcal{N}_A\,, J_A\,, T_A)$ for all basis states in the following and always presume $\delta_{\mathcal{N}'_A\mathcal{N}_A}\,\delta_{J'_AJ_A}\,\delta_{T'_AT_A}$.

With this one finds the antisymmetric $\gamma_{3\mathrm{N}}$–states by diagonalising the matrix $\langle\,\beta'_{3\mathrm{N}}|\ \frac{1}{3}\left(\mathbb{1}-2\,\widehat{\mathcal{P}}_{23}\right)\ |\,\beta_{3\mathrm{N}}\rangle$ and selecting eigenstates of the eigenvalue 1.The eigenstates will be complicated linear combinations of $\beta_{3\mathrm{N}}$–states and therefore finally only given numerically in form of weight factors of $\beta_{3\mathrm{N}}$–states.
Keeping this complication in mind, the proceeding to higher A is similar: based on the antisymmetric $\gamma_{(A-1)\mathrm{N}}$–states, a single nucleon is coupled to form the $\beta_{A\mathrm{N}}$–states (Fig. 2.3 ii)). To solve the eigenvalue problem Eq. (2.4) for A nucleons with $\widehat{\mathcal{A}} = \frac{1}{A}\left(\mathbb{1}-(A-1)\,\widehat{\mathcal{P}}_{A(A-1)}\right)$ (Eq. (2.6)) we need to go back to $\beta_{(A-1)\mathrm{N}}$–states and combine them with a single nucleon as illustrated in Fig. 2.3 i). These intermediate states are here denoted by $|\,\beta^{\star}_{A\mathrm{N}}\rangle$ and contain two single nucleons so that we can perform the coordinate transformation of the A-th and the $(A-1)$-th nucleon, $\widehat{\mathcal{P}}_{A(A-1)}$.
To shorten the notation, we identify the antisymmetric subsystem $|\,\gamma_{(A-2)\mathrm{N}}\rangle$ with $|\,\gamma_a\,\rangle$, which together with the single nucleon b forms the $\beta_{(A-1)\mathrm{N}} = \beta_b$–states; nucleon A is labelled by the index c. This notation also emphasises the analogy to the 3N case since the transposition operator $\widehat{\mathcal{P}}_{A(A-1)} = \widehat{\mathcal{P}}_{bc}$ corresponds to a transition from $(ab)\,c$ to $(ac)\,b$.

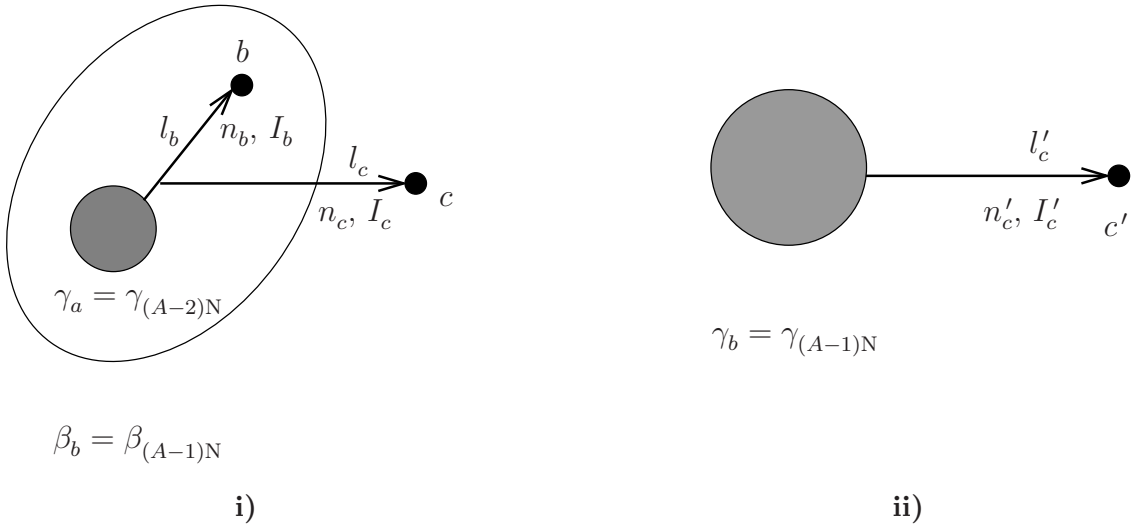

Figure 2.3: **i)** $\beta^{\star}_{AN}$–state and **ii)** β_{AN}–state

With this the antisymmetrisation matrix is calculated as:

$$\langle\, \beta'_{AN}\,|\widehat{\mathcal{P}}_{bc}|\,\beta_{AN}\,\rangle \;=\; \sum_{\beta^{\star\prime}_{AN}\beta^{\star}_{AN}} \langle\, \beta'_{AN}\,|\,\beta^{\star\prime}_{AN}\,\rangle\langle\, \beta^{\star\prime}_{AN}|\widehat{\mathcal{P}}_{bc}|\,\beta^{\star}_{AN}\,\rangle\langle\, \beta^{\star}_{AN}\,|\,\beta_{AN}\,\rangle\,. \quad (2.20)$$

For comprehensibility, this sum can also be shown in a descriptive way:

$$\langle\, \beta'_{AN}\,|\widehat{\mathcal{P}}_{bc}|\,\beta_{AN}\,\rangle \;=\; \Big\langle \bullet\!\!-\!\!\cdot \;\Big|\; \cdot\!\!\diagup\!\!\bullet \Big\rangle \Big\langle \cdot\!\!\diagup\!\!\bullet \;\Big|\, \widehat{\mathcal{P}}_{bc} \,\Big|\; \bullet\!\!\diagdown\!\!\cdot \Big\rangle \Big\langle \bullet\!\!\diagdown\!\!\cdot \;\Big|\; \cdot\!\!-\!\!\bullet \Big\rangle\,, \quad (2.21)$$

where single nucleons are depicted as solid dots and antisymmetric subsystems as shaded blobs. For this simplified notation, we assume that a sum over intermediate states is implied.
The overlap $\langle\, \beta^{\star}_{AN}\,|\beta_{AN}\rangle$ can be deduced from Fig. 2.3: if particle c (and its quantum numbers) are the same as c' (and its quantum numbers), the resulting coefficient is known from the antisymmetrisation of the $(A-1)$-nucleon system.

$$\begin{aligned} \langle\, \beta^{\star}_{AN}\,|\beta_{AN}\rangle \;&=\; \delta_{c'c}\,\langle\, \beta_{(A-1)\mathrm{N}}\,|\,\gamma_{(A-1)\mathrm{N}}\,\rangle \\ &\qquad \text{where} \quad \delta_{c'c} = \delta_{n'_c n_c}\,\delta_{l'_c l_c}\,\delta_{I'_c I_c} \end{aligned} \quad (2.22)$$

The coefficients cannot be given in an analytical form but will be calculated numerically. Here it is obvious, that antisymmetrised states have to be generated successively for $A = 3, 4, \ldots, A$. For $|\,\beta^{\star}_{AN}\rangle$ we define the Jacobi coordinates for the system $(ab)c$ analogously to Eq. (2.10):

$$\vec{\rho}_b \;=\; \frac{\vec{r}_a - \vec{r}_b}{b_b}$$

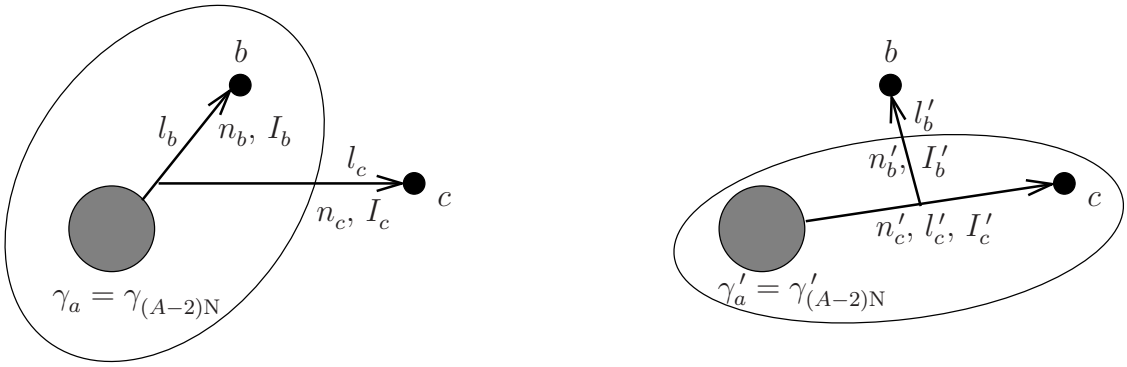

$\beta_b = \beta_{(A-1)\mathrm{N}}$ $\qquad$ $\beta'_c = \beta'_{(A-1)\mathrm{N}}$

i) $\qquad$ **ii)**

Figure 2.4: **i)** $\beta^{\star}_{A\mathrm{N}}$–state and **ii)** $\beta^{\star\prime}_{A\mathrm{N}}$–state

$$\vec{\rho}_c \;=\; \frac{\vec{r}_c - \frac{1}{m_a+m_b}\,(m_a\,\vec{r}_a + m_b\,\vec{r}_b)}{b_c} \tag{2.23}$$

and compare the assignments for the quantum numbers of $|\,\beta_{3\mathrm{N}}\rangle$ and $|\,\beta^{\star}_{A\mathrm{N}}\rangle$, as depicted in Fig. 2.1 and Fig. 2.4 i), respectively, in order to be able to lead back the expression for $\langle\,\beta^{\star\prime}_{A\mathrm{N}}|\;\widehat{\mathcal{P}}_{bc}\;|\,\beta^{\star}_{A\mathrm{N}}\rangle$ to Eq. (2.14). To account for the opposite direction of l_b and l_{12}, the coordinate $\vec{\rho}_b$ acquires a phase $(-1)^{l_b}$. The system $(ac)b$ is defined analogously including a phase $(-1)^{l'_c}$. The transposition $\widehat{\mathcal{P}}_{bc}$ leaves the γ_a–state unchanged which yields $\delta_{\Gamma'_a\Gamma_a} = \delta_{\mathcal{N}'_a\mathcal{N}_a}\,\delta_{J'_aJ_a}\,\delta_{T'_aT_a}\,\delta_{\gamma'_a\gamma_a}$.
This simple consideration fixes the required phase in order to match Eq. (2.14). Unfortunately, the coupling scheme of the β_b– and β'_c–states is not identical to that used in Eq. (2.14). Focussing on the angular momentum part of

$$\begin{aligned}
&\langle\,\beta^{\star\prime}_{A\mathrm{N}}\,|\widehat{\mathcal{P}}_{bc}|\,\beta^{\star}_{A\mathrm{N}}\,\rangle \\
&= \langle(\mathcal{N}'_c\,,J'_c\,,T'_c)\,\beta'_c\;\; n'_b\,(l'_b\,s_b)\,I'_b\,;\big\{\big[J_a\;\,(l'_c\,s_c)\,I'_c\big]J'_c\;\,I'_b\big\}J_A\;\big[\,(T_a\,t_c)T'_c\;\,t_b\big]T_A\,| \\
&\qquad |\,(\mathcal{N}_b\,,J_b\,,T_b)\,\beta_b\;\; n_c\,(l_c\,s_c)\,I_c\,;\big\{\big[J_a\;\,(l_b\,s_b)\,I_b\big]J_b\;\,I_c\big\}J_A\;\big[\,(T_a\,t_b)T_b\;\,t_c\big]T_A\rangle\,,
\end{aligned}$$

the angular momenta of $|\,\beta^{\star}_{A\mathrm{N}}\rangle$ need to be recoupled in the following way ($\delta_{\mathcal{N}'_A\mathcal{N}_A}\,\delta_{J'_AJ_A}\,\delta_{T'_AT_A}$ implied):

$$\begin{aligned}
&\big\langle\big\{\big[J_a\;\,(l'_c\,s_c)\,I'_c\big]J'_c\;\,(l'_b\,s_b)\,I'_b\big\}J_A\;\big|\big\{\big[J_a\;\,(l_b\,s_b)\,I_b\big]J_b\;\,(l_c\,s_c)\,I_c\big\}J_A\big\rangle \\
&= (-1)^{l_b+l'_c}\,(-1)^{I'_c-l'_c-s_c}\,(-1)^{I_b-l_b-s_b}
\end{aligned}$$

$$
\begin{aligned}
&\times\big\langle\big\{\big[J_a\ (s_c\ l_c')\,I_c'\big]J_c'\ (l_b'\ s_b')\,I_b'\big\}J_A\,\big|\big\{\big[J_a\ (s_b\ l_b)\,I_b\big]J_b\ (l_c\ s_c)\,I_c\big\}J_A\big\rangle\\
&=(-1)^{I_c'-s_c+I_b-s_b}\,(-1)^{J_a+s_c+l_c'+J_c'}\,(-1)^{J_a+s_b+l_b+J_b}\\
&\quad\times\sum_{S_c'S_b}\hat{I}_c'\,\hat{S}_c'\begin{Bmatrix} J_a & s_c & S_c' \\ l_c' & J_c' & I_c' \end{Bmatrix}\hat{I}_b\,\hat{S}_b\begin{Bmatrix} J_a & s_b & S_b \\ l_b & J_b & I_b \end{Bmatrix}\\
&\quad\times\big\langle\big\{\big[\,(J_a\ s_c)\,S_c'\ \ l_c'\big]J_c'\ (l_b'\ s_b)\,I_b'\big\}J_A\,\big|\big\{\big[\,(J_a\ s_b)\,S_b\ \ l_b\big]J_b\ (l_c\ s_c)\,I_c\big\}J_A\big\rangle\\
&=(-1)^{I_c'+I_b+2J_a+l_c'+J_c'+l_b+J_b}\,(-1)^{l_c'+S_c'-J_c'}\,(-1)^{l_b+S_b-J_b}\\
&\quad\times\sum_{S_c'S_b}\hat{I}_c'\,\hat{S}_c'\,\hat{I}_b\,\hat{S}_b\begin{Bmatrix} J_a & s_c & S_c' \\ l_c' & J_c' & I_c' \end{Bmatrix}\begin{Bmatrix} J_a & s_b & S_b \\ l_b & J_b & I_b \end{Bmatrix}\\
&\quad\times\big\langle\big\{\big[l_b'\ (J_a\ s_c)\,S_c'\big]J_c'\ (l_b'\ s_b)\,I_b'\big\}J_A\,\big|\big\{\big[l_b\ (J_a\ s_b)\,S_b\big]J_b\ (l_c\ s_c)\,I_c\big\}J_A\big\rangle\\
&=(-1)^{I_c'+I_b+2J_a+S_c'+S_b}\\
&\quad\times\sum_{S_c'S_b}\hat{I}_c'\,\hat{S}_c'\,\hat{I}_b\,\hat{S}_b\begin{Bmatrix} J_a & s_c & S_c' \\ l_c' & J_c' & I_c' \end{Bmatrix}\begin{Bmatrix} J_a & s_b & S_b \\ l_b & J_b & I_b \end{Bmatrix}\\
&\quad\times\big\langle\big\{\big[l_c'\ (J_a\ s_c)\,S_c'\big]J_c'\ (l_b'\ s_b)\,I_b'\big\}J_A\,\big|\big\{\big[l_b\ (J_a\ s_b)\,S_b\big]J_b\ (l_c\ s_c)\,I_c\big\}J_A\big\rangle
\end{aligned}
\tag{2.24}
$$

This expression can now be compared to Eq. (2.14). Adding the phase factor $(-1)^{l_b+l_c'}$ from above and using $d=\frac{1}{A(A-1)}$ we find the full expression for the coordinate transformation $(ab)\,c$ to $(ac)\,b$:

$$
\begin{aligned}
&\langle\,\beta_{AN}^{\star\prime}\,|\widehat{\mathcal{P}}_{bc}|\,\beta_{AN}^{\star}\,\rangle\\
&=\langle(\mathcal{N}_c'\,,J_c'\,,T_c')\,\beta_c'\ \ n_b'\,(l_b'\,s_b)\,I_b'\,;\big[\,(J_a'\,I_c')\,J_c'\ \,(l_b'\,s_b)\,I_b'\big]J_A\,\big[\,(T_a'\,t_c)T_c'\ \,t_b\big]T_A\,|\\
&\qquad|\,(\mathcal{N}_b\,,J_b\,,T_b)\,\beta_b\ \ n_c\,(l_c\,s_c)\,I_c\,;\big[\,(J_a\,I_b)\,J_b\ \,(l_c\,s_c)\,I_c\big]J_A\,\big[\,(T_a\,t_b)T_b\ \,t_c\big]T_A\rangle\\
&=\delta_{\Gamma_a'\Gamma_a}\ \ (-1)^{I_c'+I_b+2J_a+T_c'+T_b+l_b'+l_c}\\
&\quad\times\hat{I}_c'\,\hat{J}_c'\,\hat{I}_b'\ \,\hat{I}_b\,\hat{J}_b\,\hat{I}_c\ \,\hat{T}_c'\,\hat{T}_b\\
&\quad\times\sum_{S_c'S_b}\hat{S}_c'^{\,2}\,\hat{S}_b^{\,2}\begin{Bmatrix} J_a & s_c & S_c' \\ l_c' & J_c' & I_c' \end{Bmatrix}\begin{Bmatrix} J_a & s_b & S_b \\ l_b & J_b & I_b \end{Bmatrix}
\end{aligned}
$$

$$\times \sum_{LS} \hat{L}^2\, \hat{S}^2 \left\{ \begin{array}{ccc} s_c & J_a & S'_c \\ s_b & S & S_b \end{array} \right\} \left\{ \begin{array}{ccc} t_c & T_a & T'_c \\ t_b & T_A & T_b \end{array} \right\}$$

$$\times \left\{ \begin{array}{ccc} l'_c & S'_c & J'_c \\ l'_b & s_b & I'_b \\ L & S & J_A \end{array} \right\} \left\{ \begin{array}{ccc} l_b & S_b & J_b \\ l_c & s_c & I_c \\ L & S & J_A \end{array} \right\}$$

$$\times \langle n'_c\, l'_c\,,\; n'_b\, l'_b \;:\; L \,|\, n_b\, l_b\,,\; n_c\, l_c \;:\; L \rangle_{d=\frac{1}{A(A-2)}}\,, \tag{2.25}$$

We remark that the number of $\beta^{\star}_{AN}$–states always exceeds the number of β_{AN}–states. The β_{AN}–states are more restricted by symmetry aspects, similar to $|\,\beta_{AN}\rangle$ with respect to $|\,\gamma_{AN}\rangle$, since they are a complete basis for the space of antisymmetric $(A-1)$-nucleon states while the $\beta^{\star}_{AN}$–states are a complete basis for the space of antisymmetric $(A-2)$-nucleon states. Therefore we can always describe the β_{AN}–states completely in terms of the $\beta^{\star}_{AN}$–states, but not vice versa.
We also note that the HO basis allows one to construct antisymmetrised states that are independent of ω. Once a basis is evaluated, it can be employed for all ω. This is obviously important for the application.

With this method of coordinate transformation different sets of basis states can be constructed. To include NN- and few-N forces to the nuclear potential in a simple way we perform the transformation in such a way that antisymmetric 2N- or few-N states are separated. This formalism is discussed in the following section.

2.2 Matrix elements of n-body operators

For the calculation of the energies we need to solve the eigenvalue equation

$$\sum_{\Gamma_{AN}} \langle\, \Gamma'_{AN}\,|\widehat{H}|\,\Gamma_{AN}\,\rangle \langle\, \Gamma_{AN}\,|\,\Psi\,\rangle = E_b^{(AN)}\, \langle\, \Gamma'_{AN}\,|\,\Psi\,\rangle\,. \tag{2.26}$$

The eigenvalue equation is readily solved using standard methods so that the problem is reduced to the calculation of the matrix elements of the Hamiltonian

$$\widehat{H} = \widehat{T}_{AN} + \sum_{\text{pairs}} \widehat{V}_{\text{NN}} + \sum_{\text{triples}} \widehat{V}_{\text{3N}} + \sum_{\text{quadruples}} \widehat{V}_{\text{4N}} + \ldots \tag{2.27}$$

As shown in App. A.2, the kinetic energy can be written as

$$\widehat{T}_{AN} = \sum_{i<j} \frac{2}{A}\, \widehat{T}_{ij}\,, \tag{2.28}$$

where $\widehat{T}_{ij} = p_{ij}^2/m_{\rm N}$ is the relative kinetic energy of the pair (ij). Using the antisymmetry of the basis states, we can simplify the expression for the matrix elements to

$$\begin{aligned}\langle\,\Gamma'_{AN}\,|\widehat{H}|\,\Gamma_{AN}\,\rangle &= \binom{A}{2}\langle\,\Gamma'_{AN}\,|\left(\frac{2}{A}\,\widehat{T}_{12}+\widehat{V}_{12}\right)|\,\Gamma_{AN}\,\rangle \\ &\quad+\binom{A}{3}\langle\,\Gamma'_{AN}\,|\widehat{V}_{123}|\,\Gamma_{AN}\,\rangle \\ &\quad+\ldots \end{aligned} \tag{2.29}$$

Therefore, we want to show in this section how such matrix elements can be evaluated in the to our experience most efficient way. We start with the example of two-body operators for $A = 3$ and generalise these to the more complex cases. For the triton (^{3}H) or ^{3}He we make use of the $\langle\,\beta\,|\,\gamma\,\rangle$–coefficients of the 3N-system. As pointed out in the previous section, the $\gamma_{3\rm N}$–states can completely be expressed in terms of the $\beta_{3\rm N}$–states. The $\beta_{3\rm N}$–states are constructed as a single nucleon coupled to an antisymmetric 2N–state, Eq. (2.9), which is then used to calculate the two-nucleon contribution of the binding energy:

$$\begin{aligned}&E_b^{(3\rm N)}\,\langle\,\Gamma'_{3\rm N}\,|\,\Psi\,\rangle \\ &\quad=\sum_{\Gamma_{3\rm N}}\langle\,\Gamma'_{3\rm N}\,|\widehat{H}|\,\Gamma_{3\rm N}\,\rangle\,\langle\,\Gamma_{3\rm N}\,|\,\Psi\,\rangle \\ &\quad=\bigcup_{\mathcal{N}'_3,\mathcal{N}_3}3\times\sum_{\gamma_{3\rm N}}\sum_{\beta'_{3\rm N}\beta_{3\rm N}}\langle\,\gamma'_{3\rm N}|\,\beta'_{3\rm N}\rangle\langle\,\beta'_{3\rm N}|\left(\frac{2}{3}\,\widehat{T}_{12}+\widehat{V}_{12}\right)|\,\beta_{3\rm N}\rangle\langle\,\beta_{3\rm N}|\,\gamma_{3\rm N}\rangle\langle\,\gamma_{3\rm N}\,|\,\Psi\,\rangle\end{aligned} \tag{2.30}$$

For $A > 3$ the two-nucleon contribution can be calculated similarly if we are able to identify an antisymmetric 2N-subsystem from $|\,\gamma_{AN}\rangle$. To this aim we consider $\beta^\star_{AN}$–states and perform a coordinate transformation such that the antisymmetric $(A-2)$-nucleon system couples as a spectator to an antisymmetric 2N–state, as indicated in Fig. 2.5. These states will be denoted by $|\,\tilde{\beta}^{(2)}_{AN}\rangle$; the superscript (2) indicates which antisymmetric subsystem is separated. The projection onto the completely antisymmetrised A-nucleon states $\langle\,\gamma_{AN}|\,\tilde{\beta}^{(2)}_{AN}\rangle$ is calculated via:

$$\begin{aligned}\langle\,\gamma_{AN}\,|\tilde{\beta}^{(2)}_{AN}\rangle &= \sum_{\beta\beta^\star}\langle\,\gamma\,|\,\beta\,\rangle\langle\,\beta\,|\,\beta^\star\,\rangle\langle\beta^\star\,|\,\tilde{\beta}^{(2)}\,\rangle \\ &= \end{aligned} \tag{2.31}$$

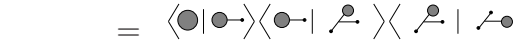

For simplicity the subscript AN is omitted on the right-hand side. The transition $\langle\beta^\star_{AN}\,|\,\tilde{\beta}^{(2)}_{AN}\,\rangle$ requires another recoupling of $\langle\beta^\star_{AN}\,|$:

$$\langle\beta^\star_{AN}\,| = \langle\big(\mathcal{N}_{A-1},J_{A-1},T_{A-1}\big)\beta_{(A-1)\rm N}\;\; n_2\,(l_2\,s_2)\,I_2;$$

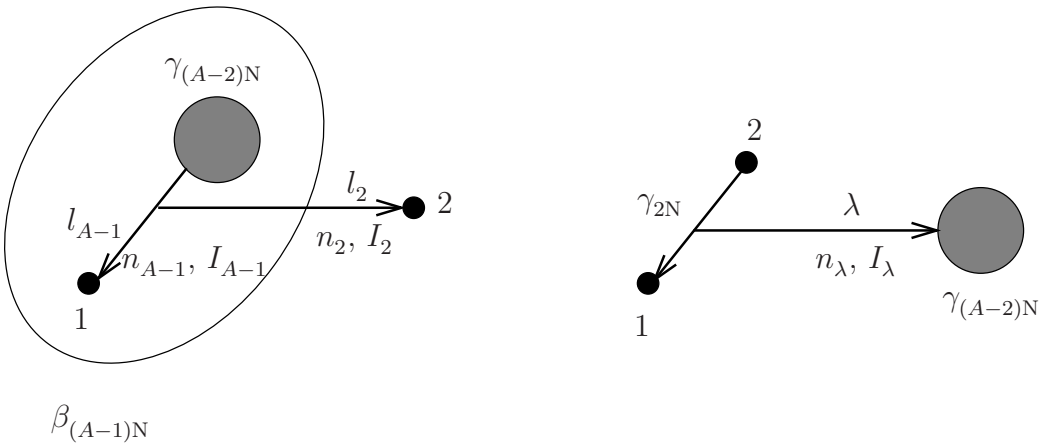

i) **ii)**

Figure 2.5: $\beta^{\star}_{A\mathrm{N}}$–state (**i)**) and $\tilde{\beta}^{(2)}_{A\mathrm{N}}$–state (**ii)**); solid blobs denote single nucleons.

$$\left\{\left[J_{A-2}\ \left(l_{A-1}\,s_1\right)I_{A-1}\right]J_{A-1}\ I_2\right\}J_A\left[\left(T_{A-2}\,t_1\right)T_{A-1}\,t_2\right]T_A\right| \qquad (2.32)$$

so that the angular momenta couple as follows:

$$\begin{aligned}
&\Big\langle\left\{\left[J_{A-2}\ \left(l_{A-1}\,s_1\right)I_{A-1}\right]J_{A-1}\ \left(l_2\ s_2\right)I_2\right\}J_A\Big| \\
&\quad=(-1)^{I_{A-1}-l_{A-1}-s_1} \\
&\quad\times\Big\langle\left\{\left[J_{A-2}\ \left(s_1\,l_{A-1}\right)I_{A-1}\ J_{A-2}\right]J_{A-1}\ \left(l_2\ s_2\right)I_2\right\}J_A\Big| \\
&\quad=(-1)^{I_{A-1}-l_{A-1}-s_1+J_{A-2}+s_1+l_{A-1}+J_{A-1}} \\
&\qquad\times\sum_{S_{A-1}}\hat{I}_{A-1}\,\hat{S}_{A-1}\left\{\begin{array}{ccc}J_{A-2}&s_1&S_{A-1}\\ l_{A-1}&J_{A-1}&I_{A-1}\end{array}\right\} \\
&\qquad\times\ \Big\langle\left\{\left[\left(J_{A-2}\,s_1\right)\ S_{A-1}\,l_{A-1}\right]J_{A-1}\ \left(l_2\ s_2\right)I_2\right\}J_A\Big| \\
&\quad=(-1)^{I_{A-1}+J_{A-2}+J_{A-1}-J_{A-1}+l_{A-1}+S_{A-1}} \\
&\qquad\times\sum_{S_{A-1}}\hat{I}_{A-1}\,\hat{S}_{A-1}\left\{\begin{array}{ccc}J_{A-2}&s_1&S_{A-1}\\ l_{A-1}&J_{A-1}&I_{A-1}\end{array}\right\} \\
&\qquad\times\Big\langle\left\{\left[l_{A-1}\ \left(J_{A-2}\,s_1\right)\ S_{A-1}\right]J_{A-1}\ \left(l_2\ s_2\right)I_2\right\}J_A\Big| \\
&\quad=(-1)^{I_{A-1}+J_{A-2}+l_{A-1}+S_{A-1}-S_{A-1}+s_1+J_{A-2}} \\
&\qquad\times\sum_{S_{A-1}}\hat{I}_{A-1}\,\hat{S}_{A-1}\left\{\begin{array}{ccc}J_{A-2}&s_1&S_{A-1}\\ l_{A-1}&J_{A-1}&I_{A-1}\end{array}\right\}
\end{aligned}$$

$$\times\Big\langle \Big\{\big[l_{A-1}\ \big(s_1\ J_{A-2}\big)\ S_{A-1}\big]J_{A-1}\ (l_2\ s_2)\,I_2\Big\}J_A\Big|$$

$$= (-1)^{I_{A-1}+2J_{A-2}+l_{A-1}+s_1-T_{A-1}+t_1+T_{A-2}}$$
$$\times \sum_{S_{A-1}} \hat{I}_{A-1}\,\hat{S}_{A-1} \left\{ \begin{array}{ccc} J_{A-2} & s_1 & S_{A-1} \\ l_{A-1} & J_{A-1} & I_{A-1} \end{array} \right\}$$
$$\times\Big\langle \Big\{\big[l_{A-1}\ \big(s_1\ J_{A-2}\big)\ S_{A-1}\big]J_{A-1}\ (l_2\ s_2)\,I_2\Big\}J_A\Big| \qquad (2.33)$$

Defining $|\,\tilde{\beta}^{(2)}_{AN}\,\rangle$ as

$$|\,\tilde{\beta}^{(2)}_{AN}\,\rangle = |\,(\mathcal{N}_{12},\,J_{12},\,T_{12})\,\gamma_{2N}\ \ n_\lambda\,\lambda\ \big(\mathcal{N}_{A-2},\,J_{A-2},\,T_{A-2}\big)\,\gamma_{(A-2)N}\,;$$
$$\Big\{\,[l_{12}\ (s_1\,s_2)\,s_{12}]\,J_{12}\ \big(\lambda\,J_{A-2}\big)\,I_\lambda\Big\}J_A\ \ \big[(t_1\,t_2)\,T_{12}\,T_{A-2}\big]\,T_A\rangle, \qquad (2.34)$$

the individual quantum numbers for the transition $\langle\,\beta^\star_{AN}\,|\,\tilde{\beta}^{(2)}_{AN}\,\rangle$ can be identified with those of Eq.s (2.15) - (2.19):

$$\langle\,\beta^\star_{AN}\,|\,\tilde{\beta}^{(2)}_{AN}\,\rangle = (-1)^{I_{A-1}+2J_{A-2}+l_{A-1}+s_1-T_{A-1}+T_{A-2}+t_1}$$
$$\times \sum_{S_{A-1}} \hat{I}_{A-1}\,\hat{S}_{A-1} \left\{ \begin{array}{ccc} J_{A-2} & s_1 & S_{A-1} \\ l_{A-1} & J_{A-1} & I_{A-1} \end{array} \right\}$$
$$\times\Big\langle \Big\{\big[l_{A-1}\ \big(s_1\ J_{A-2}\big)S_{A-1}\big]J_{A-1}\ (l_2\ s_2)I_2\Big\}J_A\ \ \big[\,\big(t_1\ T_{A-2}\big)\,T_{A-1}\ \ t_2\big]T_A\Big|$$
$$\Big|\Big\{\big[l_{12}\ (s_1\,s_2)\,s_{12}\big]J_{12}\ \big(\lambda\,J_{A-2}\big)\,I_\lambda\Big\}J_A\ \ \big[\,(t_1\,t_2)\,T_{12}\,T_{A-2}\big]T_A\Big\rangle$$

$$= (-1)^{3J_{A-2}+I_{A-1}+l_{A-1}+l_2+\lambda+s_{12}+s_1+s_2+T_{12}+t_1+t_2+2T_{A-2}}$$
$$\times\,\hat{J}_{A-1}\,\hat{I}_2\,\hat{J}_{12}\,\hat{I}_\lambda\,\hat{s}_{12}\,\hat{T}_{12}\,\hat{T}_{A-1}\,\hat{I}_{A-1}$$
$$\times \sum_{S_{A-1}} (-1)^{S_{A-1}}\,\hat{S}^2_{A-1} \left\{ \begin{array}{ccc} J_{A-2} & s_1 & S_{A-1} \\ l_{A-1} & J_{A-1} & I_{A-1} \end{array} \right\}$$
$$\times \sum_{LS} \hat{L}^2\,\hat{S}^2 \left\{ \begin{array}{ccc} s_2 & s_1 & s_{12} \\ J_{A-2} & S & S_{A-1} \end{array} \right\} \left\{ \begin{array}{ccc} t_2 & t_1 & T_{12} \\ T_{A-2} & T_A & T_{A-1} \end{array} \right\}$$
$$\times \left\{ \begin{array}{ccc} l_{A-1} & S_{A-1} & J_{A-1} \\ l_2 & s_2 & I_2 \\ L & S & J_A \end{array} \right\} \left\{ \begin{array}{ccc} l_{12} & s_{12} & J_{12} \\ \lambda & J_{A-2} & I_\lambda \\ L & S & J_A \end{array} \right\}$$
$$\times\,\langle n_{A-1}\,l_{A-1},\ n_2\,l_2\ :\ L\,|\,n_{12}\,l_{12}\,,\ n_\lambda\,\lambda\ :\ L\rangle_{d=\frac{A-2}{A}} \qquad (2.35)$$

Again we regard the completeness of these states with respect to each other which leads to the following orthogonality relations in addition to Eq. (2.5):

$$\sum_{\beta^\star_{AN}} \langle\, \tilde\beta^{(2)\prime}_{AN} \,|\, \beta^\star_{AN} \,\rangle\langle\, \beta^\star_{AN} \,|\, \tilde\beta^{(2)}_{AN} \,\rangle \;=\; \delta_{\tilde\beta^{(2)\prime}_{AN}\tilde\beta^{(2)}_{AN}} \tag{2.36}$$

$$\sum_{\tilde\beta^{(2)}_{AN}} \langle\, \beta'_{AN} \,|\, \tilde\beta^{(2)}_{AN} \rangle\langle\, \tilde\beta^{(2)}_{AN} \,|\, \beta_{AN} \,\rangle \;=\; \delta_{\beta'_{AN}\beta_{AN}} \tag{2.37}$$

$$\sum_{\tilde\beta^{(2)}_{AN}} \langle\, \gamma'_{AN} \,|\, \tilde\beta^{(2)}_{AN} \rangle\langle\, \tilde\beta^{(2)}_{AN} \,|\, \gamma_{AN} \,\rangle \;=\; \delta_{\gamma'_{AN}\gamma_{AN}} \tag{2.38}$$

Furthermore, Eq. (2.36) also yields $\delta_{\beta^{\star\prime}_{AN}\beta^\star_{AN}}$ if the 2N-subsystem of $|\,\tilde\beta^{(2)}_{AN}\rangle$ is not restricted to antisymmetric states but covers the full two-nucleon space:

$$\sum_{\tilde\beta^{(2)}_{AN}} \langle\, \beta^{\star\prime}_{AN} \,|\, \tilde\beta^{(2)}_{AN} \,\rangle\langle\, \tilde\beta^{(2)}_{AN}| \,\beta^\star_{AN} \,\rangle \;=\; \delta_{\beta^{\star\prime}_{AN}\beta^\star_{AN}} \tag{2.39}$$

With the $\langle\, \gamma_{AN} \,|\, \tilde\beta^{(2)}_{AN} \,\rangle$-coefficients the two-nucleon contribution to the binding energy takes a similar form as Eq. (2.30):

$$\begin{aligned}
&E_b^{(AN)}\, \langle\, \Gamma'_{AN} \,|\, \Psi \,\rangle \\
&= \sum_{\Gamma_{AN}} \langle\, \Gamma'_{AN} \,|\widehat{H}|\, \Gamma_{AN} \,\rangle\, \langle\, \Gamma_{AN} \,|\, \Psi \,\rangle \\
&= \bigcup_{\mathcal{N}'_A,\mathcal{N}_A} \binom{A}{2} \times \sum_{\gamma_{AN}} \sum_{\tilde\beta^{(2)\prime}_{AN}\tilde\beta^{(2)}_{AN}} \langle\, \gamma'_{AN}|\, \tilde\beta^{(2)\prime}_{AN} \rangle\langle \tilde\beta^{(2)\prime}_{AN} \,|\left(\frac{2}{A}\,\widehat{T}_{12} + \widehat{V}_{12}\right)|\, \tilde\beta^{(2)}_{AN}\rangle\langle \tilde\beta^{(2)}_{AN} \,|\gamma_{AN}\rangle\langle\gamma_{AN}|\Psi\rangle
\end{aligned} \tag{2.40}$$

This formalism provides a straight forward extension to the inclusion of few-N forces: performing an appropriate coordinate transformation i-nucleon subsystems can be separated from A-nucleon states such that they are coupled to an antisymmetric $(A-i)$-nucleon state as spectator. The orthogonality relation (2.38) holds for all $\langle\, \tilde\beta^{(i)}_{AN}|\, \gamma_{AN} \,\rangle$. Accordingly, for nuclei with $A > 4$ the construction of $\tilde\beta^{(3)}_{AN}$–states, where $|\,\gamma_{3N}\rangle$ couple to $|\,\gamma_{(A-3)N}\rangle$, includes 3NF in a convenient way. The projections onto $|\,\gamma_{AN}\,\rangle$ require a sum over three intermediate states:

$$\begin{aligned}
\langle\gamma_{AN}\,|\tilde\beta^{(3)}_{AN}\rangle \;&=\; \sum_{\tilde\beta^{(2)}\,\beta^{(2)\star}\,\hat\beta^{(2)}} \langle\gamma|\tilde\beta^{(2)}\rangle\langle\, \tilde\beta^{(2)}|\, \beta^{(2)\star}\rangle\langle\beta^{(2)\star}|\hat{\beta^{(2)}}\rangle\langle\hat{\beta^{(2)}}|\tilde{\beta^{(3)}}\rangle \\
&=\; \langle\bullet|\!-\!\bullet\rangle\langle\bullet\!-\!\bullet\,|\,\bullet\!-\!\bullet\rangle\langle\bullet\!-\!\bullet\,|\,\bullet\!-\!\bullet\rangle\langle\bullet\!-\!\bullet\,|\,\bullet\!-\!\bullet\rangle\,.
\end{aligned} \tag{2.41}$$

Their derivation is outlined in App. B.

Chapter 3

Implementation

As discussed in the previous chapter the antisymmetrisation of basis states and the calculation of binding energies represent eigenvalue problems, the former of the matrix $\mathcal{M}_{\beta'\beta} = \langle\, \beta'_{AN} | \widehat{\mathcal{A}} |\, \beta_{AN} \rangle$ with the dimension $\beta_{max} \times \beta_{max}$, the latter of $\mathcal{M}_{\Gamma'\Gamma} = \langle\, \Gamma'_{AN} | \widehat{H} |\, \Gamma_{AN} \rangle$ with the dimension $\Gamma_{max} \times \Gamma_{max}$. Considering NN forces only, the calculation of both matrices require a double sum, for $\mathcal{M}_{\beta'\beta}$ over $\beta^{\star\prime}_{AN}$ and $\beta^{\star}_{AN}$, and for $\mathcal{M}_{\Gamma'\Gamma}$ over $\tilde{\beta}^{(2)\prime}_{AN}$ and $\tilde{\beta}^{(2)}_{AN}$. All numbers increase considerably with A and $\mathcal{N}_A$. Since not only the number of β–states exceeds the number of γ–states approximately by a factor of A, but also the number of $\beta^\star$–states is approximately twice as large as the number of $\tilde{\beta}^{(2)}$–states, the antisymmetrisation is the most memory consuming part of the formalism, apart from the 3NF coefficients $\langle\, \tilde{\beta}^{(2)}_{AN} \,|\, \gamma_{AN} \,\rangle$. Furthermore, the number of $\beta^\star$–states even exceeds the number of β–states approximately by a factor of $(A-1)$. From Eq. (2.22) this becomes evident since the projection $\langle\, \beta^{\star}_{AN} \,|\, \beta_{AN} \,\rangle$ is the overlap $\langle\, \beta \,|\, \gamma \,\rangle$ of the $(A-1)$-nucleon system times a δ-function for the spectator nucleon and since there are $(A-1)$-times more β– than γ–states in the $(A-1)$-nucleon system. Though the antisymmetriation can be done ($\mathcal{N}_A$, J_A, T_A)-blockwise, this results in data that requests memory capacity of the order of several GB. Therefore, the storage of the data as well as the evaluation of eigenvalues and eigenvectors needs to be parallelised in a highly efficient way. Tables 3.1 and 3.2 show examples for the increase of β_{max} with A, $\mathcal{N}_A$ and J_A, and for the relation of the numbers of γ-, β- and $\beta^\star$–states, respectively.

To achieve an efficient parallelisation we use several libraries for the calculations: For the matrix eigenvalue equations we employ the routines of the library ScaLAPACK (Scalable Linear Algebra Package) that are fairly well parallelised and sufficient for our purposes. They work on completely distributed matrices which is essential for an efficient use of the available memory. Therefore, a similarly efficient calculation of the matrix elements is challenged. We found that compromises have to be made here between an efficient use of memory and a reduction of communication time. For the communication we choose the library

$\mathcal{N}_A$	$A = 4$ $J_4 = 4$, $T_4 = 1$	$A = 5$ $J_5 = 7/2$, $T_5 = 1/2$	$A = 6$ $J_6 = 3$, $T_6 = 1$	$A = 7$ $J_7 = 1/2$, $T_7 = 1/2$
5	250	831	1519	987
6	571	2231	4856	3340
7	1139	5258	13499	9957
8	2065	11248	33756	26954
9	3485	22309		
10	5565	41610		

J_A	$A = 4$ $\mathcal{N}_4 = 10$, T = 1	J_A	$A = 5$ $\mathcal{N}_5 = 10$, T = 1/2	J_A	$A = 6$ $\mathcal{N}_6 = 8$, T = 1
2	4812	3/2	31532	1	23411
3	5553	5/2	39756	2	32218
4	5565	7/2	41610	3	33756
5	5001	9/2	38074	4	29303
6	4073	11/2	31021	5	21615

Table 3.1: Increase of β_{max} with $\mathcal{N}_A$ for the largest blocks (upper table) and with J_A (lower table) for several A.

	$A=4$ J=3, T=1			$A=5$ J=7/2, T=1/2			$A=6$ J=3, T=1		
$\mathcal{N}_A$	γ_{max}	β_{max}	$\beta^{\star}_{max}$	γ_{max}	β_{max}	$\beta^{\star}_{max}$	γ_{max}	β_{max}	$\beta^{\star}_{max}$
2	3	12	39						
3	13	52	162	11	61	264	8	74	481
4	37	151	463	48	258	1084	49	391	2294
5	88	353	1073	159	831	3431	217	1519	8473
6	178	715	2165	433	2231	9117	718	4856	26277

Table 3.2: Examples for the relation $\beta^{\star}_{max} \approx (A-1)\times\beta_{max} \approx (A-1)\times A\times\gamma_{max}$.

MPI (Message Passing Interface). Both ScaLAPACK and MPI provide the possibility to build groups of processes that can exchange data in a way that is independent of each other. This enables us to define a practical compromise of data distribution and reduction of communication time. In MPI language, these groups are called communicator. Since we use a two-dimensional arrangement of processes, the communicator can usually also be chosen as two-dimensional. For a descriptive illustration of the parallelisation we will therefore denote these two dimensions of the communicator by '*row*' and '*col*' so that the number of processes is $\mathrm{npe} = \mathrm{npe}_{row} \cdot \mathrm{npe}_{col}$.
The definition of the antisymmetrised states is given by the weights of β–states in a fully antisymmetrised γ–state. These coefficients form large datasets that need to be written to disk machine-independently. Since the data is generated in a distributed way, parallel input/output (I/O) will be required. Apart from saving such data, an efficient reading is required, since the coefficients of the $(A-1)$-nucleon system need to be retrieved for the evaluation of antisymmetrised A-nucleon states. This task can be performed by the parallel I/O library HDF5. HDF5 enables us to write distributed data globally to disk and generates machine independent files. With this all coefficients that are generated once can also be read in in every desired distribution with HDF5 which helps to save memory capacity for each run.
The following section will be devoted to the considerations of these aspects. For readability we omit the subscript AN throughout this chapter and label only the $(A-1)$-nucleon system.

3.1 Parallelisation scheme

We illustrate the parallelisation of double sums with the example of $\mathcal{M}_{\beta'\beta}$. The two-dimensional communicator is used to distribute two of the involved indices. Here, notations like $\beta^{\star}_{col}$ and $\beta^{\star\prime}_{row}$ imply that $\beta^{\star}$ is distributed over *col*–processes and $\beta^{\star\prime}$ over *row*–processes. The sums are separated into two steps :

$$\mathcal{M}'_{\beta'\beta^{\star\prime}_{row}} = \sum_{\beta^{\star}_{col}} \langle\, \beta' \,|\, \beta^{\star}_{col} \,\rangle \langle\, \beta^{\star}_{col} \,|\widehat{\mathcal{P}}_{bc}|\, \beta^{\star\prime}_{row} \,\rangle \tag{3.1}$$

With this the matrix $\langle\, \beta^{\star} \,|\widehat{\mathcal{P}}_{bc}|\, \beta^{\star\prime} \,\rangle$ (calculated from Eq. (2.25)) with the largest dimension is most widely distributed in both indices and the sum is performed locally followed by one communication over *col*, corresponding to a MPI REDUCE operation. The intermediate result $\mathcal{M}'_{\beta'\beta^{\star\prime}_{row}}$ is not distributed in its first index in order to minimise the communication for this step but distributed in its second index. This choice is advisable since $\beta^{\star}_{max}$ is $(A-1)$-times larger than β_{max}. Consequently we need to keep both distributions of the $\beta^{\star}$-coefficientsThe projection $\langle\, \beta' \,|\, \beta^{\star} \,\rangle$ contains the overlap $\langle\, \gamma \,|\, \beta \,\rangle$ of the $(A-1)$-nucleon system. Though $\mathcal{N}$, J and T are conserved for the A-nucleon system, this does not constrain these

quantum numbers of the $(A-1)$-nucleon system. Therefore, all blocks of the $(A-1)$-nucleon system need to be known for the antisymmetrisation which illustrates again the large quantity of data, even though the overlaps are distributed in one index over *col*-processes, $\langle\, \gamma \,|\, \beta_{col} \,\rangle$, to match $\langle\, \beta' \,|\, \beta^{\star}_{col} \,\rangle$ of the sum.

The second step is

$$\mathcal{M}''_{\beta' \beta_{col}} = \sum_{\beta^{\star\prime}_{row}} \mathcal{M}'_{\beta' \beta^{\star\prime}_{row}} \langle\, \beta^{\star\prime}_{row} \,|\, \beta_{col} \,\rangle \,. \tag{3.2}$$

Again, the projection $\langle\, \beta^{\star} \,|\, \beta \,\rangle$, i.e. the overlap $\langle\, \beta \,|\, \gamma \,\rangle$ of the $(A-1)$-nucleon system, needs to be known as input. Here, this overlap is distributed as $\langle\, \beta_{row} \,|\, \gamma \,\rangle$ to match the distribution of $\beta^{\star\prime}_{row}$ of the sum; the second index remains undistributed to minimise the communication as in the first step. Then the sum can again be performed locally and the result is obtained using a MPI REDUCE step over row. As the second index of $\mathcal{M}''_{\beta' \beta_{col}}$ is already distributed over *col*, each of the npe_{row} picks out its local β'_{row} from $\mathcal{M}''_{\beta' \beta_{col}}$ for the final result $\mathcal{M}_{\beta'_{row} \beta_{col}}$. The routines of ScaLAPACK diagonalise $\mathcal{M}_{\beta'_{row} \beta_{col}}$ and give back the eigenvalues 0 or 1 and their corresponding eigenvectors which solves the matrix eigenvalue equation Eq. (2.4).
With similar considerations we split the double sums of $\mathcal{M}_{\Gamma'\Gamma}$ (Eq. (2.40)) and of Eq. (2.31) to evaluate the projection $\langle\, \gamma \,|\, \tilde{\beta}^{(2)} \,\rangle$. $\tilde{\beta}^{(2)}_{max}$ differs from $\beta^{\star}_{max}$ by a factor of 1/2 due to the additional antisymmetry in the 2N-subsystem, still it exceeds β_{max} by $(A-1)/2$. Therefore the overlap $\langle \beta^{\star} \,|\, \tilde{\beta}^{(2)} \rangle$ needs to be distributed in both directions. Even more careful considerations are necessary for the parallelisation of the triple sum for the projection $\langle\, \gamma \,|\, \tilde{\beta}^{(3)} \,\rangle$ (App. B). With the orthogonality relations, Eqs. (2.5), (2.36)- (2.39) , we are able to verify the completeness and the antisymmetry of the respective states.
Now HDF5 enables us to store these A-nucleon bookkeepings in a convenient way that takes account for the $(\mathcal{N}, J, T)$-block structure of our formalism by subdividing the data into groups. Each group may contain several datasets. As an example, for the antisymmetrisation these are the β- and γ-bookkeepings, i.e. the number of β–states β_{max} and the quantum numbers n, l, I, $\left(\mathcal{N}_{A-1}, J_{A-1}, T_{A-1}\right) \gamma_{(A-1)\mathrm{N}}$ for each β, the number of γ–states γ_{max} and the overlaps $\langle\, \beta \,|\, \gamma \,\rangle$ (Eq. (2.25)), while the γ–states are uniquely defined by the quantum numbers of their $(\mathcal{N}, J, T)$-block and a counting index. The parity of the states is determined by $\mathcal{N}$. From these files, the relevant information on the A-nucleon system can be read in when proceeding to $A+1$ in both required distributions. Going to higher model spaces already existing groups, i.e. $(\mathcal{N}, J, T)$-blocks, can be skipped, and new groups are simply appended to the database. Thus bookkeepings can be extended block by block for each A.

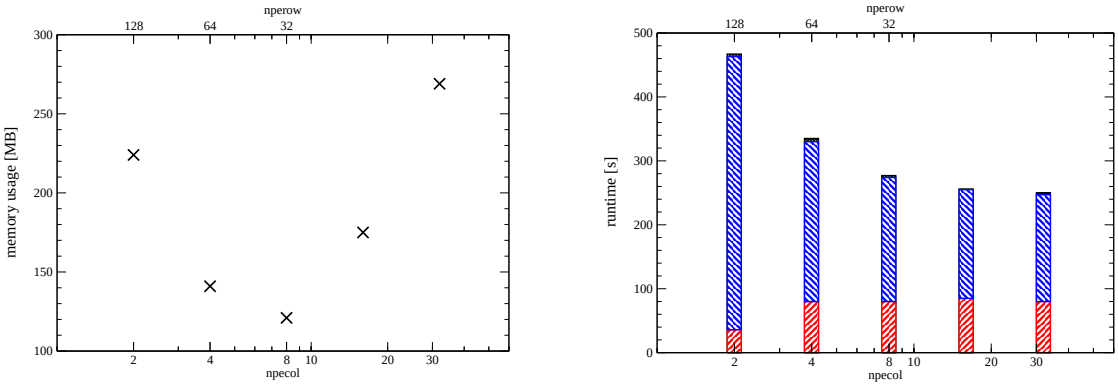

Figure 3.1: Memory usage (left) for several distributions of $\text{npe}_{row} \times \text{npe}_{col}$ for calculations on 128 nodes x 2 tasks/node = 256 tasks and their runtime behaviour (right). The total runtime is composed of the runtime for reading existing bookkeepings with HDF5 (I/O–time, red)and the runtime for the evaluation of the antisymmetrisation matrix and its solution with ScaLAPACK (γ–book time, blue).

3.2 Performance and scaling

The calculations were performed on JUQUEEN (Jülich Blue Gene/Q) with a memory capacity of 16 GB per node and 16 cores per node.
To test the parallelisation we analyse the efficiency for the antisymmetrisation of 6N states regarding the memory usage and the runtime. In the model space of $\mathcal{N} = 6$, the dimensions of the largest ($\mathcal{N}$, J, T)-block are $\gamma_{max} = 133$, $\beta_{max} = 901$ and $\beta^{\star}_{max} = 4691$. The memory usage, which is the most limiting aspect for this formalism, depends on the number and the distribution of the parallel processes, and in particular on the partition of the communicators *row* and *col*. As shown in the left diagram of Fig 3.1 a choice of 4 times as many *row*-distributed as *col*-distributed processes, $\text{npe}_{row} = 4\times\ \text{npe}_{col}$, optimises the memory usage and the runtime (Fig 3.1, right diagram). This factor originates from the above described evaluation of $\mathcal{M}_{\beta'\beta}$ (Eq.s (3.1) and (3.2)): the dimension of $\mathcal{M}'$, which is $\beta_{max} \times \beta^{\star}_{max}$, outnumbers the dimension of $\mathcal{M}''$ ($\beta_{max} \times \beta_{max}$) approximately by a factor of $(A-1)$, therefore an $(A-1)$-times higher parallelisation in the *row*-direction is necessary to get a balanced memory usage.
The dependence of the memory usage and the runtime on the number of tasks is illustrated in Fig. 3.2. Since we distribute in the two directions *row* and *col*, we need to multiply the number of tasks by a factor of 4, i.e. a factor of 2 for each direction simultaneously, to divide the memory usage by a factor of 2 (upper left diagram). In this sense, we observe a good memory scaling up to npe = 64, larger partitions are unfavourable due to the rather small dimension of this example.
Similarly, the runtime scaling is acceptable though not ideal up to npe = 64 (up-

per right diagram): the total I/O-time does not decrease, however, its percentage of the total runtime is considerably smaller than that of the time to evaluate and solve the matrix $\mathcal{M}_{\beta'_{row}\beta_{col}}$, called γ–book time in the following, so that this effect is less significant. The γ–book time decreases measurably (though not about a factor of 4 but approximately a factor of 3).
We also examined the behaviour of this test calculation with npe = 1024 and npe = 4096 where we observe an enormous increase of the I/O-time for the HDF5 routines. This turns out to be a serious problem for large dimensions where the I/O-time dominates the total runtime by far. For this reason we prefer small numbers of tasks for the further calculations and ensure the required memory capacity by choosing the number of tasks per node accordingly. Though a small number of tasks increases the scalapack/gammabook-time this was more efficient at this point. Further studies on the parallel I/O are in progress.
From the third diagram of Fig. 3.2 we deduce that, fortunately, the number of tasks per node has no significant influence on the runtime. Therefore, we are able to choose the number of tasks per node according to the required memory per task, which will be the full capacity (16 GB/task $\widehat{=}$ 1 task/node) for very large dimensions.
So far, the largest production run was performed on 16384 tasks to calculate $\gamma_{max} = 8239$ basis states in terms of $\beta_{max} = 41610$ for $A = 5$, $\mathcal{N} = 10$, $J = 7/2$ and $T = 1/2$ with a runtime of 24 minutes. It will be interesting if further improvement of the performance will be possible once the parallel I/O has been better analysed.

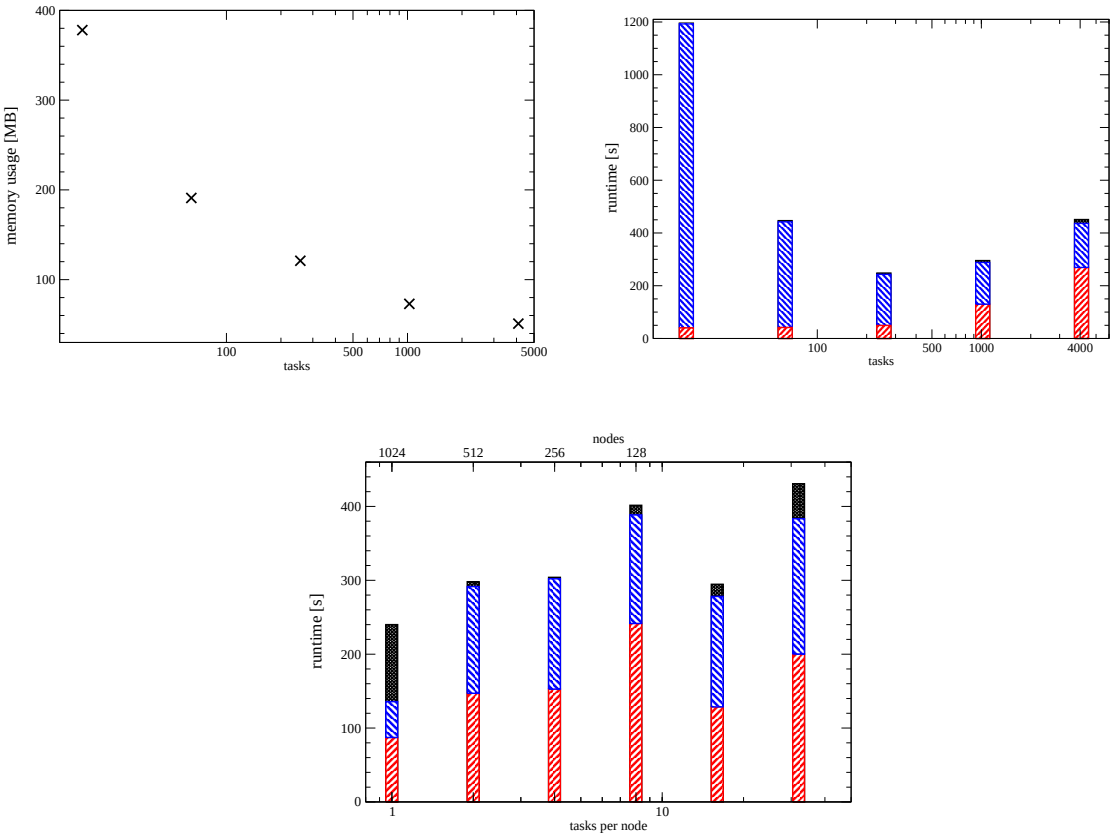

Figure 3.2: Upper diagrams: Memory usage and runtime dependent on the number of tasks ($\text{npe}_{row} \times \text{npe}_{col} = 8 \times 2$, 16×4, 32×8, 64×16, and 128×32, respectively; tasks per node = 4). Lower diagram: Runtime behaviour of calculations with 1024 tasks and 1, 2, 4 and 8 tasks per node, $\text{npe}_{row} \times \text{npe}_{col} = 64 \times 16$. Color code as described in Fig. 3.1

3.3 NN contribution to the binding energy

Considering NN forces, the matrix eigenvalue equation for the solution of the Schrödinger equation, Eq. (2.40), can be solved in a convenient way employing the above described $\tilde{\beta}^{(2)}$-bookkeeping due to the separation of antisymmetric 2N–states.
The matrix elements of the kinetic energy simplifies working in momentum space and in natural units, derived explicitly in App. A.1. With Eq. (A.9) the following standard expression holds:

$$\begin{aligned}\langle \tilde{\beta}^{(2)\prime} \,|\, \widehat{T}_{12} \,|\, \tilde{\beta}^{(2)} \rangle &= \delta_{\Gamma'_{(A-2)\mathrm{N}}\Gamma_{(A-2)\mathrm{N}}} \times \tfrac{1}{2}\,\omega\,\delta_{l'_{12}l_{12}} \\ &\quad \times \Big(-\delta_{n'_{12},(n_{12}+1)} \sqrt{(n_{12}+1)\,(n_{12}+l_{12}+3/2)} \\ &\qquad + \delta_{n'_{12},n_{12}}\,(2n_{12}+l_{12}+3/2) \\ &\qquad - \delta_{n'_{12},(n_{12}-1)} \sqrt{(n_{12}+1)\,(n_{12}+l_{12}+1/2)}\,\Big)\end{aligned} \tag{3.3}$$

This is, for the first time, ω dependent.
The matrix elements of the potential,

$$\begin{aligned}\langle \tilde{\beta}^{(2)\prime} \,|\, \widehat{V}_{\mathrm{NN}} \,|\, \tilde{\beta}^{(2)} \rangle &= \delta_{\Gamma'_{(A-2)\mathrm{N}}\Gamma_{(A-2)\mathrm{N}}} \times (-1)^{n'_{12}+n_{12}+\left(l'_{12}-l_{12}\right)/2}\; b_{12}^3 \\ &\quad \times \int dp'_{12}\; {p'_{12}}^2\; \hat{R}_{n'_{12}\,l'_{12}}(\tilde{p}'_{12}) \int dp_{12}\; p_{12}^2\; \hat{R}_{n_{12}\,l_{12}}(\tilde{p}_{12})\;\; V_{\mathrm{NN}}\,(\vec{p}\,'_{12},\vec{p}_{12})\;,\end{aligned} \tag{3.4}$$

contains the dimensionless radial HO wave functions $R_{n_{12}\,l_{12}}(\tilde{p}_{12})$ as defined in Eq. (A.6). The symmetric, charge-independent NN potential consists of three different charge-dependent components $V_{\mathrm{NN}}^{T\,m_T}$, according to the three different pairs of nucleons nn, pp ($T = 1$,$m_T = -1$ and $m_T = 1$, respectively) and np ($T = 0$). To account for their individual contribution, we consider the coefficients $c_{T\,m_T}$ from [86] to sum up these charge-dependent potentials:

$$V_{\mathrm{NN}} = \sum_{m_T} c_{T\,m_T} V_{\mathrm{NN}}^{T\,m_T}\;,$$

$$c_{00} = 1$$

$$c_{1\,1} = \frac{4Z\,(Z-1)}{3A\,(A-2)+4T\,(T+1)}$$

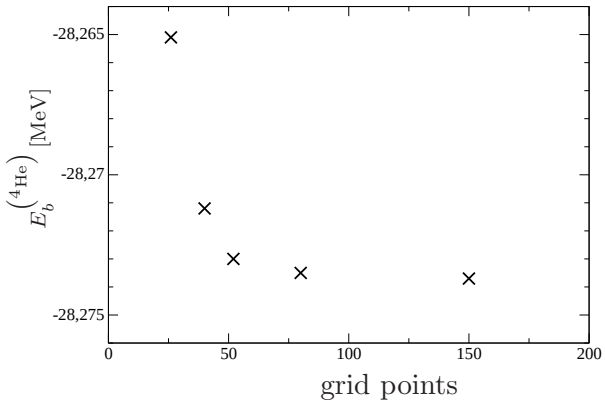

Figure 3.3: Convergence with the number of grid points for the potential V_{SRG}.

$$
\begin{aligned}
c_{1\,0} &= \frac{8NZ - A\,(A-1) + 4T\,(T+1)}{3A\,(A-2) + 4T\,(T+1)} \\
c_{1\,-1} &= \frac{4N\,(N-1)}{3A\,(A-2) + 4T\,(T+1)} \\
&\text{with normalisation } \sum_{m_T} c_{T\,m_T} = 1\,,
\end{aligned}
\tag{3.5}
$$

where N denotes the number of neutrons and Z the number of protons. Furthermore, we restrict the evaluation of Eq. (3.4) to $J_{\mathrm{NN}} = 6$ since we estimate that only the corresponding partial waves are relevant, and optimise the integration by interpolating the potential using cubic hermitean splines of App.B of [87] which reduces the number of actual evaluations of the potential.
Throughout this work, we employ the NN-only V_{SRG} evolved from the 500 MeV N^{3}LO NN potential from Ref. [26] including the electromagnetic interaction with different cutoffs λ for our calculations. Further input parameters are the nucleon mass $m_{\mathrm{N}} = 938.92$ MeV and $\hbar c = 197.33$ MeV·fm. Test calculations with $\lambda = 1.5$ fm^{-1} showed that the binding energy of ^{4}He is converged up to 1 keV for a number of 120 grid points for the potential matrix and 200 interpolation points for momenta p'_{12} and p_{12} from 0 fm^{-1} to 4 fm^{-1}. The runtime is not affected significantly by an increase of these grid points since they parameterise simple sums that can be well parallelised with respect to p'_{12} and p_{12}, whereas the number of internal grid points for the V_{SRG} evolution needs to be regarded more carefully. Fig. 3.3 shows the convergence of the binding energy of ^{4}He with this number. Since we observe an immense increase of the runtime for a larger number of grid

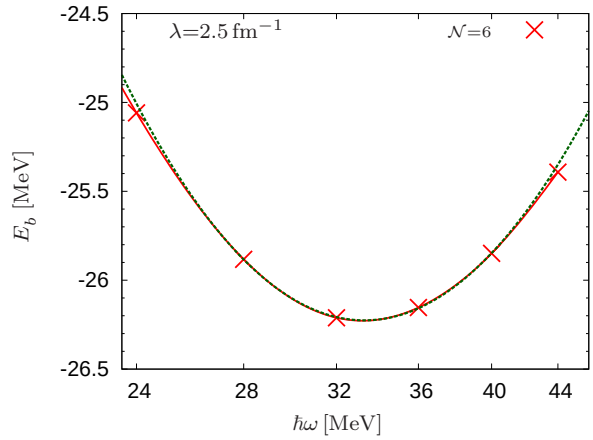

Figure 3.4: Example of the ω-dependence of the ^{4}He binding energy; $\lambda = 2.5$ fm^{-1} and $\mathcal{N} = 6$. The red crosses depict the results of the calculations, the dashed green line illustrates the fit to $E_b(\omega)$. The solid red line is generated using cubic splines to guide the eye.

points a minimum choice is important. Here we decided on 52 grid points due to the convergence of the binding energy up to 1 keV likewise. With this we are able to solve the eigenwert problem for the Schrödinger equation, Eq.(2.40).
First investigations of the convergence of the binding energy of ^{4}He with $\mathcal{N} =$ 4, 6, 8 and 10 are illustrated in Fig. 3.5. Since the oscillator length b depends on ω (Eq. (2.11)) there is an ω_{opt} for which the ^{4}He wave function is optimal parameterised by the HO wave functions in the given model space. Consequently, calculations with ω_{opt} give the lowest results of E_b for each $\mathcal{N}$, $E_{\omega\mathcal{N}}$. To find this value we apply the following technique, exemplified for $\lambda = 2.5$ fm^{-1} in the model space of $\mathcal{N} = 6$ in Fig. 3.4: To approximate $E_b(\omega)$ we choose a logarithmic scale for $\hbar\omega$ and fit a polynomial of second degree around the minimum of the curve, denoted by the dashed line, with the following ansatz:

$$E_b(\omega) = E_{\omega\mathcal{N}} + \kappa \left(log(\omega) - log\left(\omega_{opt}\right)\right)^2 . \tag{3.6}$$

A Taylor expansion around the minimum gives a measure for the variation of $E_{\omega\mathcal{N}}$, $\Delta E_{\omega\mathcal{N}}$, if ω_{opt} is changed by a small variation $\Delta\omega$ around this minimum:

$$\Delta E_{\omega\mathcal{N}} = \frac{\kappa}{\omega_{opt}^2} (\Delta\omega)^2 , \tag{3.7}$$

which is indicated by the error bars. For a realistic measure of uncertainty it turned out that $\hbar(\Delta\omega) = 2$ MeV is a reasonable choice.
We assume this ansatz for all examined nuclei and refer to the subsequent chapter for a more detailed discussion of the ω-dependence of the binding energies.
The test calculations of the ^{4}He binding energy with $\lambda = 1.5$ fm^{-1} are converged

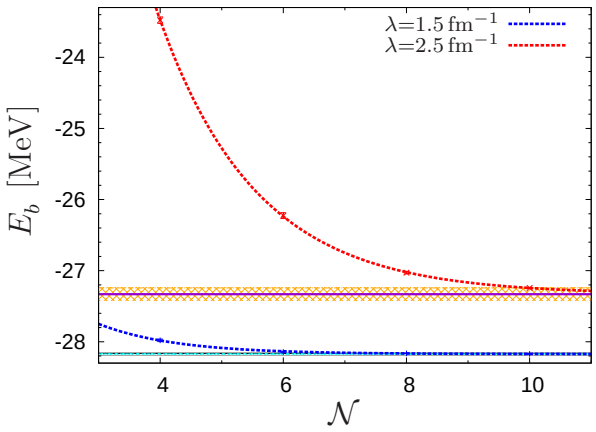

Figure 3.5: Example for the extrapolation of the ^{4}He binding energy. Values with error bars are the results of the calculations and their variation with ω, dashed lines the exponential curve fit (red: $\lambda = 2.5$ fm^{-1}, blue: $\lambda = 1.5$ fm^{-1}), and the solid lines denote the extrapolated value E_∞ (violet: $\lambda = 2.5$ fm^{-1}, black: $\lambda = 1.5$ fm^{-1}). The error estimates are depicted as bands around E_∞, for $\lambda = 1.5$ fm^{-1} hardly discernable (light blue line; $\lambda = 2.5$ fm^{-1}: orange band).

within 10 keV in the model space of $\mathcal{N} \geq 8$. For larger λ as well as for heavier nuclei, Bogner *et al.* motivate a method to extrapolate the ground-state energies with truncation at $\mathcal{N}$ to determine the parameter E_∞ with $\mathcal{N} = \infty$ in Ref. [68] based on the following ansatz:

$$E_{\omega\mathcal{N}} = E_\infty + A_\omega \, e^{-b_\omega \mathcal{N}} \,, \tag{3.8}$$

where A_ω and b_ω are constants to be determined from calculations in limited model spaces. For the curve fitting we assign different weights to each $E_{\omega\mathcal{N}}$ that depend on the slope between $E_{\omega\mathcal{N}}$ and $E_{\omega(\mathcal{N}+2)}$ in order to enhance the results of larger model spaces that are close to E_∞. This curve fitting is depicted as dashed lines in Fig. 3.5. For $A > 4$ we notice that curves of the smallest model space are considerably separated from those of larger model spaces which largely influences the extrapolation to E_∞. Therefore, the results from $\mathcal{N} = A - 4$ are not considered for the extrapolation.
Bogner *et al.* also suggested a method to determine a confidence interval for E_∞ by considering calculations with neighbouring values of $\hbar\omega$. Since this yields disproportional small error estimates, we prefer to estimate the deviation of E_∞ by the interval between the result of our largest model space and the extrapolated value which makes use of uncorrelated calculations to avoid an underestimation.

Chapter 4

Binding energies of selected nuclei

The aim of this thesis is to establish the new Jacobi coordinate based formulation of the NCSM. In this chapter, we show the feasibility of calculations within this scheme by means of the lighter nuclei ^{3}H, ^{4}He and ^{6}Li. Since complete calculations for ^{3}H and ^{4}He are available within the FY approach [88], the evaluation of the matrix elements for the nuclear potential can be tested appropriately with these systems. ^{6}Li is the first system where we can apply the formalism, in particular the method of extrapolating the converged values of the binding energy, in a non-trivial way. The dependence on the SRG–cutoff parameter λ can be studied for binding energies and, for the first time, also excitation energies.

4.1 The ^{3}H system

The first system we want to discuss is ^{3}H. It is the first bound state where all partial waves of the NN potential contribute. The results already show the characteristic dependence on ω and on $\mathcal{N}_3$ that we expect for larger systems. Due to the rather small dimensions, we are able to access very large model spaces such as $\mathcal{N}_3 = 18$, where the number of β– and γ– states are $\beta_{max} = 380$ and $\gamma_{max} = 127$, respectively, already with a standard desktop computer. Though larger model spaces can be obtained without difficulty they do not seem to be required for calculations involving low–momentum interactions.
With these first studies, we also inteded to get acquainted with the systematic extraction of binding energies for several ω and $\mathcal{N}_3$. Fig. 4.1 shows the results for different $\mathcal{N}_3$ dependent on $\hbar\omega$ on the left-hand side. As expected, the result for the smallest λ of the SRG interaction, $\lambda = 1.0$ fm^{-1}, is the best converged one. We observe a plateau for $\hbar\omega = 5 - 15$ MeV in the model space of $\mathcal{N}_3 = 18$ as expected for fully converged results. Based on Eqs. (3.6) and (3.7), we are able to extract the optimal value for ω and the corresponding binding energy for

λ [fm^{-1}]	NCSM	FY
1.0	-7.46 MeV	-7.460(2) MeV
1.2	-7.929 MeV	—
1.5	-8.264(1) MeV	-8.262(2) MeV
1.8	-8.334(2) MeV	—
2.0	-8.313(4) MeV	-8.309(2) MeV
2.2	-8.270(7) MeV	—
2.5	-8.185(12) MeV	-8.195(2) MeV
experiment	-8.481 MeV	

Table 4.1: Binding energy of ^{3}H calculated within NCSM and FY with error estimates.

each $\mathcal{N}_3$ systematically including an estimate of uncertainty. These results are shown on the right-hand side of Fig. 4.1 as blue symbols with error bars. Note the scale of this diagram which illustrates the extraordinarily small uncertainty for $\lambda = 1.0$ fm^{-1}. With this we extract the converged result according to Eq. (3.8), shown as the red line, with an accuracy estimate less than 1 keV. This agrees well with the FY result, indicated by the green band.
For larger cutoffs, the results converge more slowly, hence also the error bars are larger, illustrated in the lower diagrams of Fig. 4.1 and in Fig. 4.2.
Nevertheless, the so found binding energies are well converged and in agreement with FY for all cutoffs. In Tab. 4.1, our results are given in comparison to FY calculations for ^{3}H [88] explicitly.
Additionally, we note that the shifts of optimal ω is in line with naive expectations. The stronger the short-distance correlations, the larger λ, the larger is the optimal ω. At the same time, the optimal ω shifts to smaller values when increasing the model space. This is an interesting effect that we believe to be related to the long-distance behaviour of the ^{3}H wave function. The more compact ^{4}He does not show this effect. We discuss this system in the following section.

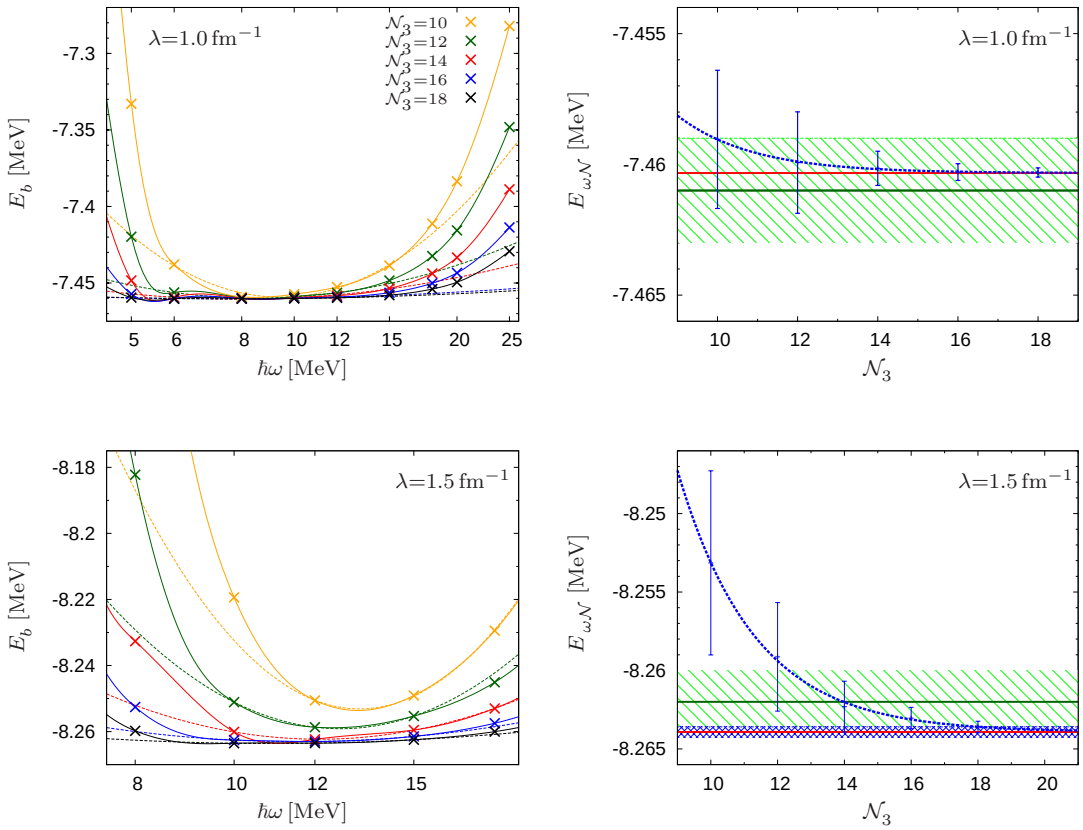

Figure 4.1: Binding energy of ^{3}H dependent on ω for several $\mathcal{N}_3$ (left diagrams) obtained using the V_{SRG} evolved from the 500 MeV N^{3}LO NN potential from Ref. [26] including the electromagnetic interaction (see Sec. 3.3); $\lambda = 1.0$ fm^{-1} and $\lambda = 1.5$ fm^{-1}, respectively. As in Fig. 3.4, the dashed lines illustrate the fit to $E_b(\omega)$ according to Eq. (3.6), the solid lines are generated using cubic splines. The right diagrams illustrate the dependence of E_b on $\mathcal{N}_3$ and the extrapolation to $\mathcal{N}_3 = \infty$, Eq. (3.8). The blue curve is the exponential curve fit, where the error bars give a relative measure of the variation with ω, the red line depicts the extrapolated value E_∞ and the blue band (if dinstinguishable) its error estimate. The dark green line is the FY result from [88] with error estimate (green band).

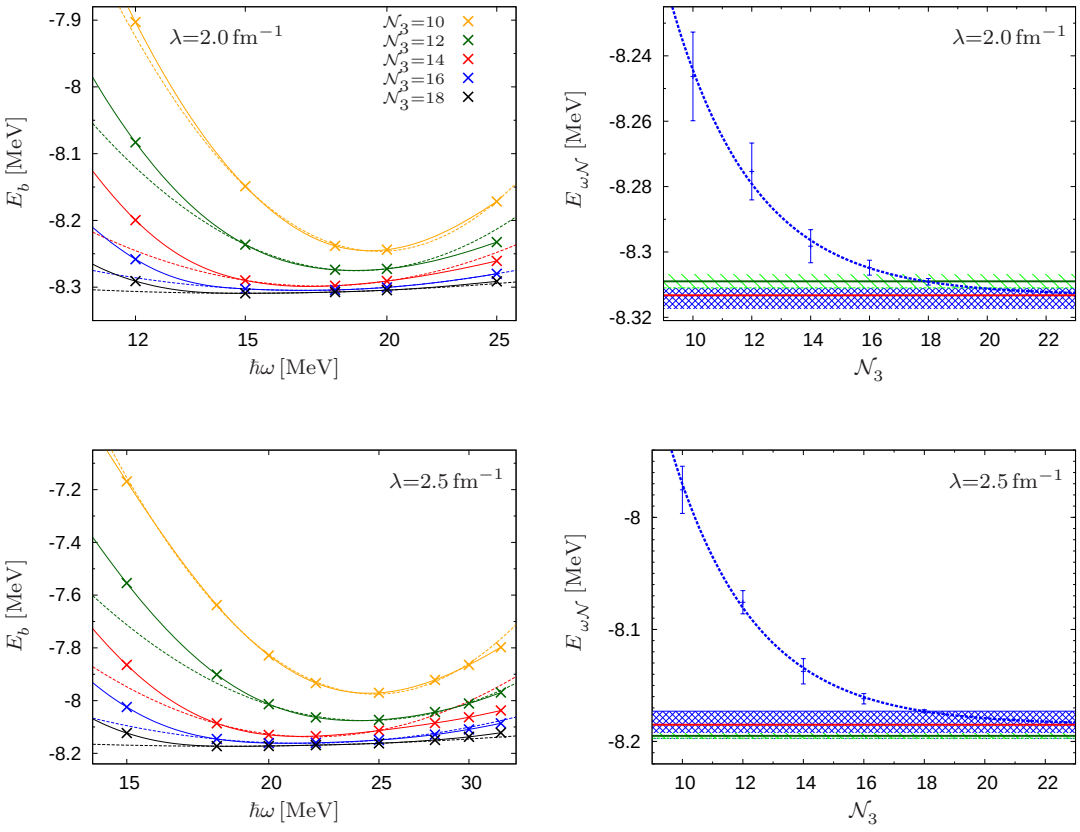

Figure 4.2: Binding energy of ^{3}H dependent on $\mathcal{N}_3$ and ω and the extrapolation to $\mathcal{N}_3 = \infty$; lines and symbols as described in Fig. 4.1.

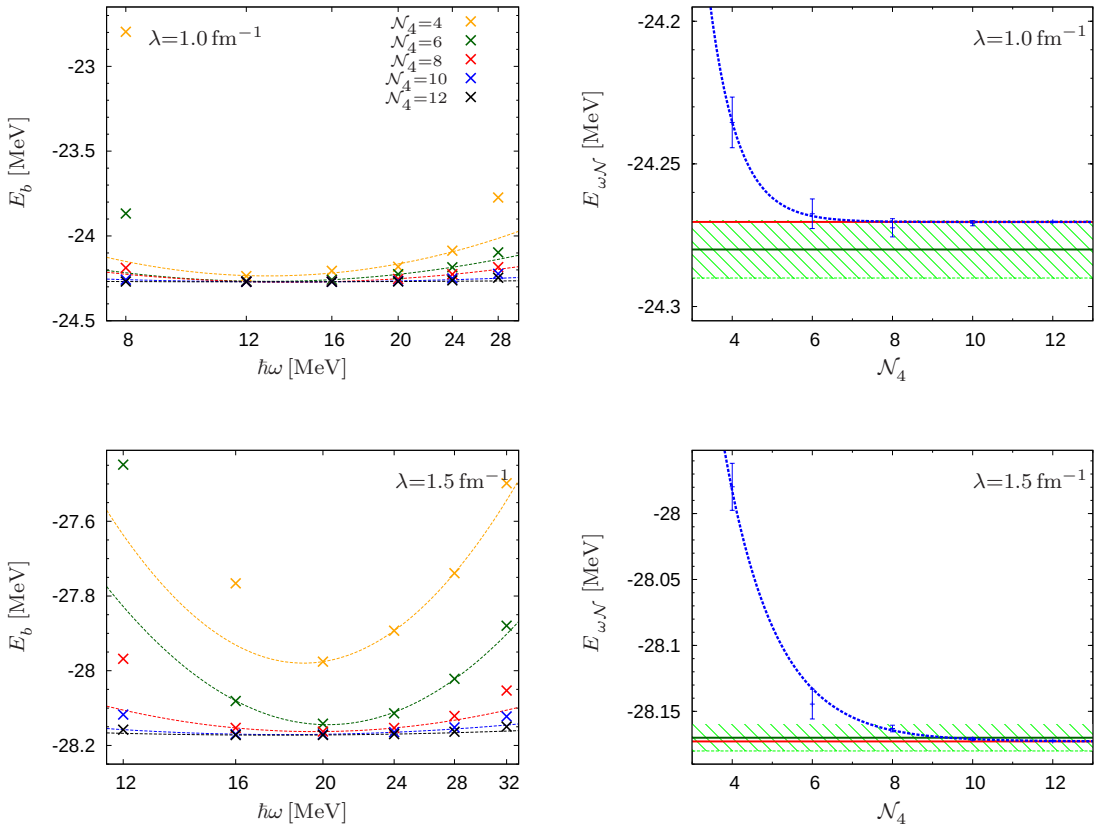

Figure 4.3: Binding energy of ^{4}He dependent on $\mathcal{N}_4$ and ω and the extrapolation to $\mathcal{N}_4 = \infty$; lines and symbols as described in Fig. 4.1.

4.2 The ^{4}He system

The ^{4}He is a different and even more simple test than ^{3}H in some aspects. As it is still an s–shell nucleus, it is dominated by $\mathcal{N}_4 = 0$ HO configurations but much more strongly bound and therefore compact. Proceeding as in the previous section, we extract converged values and error estimates that can be compared to FY [88]. The results are shown in Figs. 4.3 and 4.4.

We observe a much smoother dependence on ω than for ^{3}H. Correspondingly, convergence is achieved in much smaller model spaces which can be expected since the ^{4}He wave function drops off much faster and is therefore better parameterised by HO wave functions. This is also reflected by larger optimal ω. As mentioned in the previous section, no strong shifts of this value can be observed for increasing model spaces or cutoffs.

Here, we are also able to test the formulation of the $\tilde{\beta}^{(2)}$–states. In our largest model space of $\mathcal{N}_4 = 12$, the dimensions are $\gamma_{max} = 417$, $\beta_{max} = 1551$ and $\tilde{\beta}^{(2)}_{max} = 2380$.

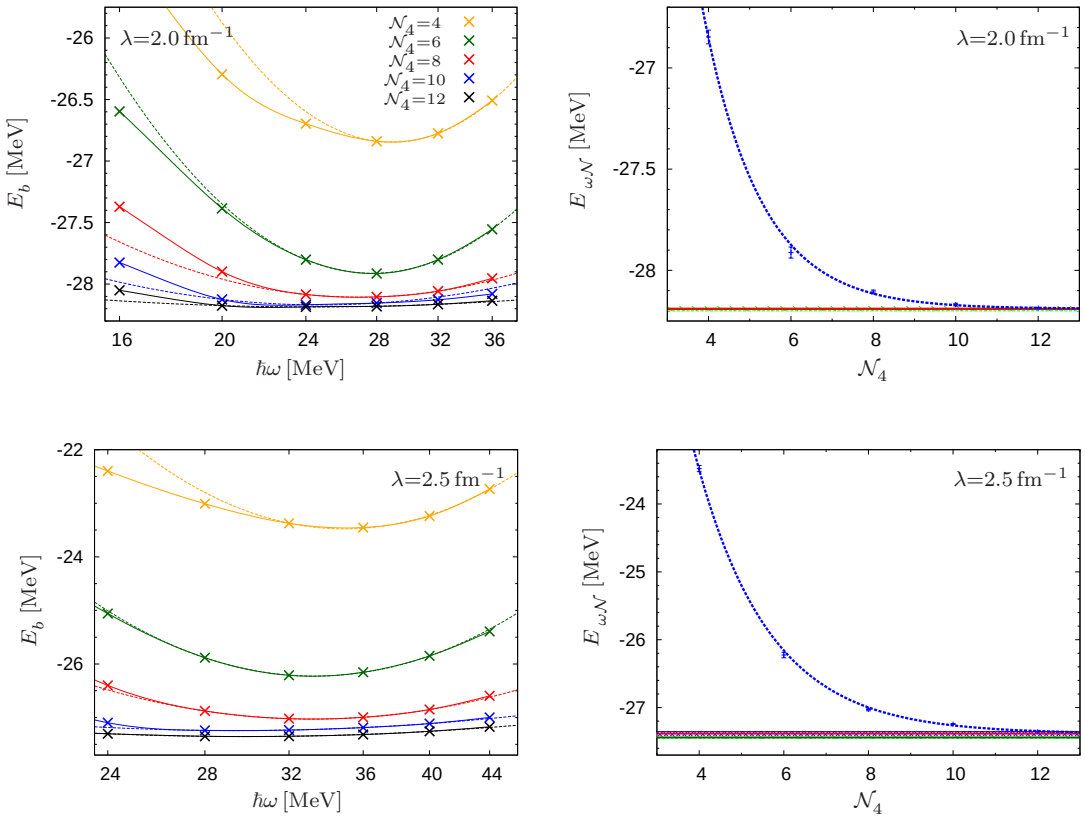

Figure 4.4: Binding energy of ^{4}He dependent on $\mathcal{N}_4$ and ω and the extrapolation to $\mathcal{N}_4 = \infty$; lines and symbols as described in Fig. 4.1.

λ [fm^{-1}]	NCSM	FY
1.0	-24.270 MeV	-24.28(1) MeV
1.2	-24.549 MeV	—
1.5	-28.173 MeV	-28.17(1) MeV
1.8	-28.396(1) MeV	—
2.0	-28.189(4) MeV	-28.19(1) MeV
2.2	-27.887(7) MeV	—
2.5	-27.384(29) MeV	-27.44(1) MeV
experiment	-28.3 MeV	

Table 4.2: Binding energy of ^{4}He calculated within NCSM and FY with error estimates. If the calculations of the NCSM are converged within 1 keV, no error estimate is specified.

The results for the extrapolated energies are in good agreement with the FY calculations, as can be seen from the right-hand sides of Figs. 4.3 and 4.4 and from Tab. 4.2.
Before turning to the more interesting p–shell nuclei, we want to emphasise that the basis states for $A = 3$ and $A = 4$ will finally be important for representing 3NF and 4NF for all HO based many-body methods including m–scheme NCSM and coupled cluster. Therefore, the results presented in this and the previous section confirm that these states can be well obtained even for large model spaces.

4.3 ^{6}Lithium

In this section, we examine the first example of a p–shell nucleus, the ^{6}Li system. These calculations are much more demanding since a large variety of antisymmetrised states for $A = 5$ needs to be available. At this point, these states have been generated up to $\mathcal{N}_5 = 10$, $J_5 = 25/2$ and $T_5 = 3/2$. Based on these, calculations for ^{6}Li in the model space of $\mathcal{N}_6 = 8$ have been accessible for $J_6 = 1$ and $J_6 = 3$ with $T_6 = 0$. We present the results for the ground state, $J^\pi\, T = 1^+\ 0$, first.

4.3.1 Ground state 1^+ 0

The binding energies are shown in Figs. 4.5- 4.7 for several ω and $\mathcal{N}_6$ for various SRG-cutoffs λ. The extraction of the optimal ω and the corresponding energies is again obtained according to Eq. (3.6). We also extrapolate converged results with Eq. (3.8) and assume that the uncertainty can be estimated by the interval between the result for our largest model space and the extrapolated value, as in the case of ^{4}He. Since the model spaces are naturally restricted more severely, this has been done based on $\mathcal{N}_6 = 4, 6$ and 8. Due to the sizeable uncertainties, larger model spaces are required, especially for cutoffs larger than 1.8 fm^{-1}, which will be available in near future. However, the pattern of convergence is very regular. Concerning the shifts of optimal ω, the values show a similar behaviour to those of ^{4}He. At least for $\lambda \leq 1.8$ fm^{-1}, they are rather insensitive to the size of the model spaces. For larger cutoffs, a quite surprising observation is that they tend to increase with $\mathcal{N}_6$ which is different to the ^{3}H case.

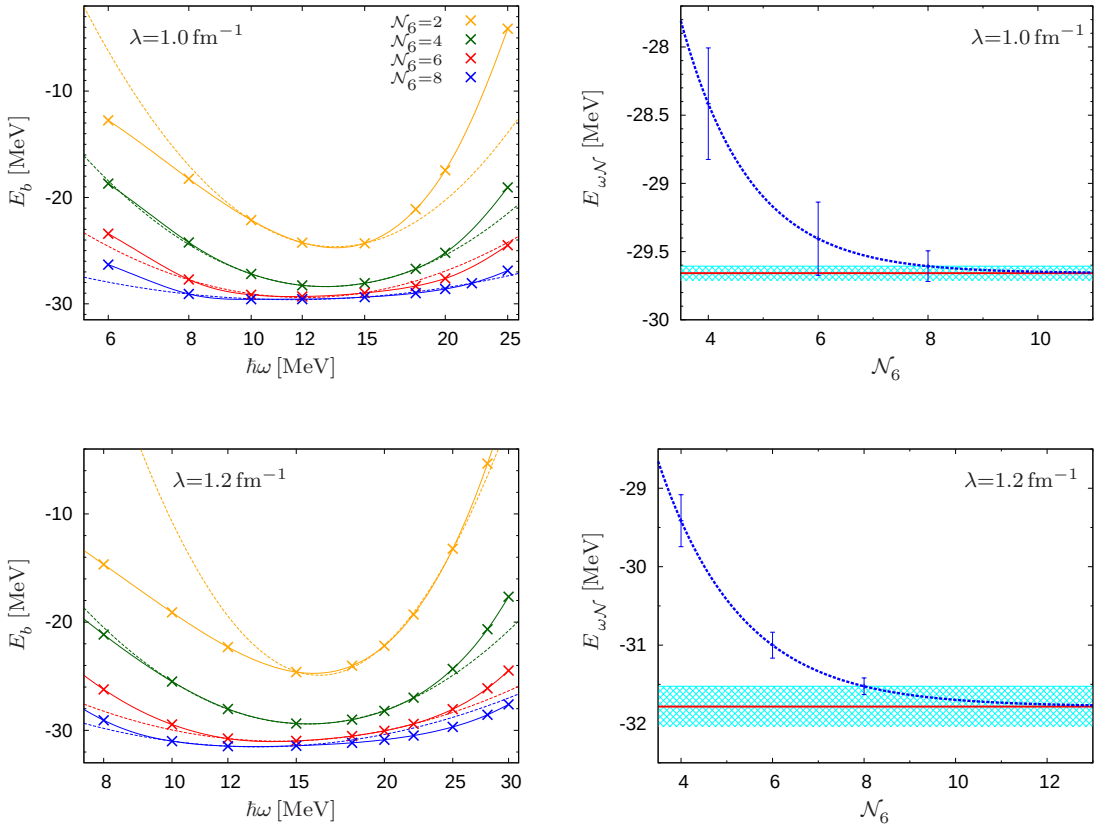

Figure 4.5: Binding energy of the ground state of ^{6}Li dependent on $\mathcal{N}_6$ and ω (left diagrams) and the extrapolation to $\mathcal{N}_6 = \infty$ (right diagrams), obtained using the V_{SRG} evolved from the 500 MeV N^{3}LO NN potential from Ref. [26] including the electromagnetic interaction (see Sec. 3.3) for $\lambda = 1.0$ fm^{-1} and $\lambda = 1.2$ fm^{-1}. Again, the dashed lines illustrate the fit to $E_b(\omega)$ according to Eq. (3.6), and the solid lines are generated using cubic splines. The blue curve shows the exponential curve fit to the results of the calculation, Eq. (3.8), depicted with the estimate of their ω variation (error bars), the red line shows the extrapolated value E_∞ and its error estimate (blue band).

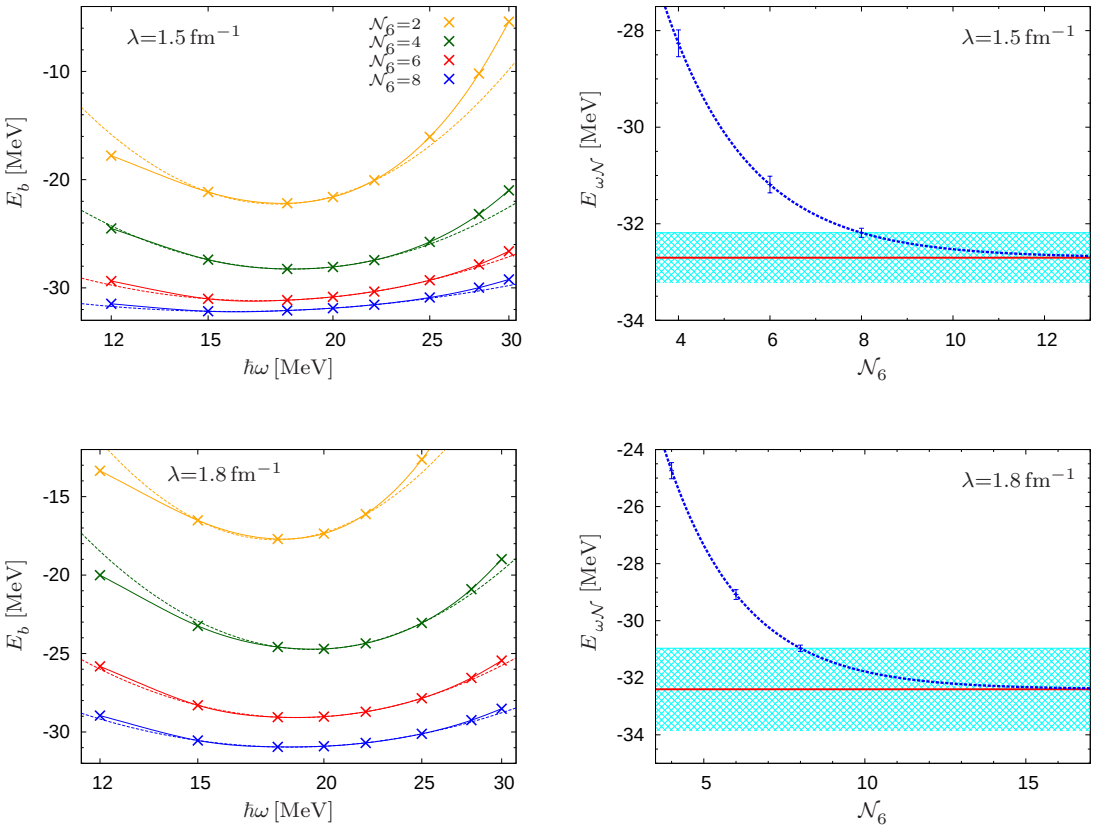

Figure 4.6: Binding energy of the ground state of ^{6}Li dependent on $\mathcal{N}_6$ and ω and the extrapolation to $\mathcal{N}_6 = \infty$ for $\lambda = 1.5$ fm^{-1} and $\lambda = 1.8$ fm^{-1}; lines and symbols as described in Fig. 4.5.

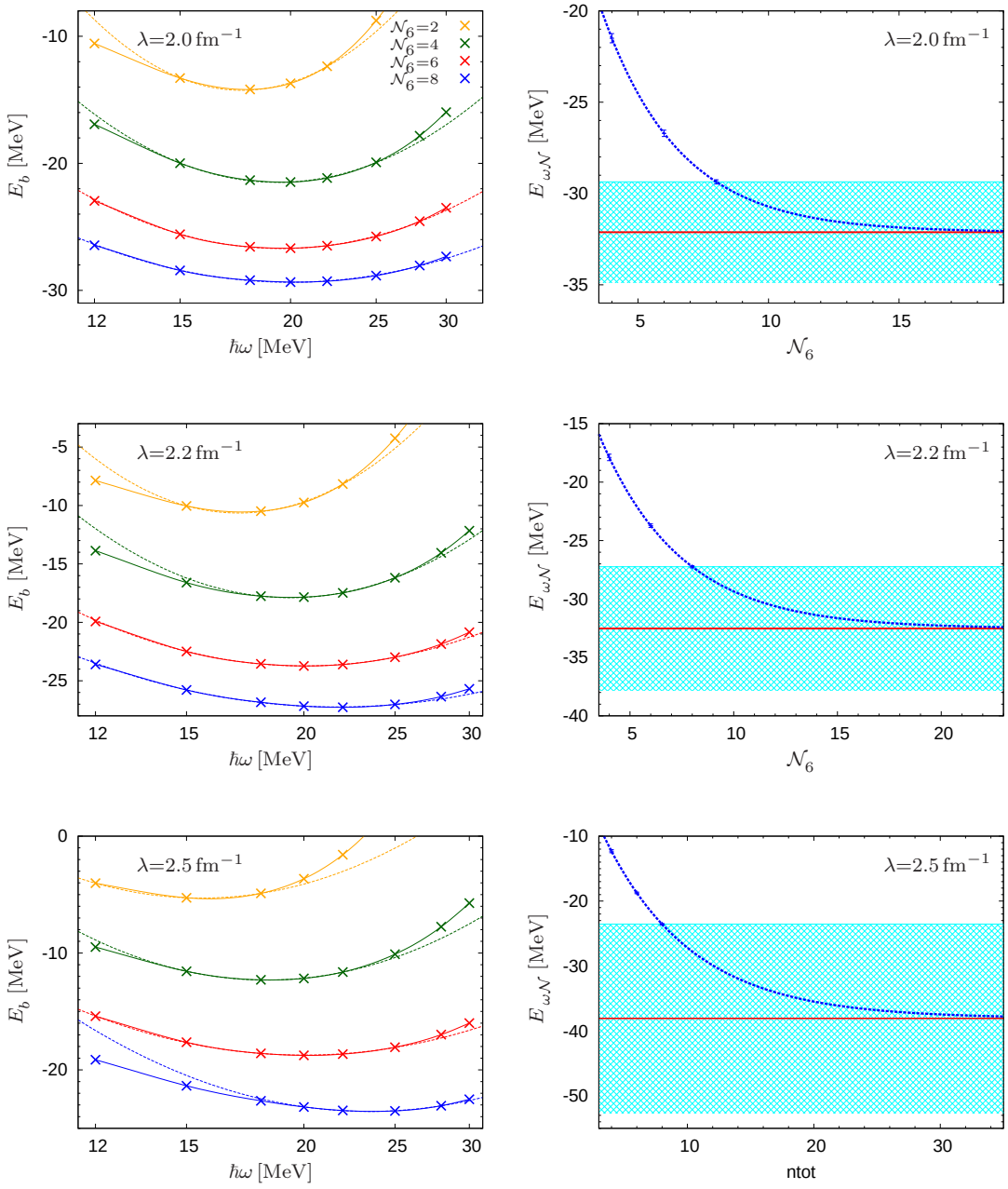

Figure 4.7: Binding energy of the ground state of ^{6}Li dependent on $\mathcal{N}_6$ and ω and the extrapolation to $\mathcal{N}_6 = \infty$ for $\lambda = 2.0$ fm^{-1}, $\lambda = 2.2$ fm^{-1} and $\lambda = 2.5$ fm^{-1}; lines and symbols as described in Fig. 4.5

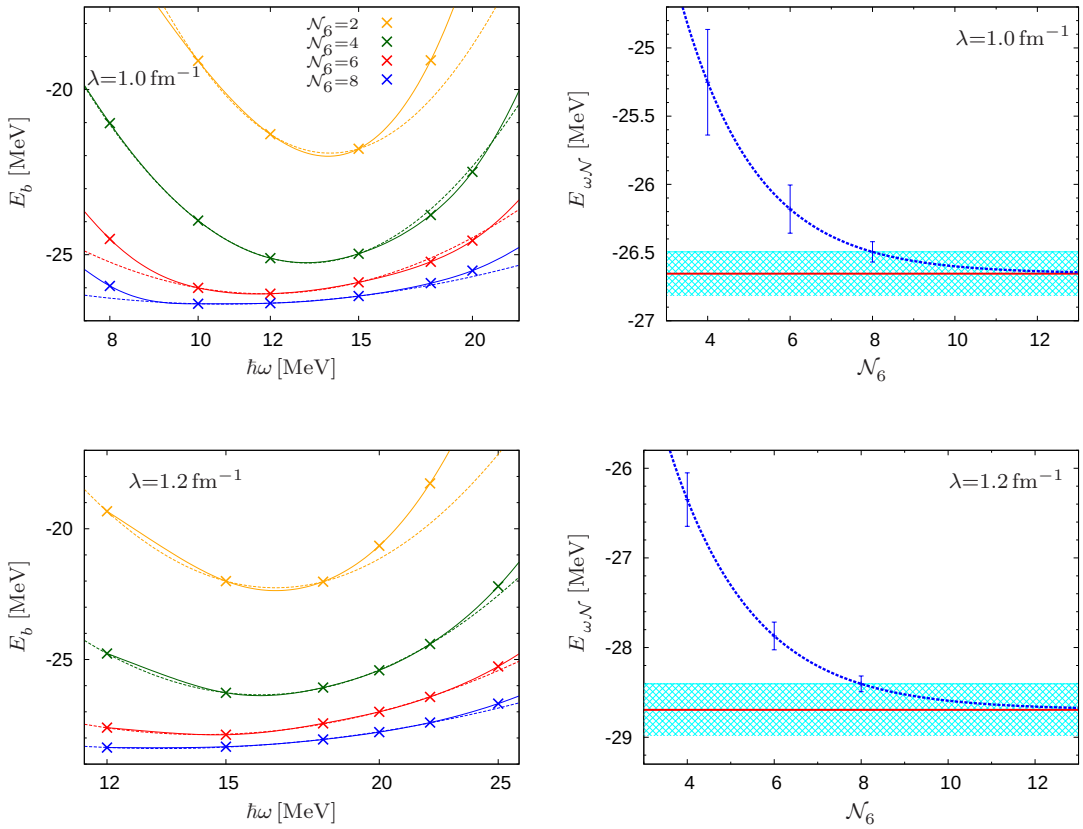

Figure 4.8: Binding energy of the lowest excited state of ^{6}Li (3^+ 0) dependent on $\mathcal{N}_6$ and ω and the extrapolation to $\mathcal{N}_6 = \infty$ for $\lambda = 1.0$ fm^{-1} and $\lambda = 1.2$ fm^{-1}; lines and symbols as described in Fig. 4.5

4.3.2 Lowest excited state 3^+ 0

The results for the lowest excited state of ^{6}Li, $J^\pi T = 3^+$ 0, are presented in Figs. 4.8 -4.10. The computational effort for these calculations is already approximately twice as large as for the ground state. The dependence of the binding energies on ω resembles that of the binding energies of the ground state not only regarding their variation with ω but also the shift of the optimal ω that tends to increase for $\lambda > 1.8$ fm^{-1}. This issue will be interesting to investigate once larger $\mathcal{N}_6$ are available or even for higher excited states.
Obtained again by extraction of optimal ω-values, the related binding energies $E_{\omega\mathcal{N}}$ show a behaviour similar to that of the ground state, as can be seen on the right-hand sides of the figures. The convergence is comparable, i.e. for $\lambda \leq 1.8$ fm^{-1}, the extrapolation gives reasonable results and error estimates, whereas the study of larger cutoffs requires larger model spaces.

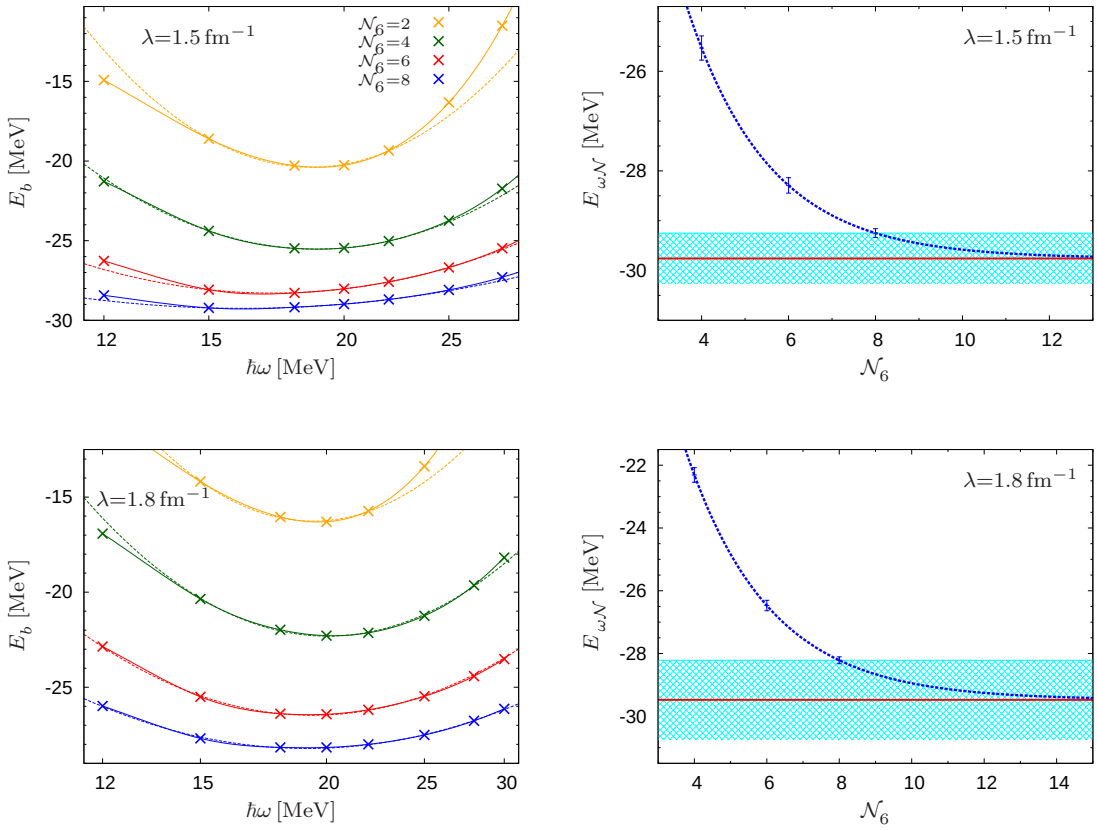

Figure 4.9: Binding energy of the lowest excited state of ^{6}Li (3^+ 0) dependent on $\mathcal{N}_6$ and ω and the extrapolation to $\mathcal{N}_6 = \infty$ for $\lambda = 1.5$ fm^{-1} and $\lambda = 1.8$ fm^{-1}; lines and symbols as described in Fig. 4.5

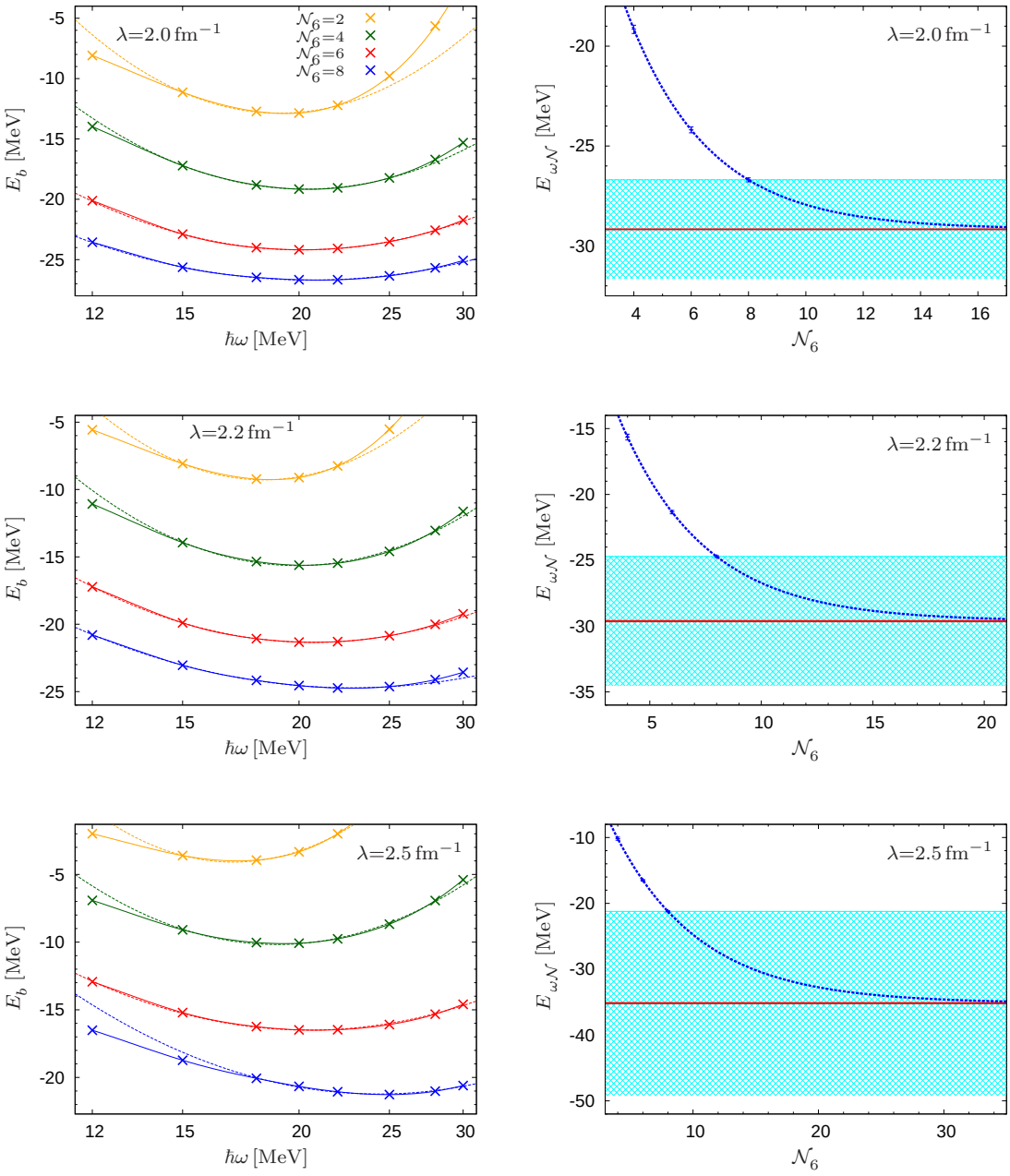

Figure 4.10: Binding energy of the lowest excited state of ^{6}Li (3^+ 0) dependent on $\mathcal{N}_6$ and omega and the extrapolation to $\mathcal{N}_6 = \infty$ for $\lambda = 2.0$ fm^{-1}, $\lambda = 2.2$ fm^{-1} and $\lambda = 2.5$ fm^{-1}. lines and symbols as described in Fig. 4.5

4.3.3 Excitation energy of 3^+ 0

Eventually, we turn to the investigation of the excitation energy of 3^+ 0, ΔE_b. Figs. 4.11 -4.13 show the ω dependence, fitted to a constant line around the optimal ω of the respective model space for both the ground state and the excited state in the left-hand sided diagrams, and the extrapolated results on the right-hand side. The error bars of $\Delta E_{\omega\mathcal{N}}$ are estimated, as before, by the interval between the result of the calculation in the largest model space and the extrapolation.
From both left-hand and right-hand side diagrams the considerable faster convergence is clearly visible. Except for $\lambda = 1.0$ fm^{-1}, the ω dependence is very similarly shaped for all cutoffs and smoothes notably with each higher $\mathcal{N}_6$ despite the rather small model spaces. This is also reflected by the strong decrease of the error bars in the right-hand side diagrams. Especially the calculations with larger cutoffs show a similarly good behaviour for all λ, although the related binding energies of 1^+ 0 and 3^+ 0 are not well converged for the larger cutoffs. The accuracy of up to 100 keV is remarkably small considering the large uncertainties of the binding energies in this range. Only the results for the largest cutoff, $\lambda = 2.5$ fm^{-1}, show somewhat larger error bars of the individual values of $\Delta E_{\omega\mathcal{N}}$. At the same time, the error estimate of the extrapolation method yields an unnaturally small uncertainty which we believe to be caused by an accidental cancellation.
The results of the calculations for ^{6}Li are summarised in Tab. 4.3. Although we expected the excitation energies to be obtained considerably faster than the binding energies, we observed a surprisingly good outcome. 3NF calculations of the excitation energies are especially promising since they are measurably influenced by 3NF. This can be seen for example by investigating the cutoff dependence, which is discussed in the following section.

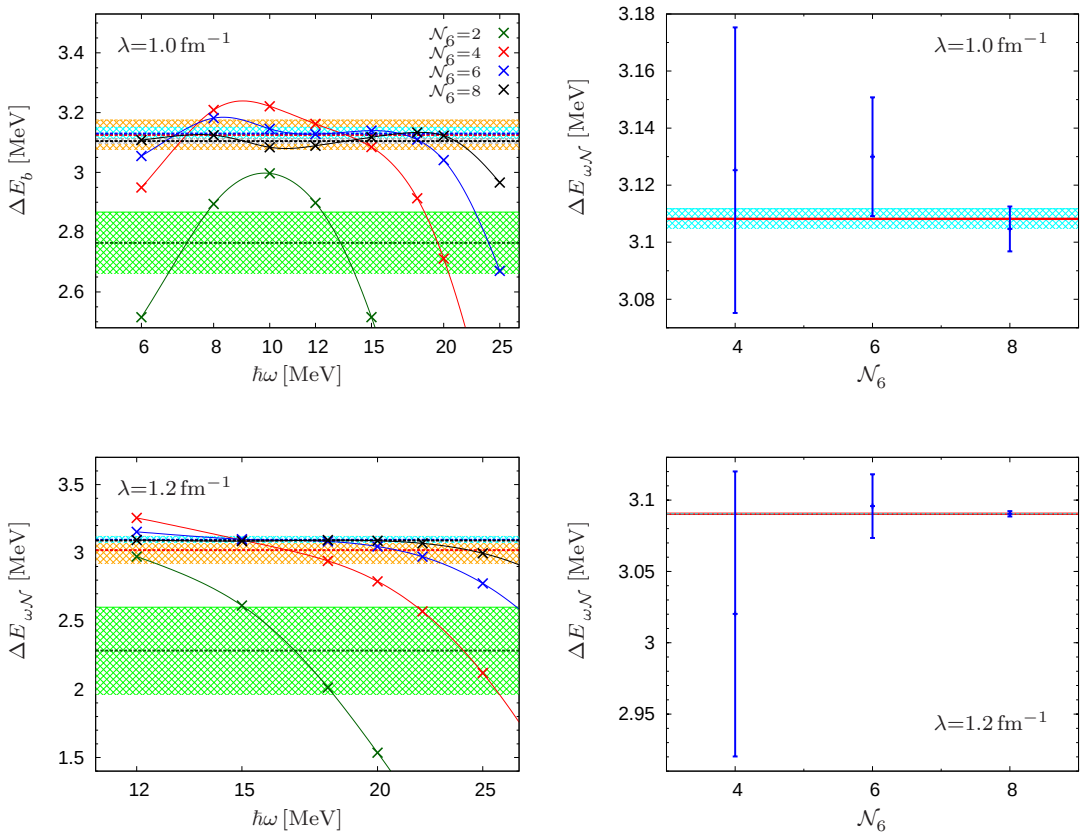

Figure 4.11: Excitation energy of ^{6}Li (3^+ 0) dependent on ω for several $\mathcal{N}_6$ (left diagrams). The shaded bands are error estimates from a standard fit procedure. The right diagrams show the extrapolated values, their uncertainty is shown as blue bands; $\lambda = 1.0$ fm^{-1} and $\lambda = 1.2$ fm^{-1}.

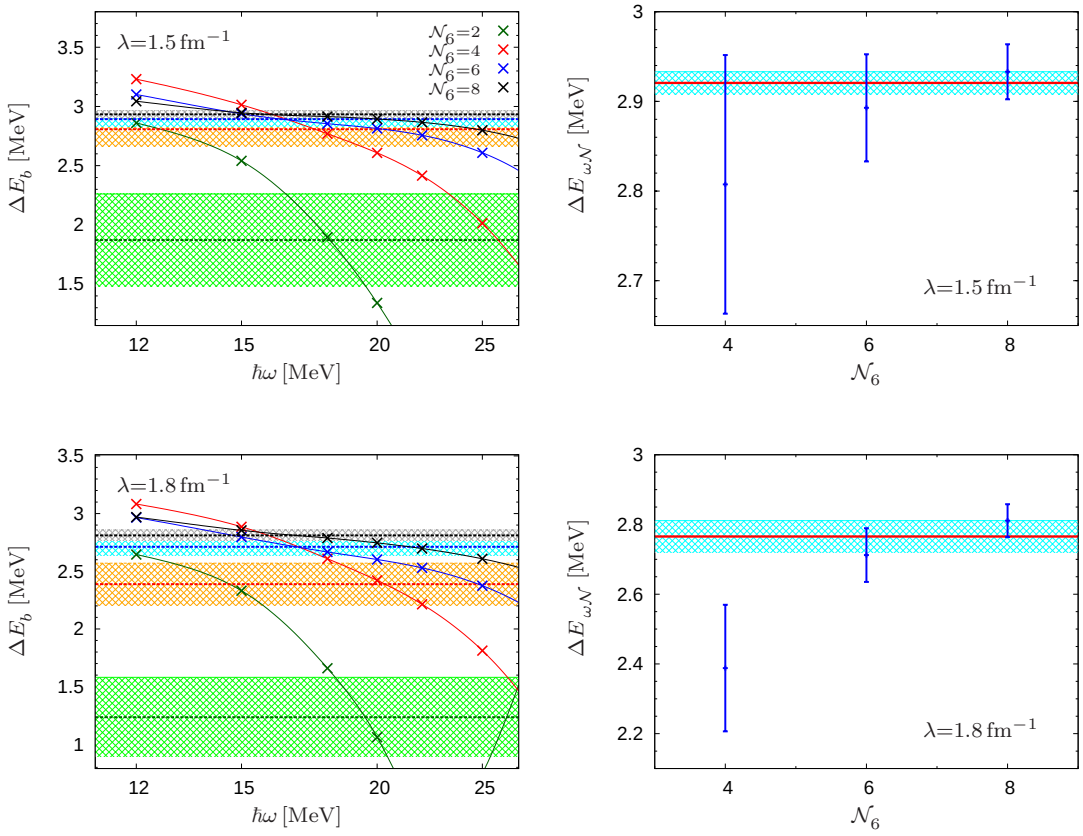

Figure 4.12: Excitation of ^{6}Li (3^+ 0), $\lambda = 1.5$ fm^{-1} and $\lambda = 1.8$ fm^{-1}; lines and symbols as described in Fig. 4.11.

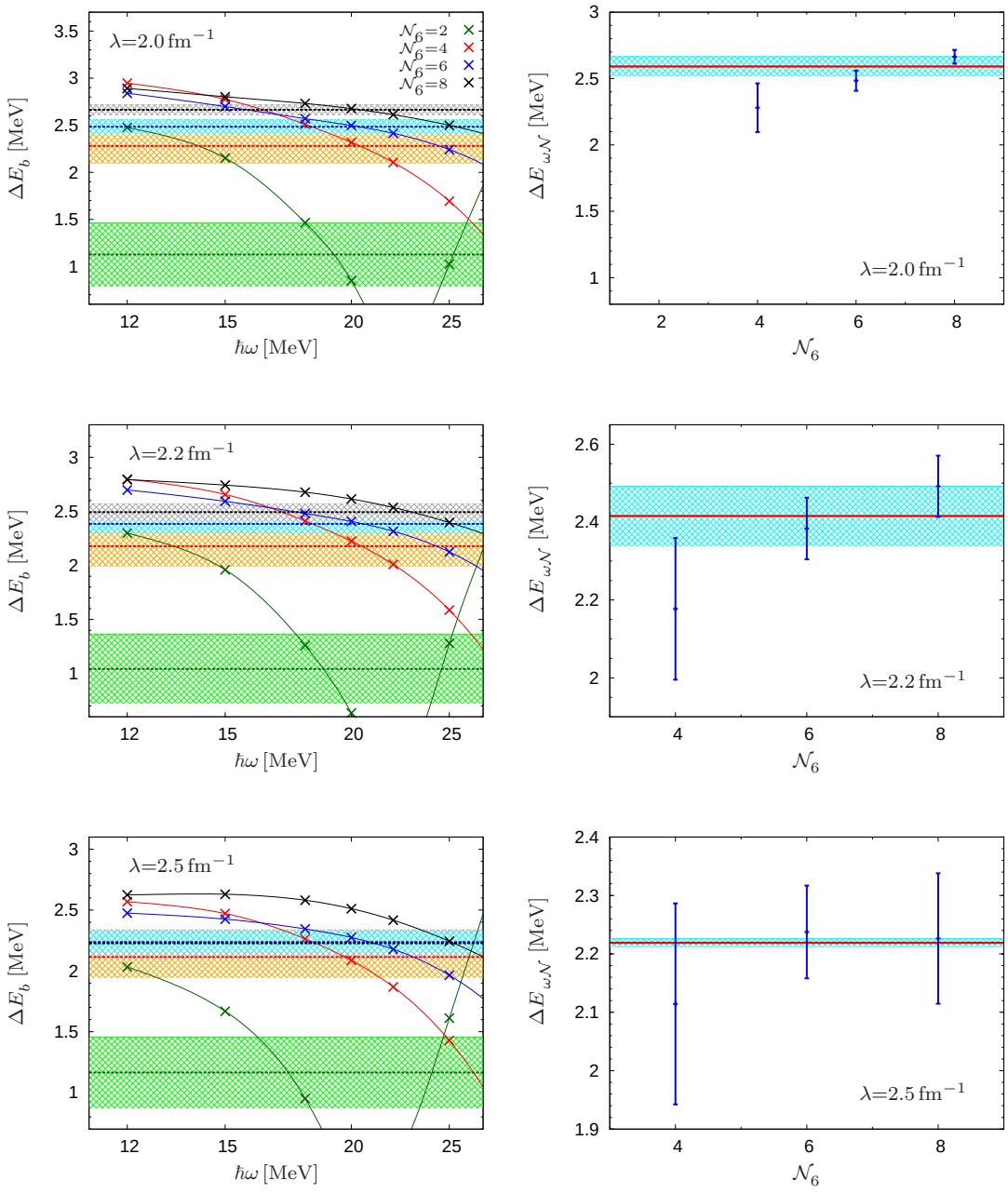

Figure 4.13: Excitation of ^{6}Li (3^+ 0), $\lambda = 2.0$ fm^{-1}, $\lambda = 2.2$ fm^{-1} and $\lambda = 2.5$ fm^{-1}.

λ [fm^{-1}]	1^+ 0	3^+ 0	excitation
1.0	-29.66(5) MeV	-26.65(16) MeV	3.11 MeV
1.2	-31.78(25) MeV	-28.69(29) MeV	3.09 MeV
1.5	-32.70(52) MeV	-29.76(51) MeV	2.92(1) MeV
1.8	-32.40(144) MeV	-29.48(126) MeV	2.77(5) MeV
2.0	-32.12(276) MeV	-29.17(247) MeV	2.59(7) MeV
2.2	-32.53(528) MeV	-29.63(491) MeV	2.42(8) MeV
2.5	-38.07(1452) MeV	-35.17(1395) MeV	2.22(1) MeV
experiment	-32.0 MeV	-29.81 MeV	2.19 MeV

Table 4.3: Explicit results for the binding energies of ^{6}Li (1^+ 0, 3^+ 0) and of the excitation energy, respectively. The error of the excitation energy for $\lambda = 2.5$ fm^{-1} is presumably underestimated due to an accidental cancellation. Instead we assume an error of 0.1 MeV. For comparison, the experimental values are also given for the ground state [68], and for the excited state and the excitation energy [89].

4.4 Cutoff dependence

The cutoff dependence of ^{3}H and ^{4}He, shown in Fig. 4.14 together with the cutoff dependence of ^{6}Li (1^+ 0, 3^+ 0 and excitation energy, respectively), show a well-known behaviour. As λ sets the scale for the relevant low momenta, small λ exclude pions as comparably heavy in relation to this scale. The EFT for this momentum range is the so-called pion–less EFT where 3NF appear at LO already, resulting in a strong cutoff dependence. Our considerations explicitly include the pions as relevant degrees of freedom, therefore the larger cutoffs are of more interest here, and for the analysis of the cutoff dependence we leave out the results for the smallest λ. With this we estimate the cutoff dependence and thus the contribution of higher order effects such as the 3NF to be of the order of ~ 0.5 MeV for ^{3}H and of ~ 2 MeV for ^{4}He, respectively, which is a lower bound of uncertainty.
A similarly shaped curve is observed for both 1^+ 0 and 3^+ 0 of ^{6}Li, where we do not consider the results for $\lambda > 2.0$ fm^{-1}. As they are not converged, their estimated uncertainty is considerably larger than the observed cutoff dependence of ~ 1 MeV and thus gives no exploitable information. However, this emphasises the need for an extension of the accessible model spaces to make calculations for larger cutoffs feasible.
Though the binding energies of 1^+ 0 and 3^+ 0 are not converged for larger λ, the diagram for the excitation energy shows a reasonable dependence in the full momentum range considered. The error bars do not superpose the variation of the results with λ which indicates a significant contribution of ~ 1 MeV from higher order effects. Calculations including 3NF additionally will show how this dependence decreases explicitly.

Another well-known behaviour is reflected in the so-called Tjon line, pictured in Fig. 4.15. Neglecting higher order effects, the binding energies reveal a correlation to the binding energy of ^{3}H. Though this correlation is well reproduced for ^{4}He, for ^{6}Li the large uncertainties for $\lambda > 2.0$ fm^{-1} do not approve of consideration so far. Still, also here the behaviour for smaller λ encourages the proceeding of our studies, especially regarding 3NF.

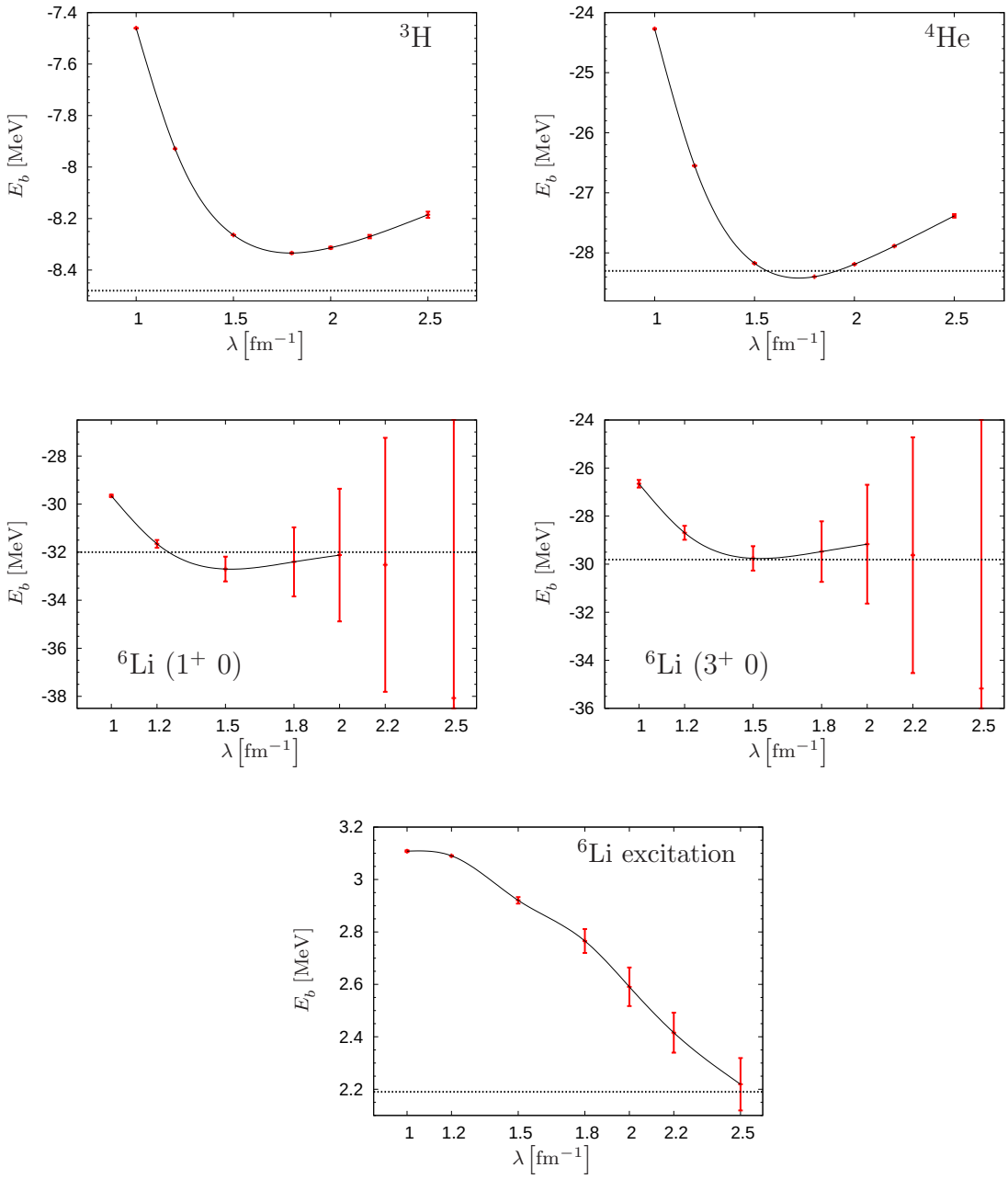

Figure 4.14: Cutoff dependence of the binding energies of ^{3}H, ^{4}He and ^{6}Li, assuming the converged values E_∞. Dotted lines denote the experimental values. The bottom diagram shows the cutoff dependence of the excitation energy.

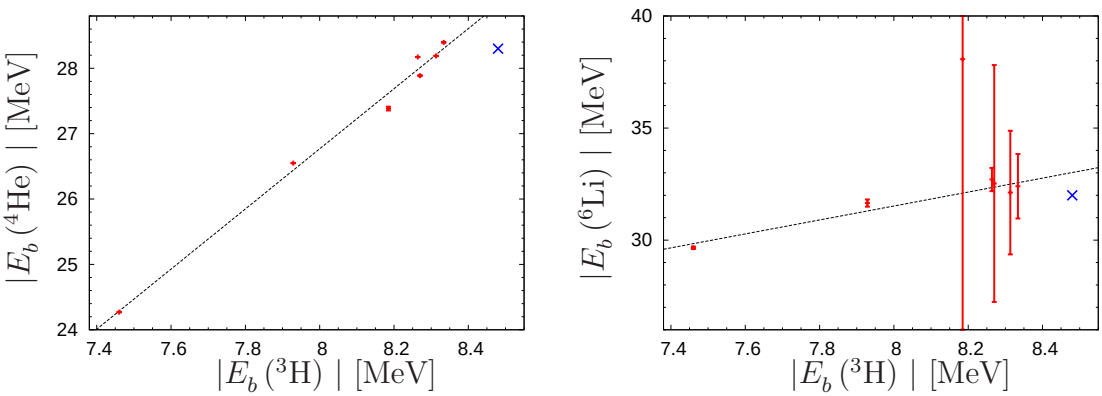

Figure 4.15: Tjon lines for ^{3}H and ^{4}He and for ^{3}H and ^{6}Li. The blue cross denotes the experimental value.

4.5 ^{7}Lithium

In Fig. 4.16, first results of calculations of ^{7}Li are illustrated. It is the first negative parity system that we investigate. Unfortunately, the considered model spaces of $\mathcal{N}_7 \leq 7$ do not allow for an extrapolation to converged values since we have to omit the results from the smallest model space. However, we are able to draw some conclusions on the upcoming calculations from the completed calculations for ^{6}Li and ^{7}Li. To this aim we order the model spaces with the difference $\delta\mathcal{N}$ of $\mathcal{N}_A$ to the smallest model space of the calculation, i.e. $\delta\mathcal{N} = \mathcal{N}_6 - 2$ and $\delta\mathcal{N} = \mathcal{N}_7 - 3$, respectively. Comparing ^{6}Li and ^{7}Li regarding the ω dependence we observe a similar behaviour of the ω dependence itself and of the individual curves for equal $\delta\mathcal{N}$. The separation between the curves for $\delta\mathcal{N} = 0$ and $\delta\mathcal{N} = 2$ is approximately twice as large as that between $\delta\mathcal{N} = 2$ and $\delta\mathcal{N} = 4$. Therefore, we assume that reasonable results may be achieved for ^{7}Li with $\mathcal{N}_7 = 9$, i.e. $\delta\mathcal{N} = 6$, on the same level as for ^{6}Li. The increase of the dimensions with $\mathcal{N}_7$ implies dimensions of $\beta_{max} \leq 90,000$, $\beta^{\star}_{max} \leq 540,000$, $\tilde{\beta}_{max} \leq 270,000$ and $\gamma_{max} \leq 13,000$ for this calculation. We are currently approaching the additionally required blocks of the 6N bookkeeping for $\mathcal{N}_6 = 9$, $J_6 = 0, \ldots, 10$ and $T_6 = 0, 1$. Once these blocks are generated, we will also be able to proceed to the lowest excited state of ^{7}Li and to study the excitation energy, both regarding the observations described for ^{6}Li concerning the ω dependence and the convergence.

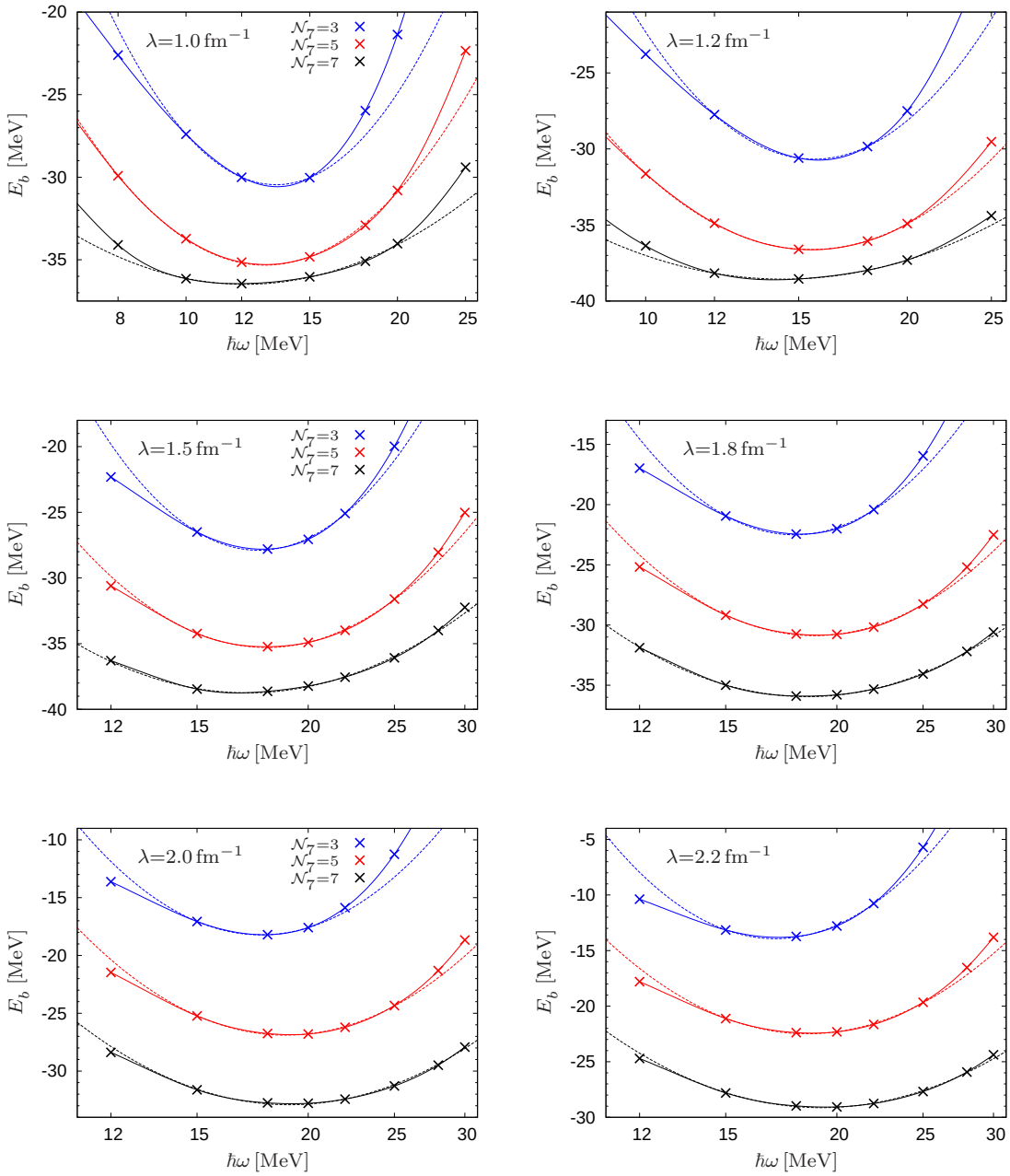

Figure 4.16: First results of the binding energy of ^{7}Li dependent on $\mathcal{N}_7$ and ω for several λ.

Chapter 5

Summary, conclusions and outlook

In this thesis, we described the development of a NCSM formalism, expressed in Jacobi coordinates in the HO basis, to solve the Schrödinger equation for bound states of few–nucleon systems. The theoretical framework of chiral EFT was explained, and the chiral expansion of the nuclear potential was introduced. We described the concept of low–momentum potentials like $V_{\text{low } k}$ and V_{SRG} and the momentum cutoff that sets the relevant scale for low– and high–momentum contributions. Additionally, we discussed existing A-body techniques and their recent developments. With this, we motivated our work.

Bound states of A-nucleon systems are described by the Schrödinger equation where the Hamiltonian depends on the relative coordinates of the nucleons. Therefore, a formulation of the basis states in Jacobi coordinates is very natural. The CM motion is separated and can simply be omitted. Since all nucleons are considered to be active, they are represented by $(A-1)$ harmonic oscillators in the HO basis. The finiteness of the basis is realised by a truncation at a chosen oscillator energy $\mathcal{N}_A$, and the results of the calculations converge with increasing model spaces. Compared to the m–scheme, where the basis states are expressed in single particle coordinates and antisymmetrised by a Slater determinant, the separation of the CM motion and the rotational symmetry reduce the number of basis states but complicate their antisymmetrisation which is traced back to a matrix eigenvalue problem. However, the conservation of the well-defined total angular momentum J_A and total isospin T_A and of the oscillator energy $\mathcal{N}_A$ results in a highly convenient block structure of the antisymmetrisation matrix. In Chapter 2 we explicitly defined the Jacobi coordinates for the 3N β–states, constructed as a single nucleon coupling to an antisymmetric 2N subsystem that satisfies the Pauli principle, and derived the antisymmetrisation matrix by applying the transposition operator $\widehat{P}_{23}$ to perform a coordinate transformation of nucleon 2 and 3. In spin–isospin space, $\widehat{P}_{23}$ operates as a recoupling, while in

configuration space the coordinate transformation of the nucleons is evaluated by HO brackets. The antisymmetrisation operator $\widehat{\mathcal{A}} = \frac{1}{3}\left(\mathbb{1} - 2\widehat{P}_{23}\right)$ is a projector with the eigenvalues 0 and 1, therefore only the physical eigenvectors corresponding to non-zero eigenvalues are kept as the antisymmetric 3N-basis states, $|\,\gamma_{3\mathrm{N}}\rangle$. This procedure can be generalised to $A > 3$ by coupling a single nucleon to $|\,\gamma_{(A-1)\mathrm{N}}\rangle$ which form the β–states of the A-nucleon system. For the antisymmetrisation the transposition operator $\widehat{P}_{23}$ is replaced by $\widehat{P}_{A(A-1)}$. To be able to calculate the coordinate transformation of the A-th and $(A-1)$-th nucleon explicitly, an intermediate type of states needs to be constructed where a single nucleon couples to a β–state of the $(A-1)$-nucleon system, labelled by $\beta^\star$. With a recoupling of these $\beta^\star$–states we showed that the construction of the antisymmetrisation matrix can be traced back to the expressions for the 3N case. Thus we demonstrated that the A-nucleon γ–states can be evaluated successively based on the $(A-1)$-nucleon system.
The solution of the Schrödinger equation forms another matrix eigenvalue problem. The kinetic energy of an A-nucleon system in Jacobi coordinates can exactly be calculated as the sum of the relative kinetic energy of two nucleons over all pairs, as outlined in App. A.2. With new basis states that separate an antisymmetric 2N-subsystem, denoted by $\tilde{\beta}^{(2)}$, these matrix elements and the NN contribution to the nuclear potential can be evaluated in a simple way. Similar to the evaluation of the transposition operator for the antisymmetrisation, these $\tilde{\beta}^{(2)}$–states are obtained by a suitable coordinate transformation applied to the single nucleons of the $\beta^\star$–states. The expression for this coordinate transformation including the required recoupling of the $\beta^\star$–states was calculated in detail. The coefficients are independent of ω and the interactions and can therefore be employed generally.
With this method, the inclusion of few–nucleon forces contributing to the nuclear potential can be realised conveniently by separating larger antisymmetric subsystems in a similar way. The explicit expression for $\tilde{\beta}^{(3)}$–states with antisymmetric 3N-subsystems was derived in App. B. Additionally, the γ-, β-, $\beta^\star$-, $\tilde{\beta}^{(2)}$- and $\tilde{\beta}^{(3)}$–states can be verified in a simple way with the constituted orthogonality relations concerning their antisymmetry and their completeness.

In Chapter 3 we described numerical aspects of our formalism. The largest part of the calculations was the antisymmetrisation of A-nucleon basis states since the relevant number, $\beta^\star_{max}$, exceeds the number of β–states by approximately a factor of $(A-1)$. Therefore, we chose the antisymmetrisation of 6N states exemplarily to test the numerical performance in detail.
The required memory capacity of several GB for these test calculations strongly demands a parallel evaluation, especially with regard to the considerable growth of data with increasing model spaces and larger A. Since both problems of this formalism – the antisymmetrisation and the solution of the Schrödinger equation

– are matrix eigenvalue equations, we employ the libraries of ScaLAPACK that compute eigenvalues and eigenvectors of a matrix by diagonalisation in a twofold distributed way. Therefore, we defined a two-dimensional communicator within the chosen library for the communication of parallel processes, MPI. According to the matrix structure of the data, these two directions of the distributions were denoted by '*row*' and '*col*'. With this we described the calculation of the antisymmetrisation matrix based on the $(A-1)$-nucleon system. The largest part, i.e. the evaluation of the transposition operator applied to the $\beta^\star$–states, is distributed most widely in both directions. The double sum over the intermediate $\beta^\star$–states was split into two steps, where we saved one index of the resulting matrix globally in order to minimise the communication of the parallel processes. With similar considerations the sums for the $\tilde{\beta}^{(2)}$– and $\tilde{\beta}^{(3)}$–projections were divided for their generation.
The so generated bookkeepingsare stored in a global database employing the routines of the parallel I/O library HDF5. They are independent of the machine, written in a universal format and thus only need to be generated once. The ability to divide data into groups provides an excellent way to extend the database for each A-nucleon system blockwise matching the block structure of our formalism since already existing blocks can be skipped and new ones appended. Since the A-nucleon bookkeepings are generated based on the $(A-1)$-nucleon system, the $(A-1)$-nucleon bookkeepings do not have to be generated repeatedly but can be read in from the database in the required distribution. Unfortunately, these HDF5 routines are much less efficient than those for writing the data which became problematic for large model spaces.
Otherwise, the test calculations showed the expected scaling concerning the number of parallel processes and their distribution in *row*- and *col*-direction, and concerning their required memory capacity.
Currently, the existing databases for $A = 3$, 4 and 5 provide the bookkeepings required for $A \geq 6$ in the model space of $\mathcal{N}_A = 10$. Due to limited accessibility of the supercomputer JUQUEEN, the generation of databases for $A = 6$ and 7 with $\mathcal{N}_A > 8$ and for $A = 8$ is ongoing and appears to be feasible.
For the calculation of the binding energies we used the NN-only V_{SRG} evolved from the 500 MeV N^{3}LO NN potential from Ref. [26] including the electromagnetic interaction, taking account of the *nn*, *np* and *pp* forces by using the coefficients $c_{T\,m_T}$ from [86]. Additionally, fit procedures for the value ω_{opt} for which the wave function is parameterised in an optimal way and for an extrapolation to $\mathcal{N}_A = \infty$ [68] including an error estimate were introduced.

With this we calculated the binding energies of ^{3}H, ^{4}He, ^{6}Li and ^{7}Li and discussed the results in Chapter 4. The required memory capacity of systems with $A > 4$ and the runtime made a high parallelisation necessary while it was possible to perform the calculations of the ^{3}H and the ^{4}He binding energy on a standard desktop computer. The results for ^{3}H and ^{4}He are converged and very accurate

for small λ and for larger λ the extrapolation method gives reliable extrapolated results. Moreover, the results agree with those calculated with a different technique (FY [88]) within the error estimate. Therefore, we did not proceed to higher model spaces but regard our calculations as benchmarks for this scheme.
For ^{6}Li, we analysed the ground state 1^+ 0 as well as the lowest excited state 3^+ 0. Since calculations of binding energies once the antisymmetrised states were generated are considerably smaller than the generation of the states itself, it was possible to study the ω dependence in all model spaces in detail. Although the model spaces are comparably small for convergence, the extrapolation method yields promising values for small λ with reasonable error estimates. While larger λ require higher model spaces for the binding energies to converge, we obtained good results for the excitation energy already in these first calculations. Considering the cutoff dependence this became even more evident. While the curve for ^{3}H and ^{4}He reproduced the well-known behaviour as expected, both the ground state and the excited state of ^{6}Li were too vaguely determined for large λ. This conclusion was underlined by the Tjon lines. However, the diagram for the excitation energy revealed a smooth dependence with meaningful error bars for all cutoffs considered which is a strong indication of the significance of higher order contributions. It is highly interesting how this dependence will decrease once the relevant bookkeepings for the inclusion of the 3NF will have been generated. Furthermore, we concluded from the results for ^{7}Li obtained so far that their behaviour is comparable to those of ^{6}Li. Therefore, it is the subject of ongoing studies to calculate the energies of higher excited states for both ^{6}Li and ^{7}Li. It is conceivable that these excitation energies will be very informative concerning the nature of the 3NF.

With the generated coefficients determining the antisymmetrised states numerous calculations can be performed efficiently to study a large variety of states including NN and 3N forces. This will be the main advantage of this Jacobi coordinate based NCSM formalism.
These new sets of states will also be the basis of hypernuclear studies with a new collaboration research center funded by the DFG (CRC 110, project B7). In a first step, it is planned to extend the basis by coordinates of a single hyperon. This can be done straightforwardly since further antisymmetrisation is not required for the distinguishable hyperon.
Meanwhile, a continous extension of the database of antisymmetrised states will allow one to study the 3NF for more and more states of more complex nuclei.
At the same time, it will be worthwhile to improve the performance of the code. Here it will be interesting to study the reading of the bookkeeping of the $(A-1)$-system in more detail. We expect that some improvements could be obtained specifically for this part of the runs.
For more complex nuclei, it will also be interesting to investigate antisymmetrised states in incomplete model spaces where the A-nucleon systems are restricted to

small angular momenta. Such truncations are part of our implementation and their practical use will be investigated in near future.

Appendix A

The Hamilton operator in HO basis

A.1 Energy eigenvalues and eigenfunctions

The eigenfunctions of the three-dimensional HO Hamiltonian $\widehat{H}_{\mathrm{HO}}$ can be separated – using spherical polar coordinates – in the usual way into an angular and a radial part:

$$\begin{aligned} \widehat{H}_{\mathrm{HO}}\,\Psi_n\left(\vec{r}\right) &= \left(\widehat{T}_{\mathrm{HO}} + \widehat{V}_{\mathrm{HO}}\right)\,\Psi_n\left(\vec{r}\right) \\ &= E_n\,\Psi_n\left(\vec{r}\right) \qquad\qquad \text{with} \\ \Psi_n\left(\vec{r}\right) &= \sum_{lm} Y_{lm}\left(\hat{r}\right)\,R_{nl}\left(r\right)\,. \end{aligned} \tag{A.1}$$

The Y_{lm} are the spherical harmonics that (can be neglected) are expanded in l for our calculations due to the spherical symmetry of the HO potential, $\hat{r}$ denotes the direction of the space coordinate $\vec{r}/r$ $(r = |\,\vec{r}\,|)$ and $R_{nl}\left(r\right)$ is the radial function of $\Psi_n\left(\vec{r}\right)$ that depends on the HO quantum number n $(n = 0, 1, 2\ldots)$, on the orbital momentum l and on the magnitude of $\vec{r}$.
The kinetic energy operator $\widehat{T}_{\mathrm{HO}}$ can be written in a very convenient way based on this ansatz, and by choosing the isotropic HO potential for $\widehat{V}_{\mathrm{HO}}$ the eigenvalues of the HO Hamiltonian can be read off since $\widehat{H}_{\mathrm{HO}}$ is diagonal for this choice. Here, this is outlined for the 2N system, hence the subscript 12 is dropped for readability.

a) <u>radial function in momentum space : Fourier transformation</u>

By performing a Fourier transformation of $\Psi_n\left(\vec{r}\right)$ we obtain the expression

of the radial function in momentum space, $R_{nl}(p)$:

$$\Psi_n(\vec{p}) = \frac{1}{(2\pi)^{3/2}} \int d^3r\, e^{i\vec{p}\cdot\vec{r}}\, \Psi_n(\vec{r})$$

$$\text{with} \quad e^{i\vec{p}\cdot\vec{r}} = \sum_{lm} 4\pi\, i^l\, j_l(p\,r)\, Y^\star_{lm}(\hat{p})\, Y_{lm}(\hat{r})$$

j_l spherical Bessel functions

$$= \frac{4\pi}{(2\pi)^{3/2}} \sum_{lm} i^l \int d^3r\, j_l(p\,r)\, Y^\star_{lm}(\hat{p})\, Y_{lm}(\hat{r})\, \Psi_n(r)$$

$$Y^\star_{lm}(\hat{p})\, Y_{lm}(\hat{r}) = Y_{lm}(\hat{p})\, Y^\star_{lm}(\hat{r})$$

$$\text{and } \Psi_n(r) = \sum_{l'\,m'} Y_{l'\,m'}(r)\, R_{nl'}(r)$$

$$= \sqrt{\frac{2}{\pi}} \sum_{lm} i^l \int d^3r\, j_l(p\,r)\, Y_{lm}(\hat{p}) \sum_{l'\,m'} Y^\star_{lm}(\hat{r})\, Y_{l'\,m'}(r)\, R_{nl'}(r)$$

$$\int d\Omega\, Y^\star_{lm}(\hat{r})\, Y_{l'\,m'}(r) = \delta_{l\,l'}\, \delta_{m\,m'}$$

$$= \sum_{lm} Y_{lm}(\hat{p})\, \sqrt{\frac{2}{\pi}}\, i^l \int dr\, r^2\, j_l(p\,r)\, R_{nl}(r)$$

$$= \sum_{lm} Y_{lm}(\hat{p})\, R_{nl}(p)$$

$$\Rightarrow \mathbf{R_{nl}(p)} = \sqrt{\frac{\mathbf{2}}{\pi}}\, \mathbf{i^l} \int \mathbf{dr\, r^2\, j_l(p\,r)\, R_{nl}(r)} \tag{A.2}$$

b) dimensionless radial function $\hat{R}_{nl}(\rho)$ in configuration space

The radial functions $R_{nl}(r)$ form a complete set of orthogonal eigenfunctions to $\widehat{H}_{\mathrm{HO}}$, in configuration space normalised to 1. By defining the characteristic oscillator length $b = \sqrt{1/(\mu\,\omega)}$ (in this case μ is the reduced mass of the deuteron and ω the angular frequency of the oscillator) the coordinate $\rho = r/b$ is dimensionless (in momentum space: $\tilde{p} = p\,b$ dimensionless; this leaves the product $(p\,r)$ invariant). The relation between the $R_{nl}(r)$ and the dimensionless $\hat{R}_{nl}(\rho)$ can easily be derived from the orthonormality

of the $R_{nl}(r)$:

$$\begin{aligned} r \longrightarrow \rho &= \frac{r}{b} \\ r &= \rho\, b \\ dr &= d\rho\, b \end{aligned}$$

$$\begin{aligned} \rightarrow \int dr\, r^2 \left|R_{nl}(r)\right|^2 &= \int d\rho\, b\, (\rho\, b)^2\; c^2 \left|\hat{R}_{nl}(\rho\, b)\right|^2 \\ &= \int d\rho\, \rho^2 \underbrace{b^3\, c^2 \left|\hat{R}_{nl}(\rho\, b)\right|^2}_{|\hat{R}_{nl}(\rho)|^2} \\ &= 1 \end{aligned}$$

$$\rightarrow c^2 = b^{-\frac{3}{2}}$$

$$\Rightarrow \mathbf{R_{nl}}(\mathbf{r}) = \mathbf{b^{-\frac{3}{2}}}\, \hat{\mathbf{R}}_{\mathbf{nl}}(\rho) \tag{A.3}$$

With this the radial functions $\hat{R}_{nl}(\rho)$ can be written in terms of the generalised Laguerre polynomials $L_n^{(\alpha)}$ [85]:

$$\hat{R}_{nl}(\rho) = (-1)^n \left[\frac{2\, n!}{\Gamma\left(n + l + \frac{3}{2}\right)}\right]^{\frac{1}{2}} \exp\left(-\frac{\rho^2}{2}\right) \rho^l\, L_n^{\left(l+\frac{1}{2}\right)}\left(\rho^2\right) \tag{A.4}$$

that satisfy the recurrence relation [90]

$$(n+1)\; L_{n+1}^{(\alpha)}(x) = (2n + \alpha + 1 - x)\; L_n^{(\alpha)}(x) - (n+\alpha)\; L_{n-1}^{(\alpha)}(x)$$

$$\leftrightarrow\; x\, L_n^{(\alpha)}(x) = -(n+1)\, L_{n+1}^{(\alpha)}(x) + (2n+\alpha+1)\, L_n^{(\alpha)}(x) - (n+\alpha)\; L_{n-1}^{(\alpha)}(x)\;. \tag{A.5}$$

c) <u>dimensionless radial function $\hat{\mathbf{R}}_{\mathbf{nl}}(\tilde{\mathbf{p}})$ in momentum space</u>

Replacing p by $\tilde{p} = p\,b$ and using the results from a) and b) the expression for the dimensionless radial function in momentum space reads:

$$\begin{aligned} R_{nl}(p) &= \sqrt{\frac{2}{\pi}}\, i^l \int d\rho\, b\, \rho^2\, b^2\, j_l\left(p\, b\, \frac{r}{b}\right)\, b^{-\frac{3}{2}}\, \hat{R}_{nl}(\rho) \\ &= b^{\frac{3}{2}} \underbrace{\sqrt{\frac{2}{\pi}}\, i^l \int d\rho\, \rho^2\, j_l(\tilde{p}\,\rho)\; \hat{R}_{nl}(\rho)}_{\equiv (-1)^n\, i^l\, \hat{R}_{nl}(\tilde{p})} \end{aligned}$$

$$\Rightarrow \mathbf{R_{nl}(p)} = \mathbf{(-1)^n\, i^l\, b^{\frac{3}{2}}\, \hat{R}_{nl}(\tilde{p})} \tag{A.6}$$

d) recurrence decomposition of $\hat{\mathbf{R}}_{\mathbf{nl}}$

The product $\tilde{p}^2\, \hat{R}_{nl}(\tilde{p})$ can be decomposed in the following way considering the recurrence relation of Eq. (A.5) and using $x\,\Gamma(x) = \Gamma(x+1)$:

$$\begin{aligned} \tilde{p}^2\, \hat{R}_{nl}(\tilde{p}) &= (-1)^n\, i^l\, \exp\left(-\frac{\tilde{p}^2}{2}\right) \tilde{p}^l \\ &\quad \times \Bigg\{ (-1)^n \left[\frac{2\,n!}{\Gamma\left(n+l+\frac{3}{2}\right)}\right]^{\frac{1}{2}} (-1)\; (n+1)\, L_{n+1}^{\left(l+\frac{1}{2}\right)}\left(\tilde{p}^2\right) \\ &\qquad + (-1)^n \left[\frac{2\,n!}{\Gamma\left(n+l+\frac{3}{2}\right)}\right]^{\frac{1}{2}} \left(2n+l+\tfrac{3}{2}\right) L_n^{\left(l+\frac{1}{2}\right)}\left(\tilde{p}^2\right) \\ &\qquad + (-1)^n \left[\frac{2\,n!}{\Gamma\left(n+l+\frac{3}{2}\right)}\right]^{\frac{1}{2}} (-1)\; \left(n+l+\tfrac{1}{2}\right) L_{n-1}^{\left(l+\frac{1}{2}\right)}\left(\tilde{p}^2\right) \Bigg\} \end{aligned}$$

$$\begin{aligned} &= (-1)^n\, i^l\, \exp\left(-\frac{\tilde{p}^2}{2}\right) \tilde{p}^l \\ &\times \Bigg\{ (n+1)\,(-1)^{n+1} \left[\frac{2\;(n+1)!}{\Gamma\left(n+1+l+\frac{3}{2}\right)} \left(\frac{2n+l+\frac{3}{2}}{n+1}\right)\right]^{\frac{1}{2}} L_{n+1}^{\left(l+\frac{1}{2}\right)}\left(\tilde{p}^2\right) \\ &\quad + \left(2n+l+\tfrac{3}{2}\right)\; (-1)^n \left[\frac{2\,n!}{\Gamma\left(n+l+\frac{3}{2}\right)}\right]^{\frac{1}{2}} L_n^{\left(l+\frac{1}{2}\right)}\left(\tilde{p}^2\right) \\ &\quad + \left(n+l+\tfrac{1}{2}\right) (-1)^{n-1} \left[\frac{2\;(n-1)!}{\Gamma\left(n-1+l+\frac{3}{2}\right)} \left(\frac{n}{n+l+\frac{1}{2}}\right)\right]^{\frac{1}{2}} L_{n-1}^{\left(l+\frac{1}{2}\right)}\left(\tilde{p}^2\right) \Bigg\} \end{aligned}$$

$$= (-1)^n\ i^l \left(\sqrt{(n+1)\left(n+l+\tfrac{3}{2}\right)}\ \hat{R}_{(n+1)l}\left(\tilde{p}\right) + \left(2n+l+\tfrac{3}{2}\right) \hat{R}_{nl}\left(\tilde{p}\right) + \sqrt{n\ \left(n+l+\tfrac{1}{2}\right)}\ \hat{R}_{(n-1)l}\left(\tilde{p}\right) \right) \tag{A.7}$$

Analogous calculations can be done for the radial functions in configuration space $\hat{R}_{nl}\left(\rho\right)$, defined in Eq. (A.4):

$$\rho^2\ \hat{R}_{nl}\left(\rho\right) = \left(\sqrt{(n+1)\left(n+l+\tfrac{3}{2}\right)}\ \hat{R}_{(n+1)l}\left(\rho\right) + \left(2n+l+\tfrac{3}{2}\right) \hat{R}_{nl}\left(\rho\right) + \sqrt{n\ \left(n+l+\tfrac{1}{2}\right)}\ \hat{R}_{(n-1)l}\left(\rho\right) \right) \tag{A.8}$$

To compute the physical eigenvalues of $\widehat{H}_{\rm HO}$ the antisymmetric part $\langle\,\gamma\,|\Psi_{nlm}\rangle$ of the HO wave function contributes. Since for the 2N system the quantum numbers of the antisymmetric α-, β- and γ–states can be identified uniquely the following calculation is formulated in terms of the γ–states with $\langle\,\vec{p}\,\gamma\,|\Psi_{nlm}\,\rangle = R_{nl}\left(p\right)$ and $\langle\,\vec{r}\,\gamma\,|\Psi_{nlm}\,\rangle = R_{nl}\left(r\right)$.
Based on the results from above we find for the expectation value of the kinetic energy operator $\widehat{T}_{\rm HO}$:

$$\begin{aligned}
\langle\,\gamma'\,|\widehat{T}_{\rm HO}|\,\gamma\,\rangle &= \int dp\, p^2\ R^{\star}_{n'l'}\left(p\right)\ \frac{p^2}{2\mu}\ R_{nl}\left(p\right) \\
&= \frac{(-1)^{n'+n}\ (-i)^{l'}\ i^l}{2\mu\, b^2} \int dp\, b\, p^2\, b^2\ \hat{R}_{n'l'}\left(\tilde{p}\right)\ p^2\, b^2\ \hat{R}_{nl}\left(\tilde{p}\right) \\
&= \frac{(-1)^{n'+n}\ i^{l-l'}}{2\mu\, b^2} \int d\tilde{p}\, \tilde{p}^{\,2} \hat{R}_{n'l'}\left(\tilde{p}\right)\ \tilde{p}^{\,2} R_{nl}\left(\tilde{p}\right) \\
&= \frac{1}{2}\,\omega\ \delta_{l'l} \left(\delta_{n'\,(n+1)}\,(-1)^{n'+n}\ \sqrt{(n+1)\left(n+l+\tfrac{3}{2}\right)} + \delta_{n'\,n}\ (-1)^{n'+n}\left(2n+l+\tfrac{3}{2}\right) + \delta_{n'\,(n-1)}\,(-1)^{n'+n}\ \sqrt{n\left(n+l+\tfrac{1}{2}\right)}\ \right)
\end{aligned} \tag{A.9}$$

Note that for the off-diagonal matrix elements $\delta_{n'\,(n+1)}$ and $\delta_{n'\,(n-1)}$ of $\widehat{T}_{\rm HO}$ this results in a phase factor $(-1)^{2n+1} = (-1)^{2n-1} = -1$ whereas for the diagonal

matrix elements $\delta_{n'\,n}$ the phase factor $(-1)^{2n}$ equals $+1$.

As a test we consider the three-dimensional isotropic harmonic oscillator potential $\mathcal{V}_{\rm HO} = \frac{1}{2}\mu\,\omega^2 r^2$ where μ, ω and r are defined as above. For the expectation value of $\widehat{\mathcal{V}}_{\rm HO}$ it is more convenient to work in configuration space:

$$\begin{aligned}
\langle\,\gamma'\,|\widehat{\mathcal{V}}_{\rm HO}|\,\gamma\,\rangle \quad &= \quad \int dr\, r^2\; R^{\star}_{n'l'}\,(r)\;\; \frac{1}{2}\mu\,\omega^2 r^2\;\; R_{nl}\,(r) \\
&\overset{\text{Eq. (A.3)}}{=} \quad \frac{\mu\,\omega^2}{2}\, b^{-3} \int d\rho\, b\;\; \rho^2\, b^2\;\, \hat{R}_{n'l'}\,(\rho)\;\; \rho^2\, b^2\;\, \hat{R}_{nl}\,(\rho) \\
&= \quad \frac{\mu\,\omega^2\, b^2}{2} \int d\rho\;\rho^2\;\hat{R}_{n'l'}\,(\rho)\;\; \rho^2\;\hat{R}_{nl}\,(\rho) \\
&\overset{\text{Eq. (A.8)}}{=} \quad \frac{1}{2}\,\omega\;\delta_{l'l} \Big(\delta_{n'\,(n+1)} \sqrt{(n+1)\left(n+l+\tfrac{3}{2}\right)} \\
&\qquad\qquad + \delta_{n'\,n}\;\left(2n+l+\tfrac{3}{2}\right) \\
&\qquad\qquad + \delta_{n'\,(n-1)}\,\sqrt{n\left(n+l+\tfrac{1}{2}\right)}\;\Big) \qquad \text{(A.10)}
\end{aligned}$$

Comparing these matrix elements to those of $\widehat{T}_{\rm HO}$ we note that they are the same except for the phase factor (-1) in the off-diagonal matrix elements of $\widehat{T}_{\rm HO}$. Therefore, the off-diagonal elements cancel in $\widehat{H}_{\rm HO} = \widehat{T}_{\rm HO} + \widehat{\mathcal{V}}_{\rm HO}$ and we finally get the well-known expression for the energy eigenvalues of the three-dimensional isotropic harmonic oscillator:

$$\begin{aligned}
\widehat{H}_{\rm HO}\,\Psi_{\mathcal{N}}\,(\vec{r}) \;&=\; E_{\mathcal{N}}\,\Psi_{\mathcal{N}}\,(\vec{r}) \qquad\qquad \text{with} \\
\Psi_{\mathcal{N}}\,(\vec{r}) \;&=\; R_{nl}\,(r) \\
E_{\mathcal{N}} \;&=\; \left(\mathcal{N}+\frac{3}{2}\right)\,\omega \qquad\quad \text{in natural units} \\
\mathcal{N} \;&=\; 2n+l \qquad\quad \text{total oscillator energy} \qquad \text{(A.11)}
\end{aligned}$$

A.2 Relative kinetic energy

For a system with $A > 2$ the kinetic energy operator $\widehat{T}_{A\rm N}$ can be expressed in terms of the kinetic energy in the 2N system, $\widehat{T}_{12}$. In the following this is shown

for the 3N system as an example.

In the center of mass frame (CM) the kinetic energy is defined as

$$\widehat{T}_{\rm 3N}^{\rm CM} = \sum_{i=1}^{3} \frac{\widehat{\vec{k}}_i^{\,2}}{2m_{\rm N}} - \frac{\widehat{\vec{P}}^{\,2}}{2M} \tag{A.12}$$

where $\vec{k}_i$ is the single nucleon momentum and $m_{\rm N}$ the mass of the i-th nucleon, respectively, $\vec{P} = \vec{k}_1 + \vec{k}_2 + \vec{k}_3$ denotes the CM momentum and $M = \sum_i m_{\rm N} = 3\, m_{\rm N}$ the total mass of the system.
Using relative or Jacobi coordinates the CM motion vanishes since $\vec{k}_1 + \vec{k}_2 + \vec{k}_3 = 0$, and we define the Jacobi momenta as:

$$\begin{aligned} \vec{p}_{12} &= \frac{1}{2}\left(\vec{k}_1 - \vec{k}_2\right) \\ \vec{p}_3 &= \frac{2}{3}\vec{k}_3 - \frac{1}{3}\left(\vec{k}_1 + \vec{k}_2\right) \end{aligned} \tag{A.13}$$

Analogous definitions hold for the set of momenta $\vec{p}_{23}$ and $\vec{p}_1$, and for the set $\vec{p}_{31}$ and $\vec{p}_2$, which yields:

$$\begin{aligned} \vec{p}_3 &= -\frac{4}{3}\,\vec{p}_{23} - \frac{2}{3}\,\vec{p}_{12} \\ \vec{p}_3 &= \frac{4}{3}\,\vec{p}_{31} + \frac{2}{3}\,\vec{p}_{12} \end{aligned}$$

Adding the squares of these equations we get:

$$\vec{p}_3^{\,2} = \frac{4}{9}\left[2\left(\vec{p}_{23}^{\,2} + \vec{p}_{23}^{\,2}\right) - \vec{p}_{12}^{\,2}\right]$$

Together with the expressions of the reduced masses (Eq. (2.12), using $\mu_3 = \frac{4}{3}\mu_{12}$ since $m_i = m_{\rm N}$) we insert this into the kinetic energy operator in Jacobi basis:

$$\begin{aligned} \widehat{T}_{\rm 3N} &= \frac{\widehat{\vec{p}}_{12}^{\,2}}{2\mu_{12}} + \frac{\widehat{\vec{p}}_3^{\,2}}{2\mu_3} \\ &= \frac{1}{3}\,\frac{\left(\widehat{\vec{p}}_{12}^{\,2} + \widehat{\vec{p}}_{23}^{\,2} + \widehat{\vec{p}}_{31}^{\,2}\right)}{\mu_{12}} \end{aligned} \tag{A.14}$$

Calculating the expectation value of $\widehat{T}_{\rm 3N}$ we make use of the total antisymmetry of the γ–states which results in a factor (-1) for every exchange of particle i and j, i.e. every two applications of the transposition operator $\widehat{\mathcal{P}}_{ij}$ leaves the

expectation value invariant. More properties of the permutation operator are given in detail in App. A.3.
Neglecting the constant factors we have:

$$\begin{aligned}\langle\gamma'\,|\,\widehat{\vec{p}}_{12}^{\,2}+\widehat{\vec{p}}_{23}^{\,2}+\widehat{\vec{p}}_{31}^{\,2}|\gamma\,\rangle &= \langle\gamma'\,|\,\widehat{\vec{p}}_{12}^{\,2}+\widehat{\mathcal{P}}_{13}\widehat{\mathcal{P}}_{23}\,\widehat{\vec{p}}_{23}^{\,2}\,\widehat{\mathcal{P}}_{23}\widehat{\mathcal{P}}_{13}+\widehat{\mathcal{P}}_{12}\widehat{\mathcal{P}}_{23}\,\widehat{\vec{p}}_{31}^{\,2}\,\widehat{\mathcal{P}}_{23}\widehat{\mathcal{P}}_{12}|\,\gamma\,\rangle \\ &= 3\;\langle\gamma'\,|\widehat{\vec{p}}_{12}^{\,2}\,|\,\gamma\,\rangle\end{aligned}$$

Thus it is shown that the factor 3 in this calculation is a symmetry factor, counting the number of pairs.

$$\Rightarrow \langle\widehat{T}_{3\mathrm{N}}\rangle = \left\langle\frac{\widehat{\vec{p}}_{12}^{\,2}}{\mu_{12}}\right\rangle = 2\,\langle\widehat{T}_{12}\rangle \tag{A.15}$$

With this the generalisation to the A-nucleon system is straight forward:

$$\begin{aligned}\widehat{T}_{A\mathrm{N}} &= \frac{1}{A}\binom{A}{2}\,2\,\widehat{T}_{12} \\ &= \frac{1}{A}\binom{A}{2}\frac{\widehat{\vec{p}}_{12}^{\,2}}{\mu_{12}}\end{aligned} \tag{A.16}$$

Analogous calculations can be done for the isotropic HO potential with 3 nucleons $\widehat{\mathcal{V}}_{3\mathrm{N}} = \frac{1}{2}\,\mu_{12}\,\omega_{12}\,r_{12}^2 + \frac{1}{2}\,\mu_3\,\omega_3\,r_3^2$, resulting in

$$\begin{aligned}\widehat{\mathcal{V}}_{A\mathrm{N}} &= \frac{1}{A}\binom{A}{2}\,\widehat{\mathcal{V}}_{12} \\ &= \frac{1}{A}\binom{A}{2}\,\mu_{12}\,\omega_{12}\,\widehat{r}_{12}^{\,2}\end{aligned} \tag{A.17}$$

A.3 General properties of the transposition operator

- Some useful properties of the transposition operator are:

$$\widehat{\mathcal{P}}_{ij}^{2} = \mathbb{1} \tag{A.18}$$

$$\widehat{\mathcal{P}}_{ij} = \widehat{\mathcal{P}}_{ji} = \widehat{\mathcal{P}}_{ij}^{-1} \tag{A.19}$$

$$\widehat{\mathcal{P}}_{ij}|\,\gamma\,\rangle = -1\,|\,\gamma\,\rangle\,, \tag{A.20}$$

where $|\,\gamma\,\rangle$ is a fully antisymmetrised state. Additionally:

$$\begin{aligned}\widehat{\mathcal{P}}_{ij}\widehat{\mathcal{P}}_{jk} &= \widehat{\mathcal{P}}_{jk}\underbrace{\widehat{\mathcal{P}}_{jk}\widehat{\mathcal{P}}_{ij}\widehat{\mathcal{P}}_{jk}}_{\widehat{\mathcal{P}}_{ik}} \\ &= \widehat{\mathcal{P}}_{jk}\widehat{\mathcal{P}}_{ik}\end{aligned} \tag{A.21}$$

and

$$\begin{aligned}\widehat{\mathcal{P}}_{ij}\widehat{\mathcal{P}}_{jk} &= \underbrace{\widehat{\mathcal{P}}_{ij}\widehat{\mathcal{P}}_{jk}\widehat{\mathcal{P}}_{ij}}_{\widehat{\mathcal{P}}_{ik}}\widehat{\mathcal{P}}_{ij} \\ &= \widehat{\mathcal{P}}_{ik}\widehat{\mathcal{P}}_{ij} \quad .\end{aligned} \tag{A.22}$$

- The full antisymmetrisation operator of the 3N-system can be completely expressed in terms of the transposition operator. Assuming an antisymmetric subsystem (12), this yields:

$$\begin{aligned}\widehat{\mathcal{A}}_{\mathrm{3N}} &= \frac{1}{3!}\sum_{\widehat{\mathcal{P}}\in\mathcal{S}_3}\varepsilon_{\widehat{\mathcal{P}}}\widehat{\mathcal{P}} \\ &= \frac{1}{6}\left(\mathbb{1} - \widehat{\mathcal{P}}_{12} - \widehat{\mathcal{P}}_{23} - \widehat{\mathcal{P}}_{31} + \widehat{\mathcal{P}}_{12}\widehat{\mathcal{P}}_{23} + \widehat{\mathcal{P}}_{23}\widehat{\mathcal{P}}_{31}\right) \\ &\overset{(12)\ \text{antisym.}}{=} \frac{1}{6}\left(\mathbb{1} + \mathbb{1} - \widehat{\mathcal{P}}_{23} - \widehat{\mathcal{P}}_{13}\widehat{\mathcal{P}}_{12}\widehat{\mathcal{P}}_{12} - \widehat{\mathcal{P}}_{23} + \widehat{\mathcal{P}}_{21}\widehat{\mathcal{P}}_{23}\right) \\ &= \frac{1}{6}\left(2\,\mathbb{1} - 3\,\widehat{\mathcal{P}}_{23} - \widehat{\mathcal{P}}_{12}\widehat{\mathcal{P}}_{23}\widehat{\mathcal{P}}_{12}\right) \\ &= \frac{1}{3}\left(\mathbb{1} - 2\,\widehat{\mathcal{P}}_{23}\right) = \frac{1}{A}\left(\mathbb{1} + (A-1)\;\widehat{\mathcal{P}}_{(A-1)A}\right)|_{A=3} \quad .\end{aligned} \tag{A.23}$$

Appendix B

Inclusion of 3NF: generation of $\tilde{\beta}^{(3)}$–states

For the inclusion of 3NF, we need to separate an antisymmetric 3N-subsystem from the γ_{AN}–state similarly to the generation of $|\,\tilde{\beta}^{(2)}_{AN}\rangle$ in Sec. 2.2. In order to perform the required coordinate transformation, two additional sets of intermediate states are needed, denoted by $|\,\beta^{(2)\star}_{AN}\,\rangle$ and $|\,\hat{\beta}^{(2)}_{AN}\,\rangle$. An illustration is depicted in Fig. B.1 i) and ii), respectively.
The $\beta^{(2)\star}$–states are constructed such that a β–state of the $(A-2)$-nucleon system is coupled to an antisymmetric 2N-subsystem, which is a spectator, while for the $\hat{\beta}^{(2)}_{AN}$–states an antisymmetric $(A-3)$-nucleon system couples to a $\beta_{3\mathrm{N}}$–state as spectator. They are defined as

$$|\,\beta^{(2)\star}_{AN}\,\rangle = |\,\big(\mathcal{N}_{(A-2)},\,J_{(A-2)},\,T_{(A-2)}\big)\,\beta_{(A-2)\mathrm{N}}\;\; n_\lambda\,\lambda\;\,(\mathcal{N}_{12},\,J_{12},\,T_{12})\,\gamma_{12}\,;$$
$$\big\{\,\big[J_{A-3}\;\big(l_{A-2}\,s_3\big)\,I_{A-2}\big]\;J_{A-2}\;(\lambda\,J_{12})\,I_\lambda\big\}J_A\;\;\big[\big(T_{A-3}\,t_3\big)\,T_{A-2}\,T_{12}\big]\,T_A\rangle, \tag{B.1}$$

and

$$|\,\hat{\beta}^{(2)}_{AN}\,\rangle = |\,(\mathcal{N}_3,\,J_3,\,T_3)\,\beta_{3\mathrm{N}}\;\; n_\lambda\,\lambda\;\,\big(\mathcal{N}_{(A-3)},\,J_{(A-3)},\,T_{(A-3)}\big)\,\gamma_{(A-3)\mathrm{N}}\,;$$
$$\big\{\,[J_{12}\;(l_3\,s_3)\,I_3]\,J_3\;\big(\lambda\,J_{A-3}\big)\,I_\lambda\big\}J_A\;\;\big[(T_{12}\,t_3)\,T_3\,T_{A-3}\big]\,T_A\rangle\,. \tag{B.2}$$

Based on these definitions, the projections onto the antisymmetric A-nucleon states an be expressed as a triple sum:

$$\langle\gamma\,|\tilde{\beta}^{(3)}\rangle \;\;=\;\; \sum_{\tilde{\beta}^{(2)}\;\beta^{(2)\star}\;\hat{\beta}^{(2)}} \langle\gamma|\tilde{\beta}^{(2)}\rangle\langle\,\tilde{\beta}^{(2)}|\,\beta^{(2)\star}\rangle\langle\beta^{(2)\star}|\hat{\beta^{(2)}}\rangle\langle\hat{\beta^{(2)}}|\tilde{\beta^{(3)}}\rangle$$

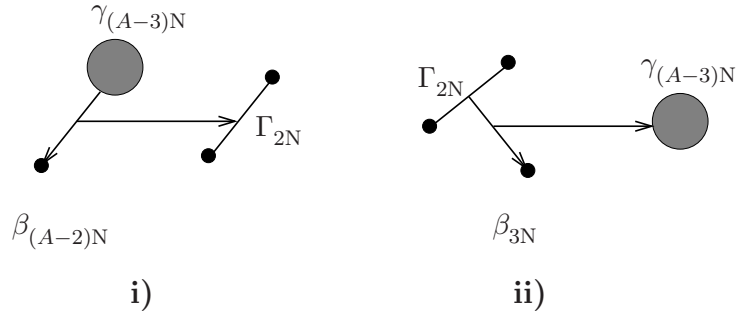

Figure B.1: Illustration of i) $\beta^{(2)\star}_{AN}$– and ii) $\hat{\beta}^{(2)}_{AN}$–states, respectively.

(B.3)

As done before we drop the subscript AN and only label the smaller subsystems here and throughout this appendix. Furthermore, we imply $\delta_{\mathcal{N}_A\mathcal{N}'_A}\,\delta_{J_AJ'_A}\,\delta_{T_AT'_A}$ as usual.
The individual transitions are explicitly evaluated in the following sections, where the coordinate transformation is performed for the overlap $\langle\, \beta^{(2)\star} |\hat{\beta}^{(2)}\,\rangle$. For the projection $\langle \gamma\,|\tilde{\beta}^{(2)}\rangle$ see Sec. 2.2.

B.1 Transition $\langle\, \tilde{\beta}^{(2)} |\, \beta^{(2)\star} \rangle$

For the transition $\langle\, \tilde{\beta}^{(2)} |\, \beta^{(2)\star} \rangle$, the quantum numbers λ, n_λ, I_λ and λ', n'_λ, I'_λ are assigned to the spectators of the $\tilde{\beta}^{(2)}$– and $\beta^{(2)\star}$–states, respectively, as illustrated in Fig. B.2.
In order to account for different couplings and directions of the spectator coordinates of $\tilde{\beta}^{(2)}$– and $\beta^{(2)\star}$–states, a recoupling of their angular momentum part is required. Then, this transition is essentially given by the overlap $\langle\, \gamma\,|\,\beta\,\rangle$ of the $(A-2)$-nucleon system which yields the δ–functions $\delta_{\mathcal{N}_{(A-2)}\mathcal{N}'_{(A-2)}}\,\delta_{J_{(A-2)}J'_{(A-2)}}\,\delta_{T_{(A-2)}T'_{(A-2)}}$.
For the explicit expression we obtain, focussing here on the recoupling:

$$
\begin{aligned}
\langle\, \tilde{\beta}^{(2)} |\, \beta^{(2)\star} \rangle \;&=\; \delta_{\Gamma'_{2\mathrm{N}}\Gamma_{2\mathrm{N}}}\;\delta_{\mathcal{N}_{(A-2)}\mathcal{N}'_{(A-2)}}\,\delta_{J_{(A-2)}J'_{(A-2)}}\,\delta_{T_{(A-2)}T'_{(A-2)}} \\
&\quad\times\Big\langle \big[J_{12}\;(\lambda\,J_{A-2})\,I_\lambda\big]J_A\,|\big\{\big[J'_{A-3}\;\big(l'_{A-2}\,s_3\big)\,I'_{A-2}\big]J'_{A-2}\;(\lambda'\,J'_{12})\,I'_\lambda\big\}J_A\Big\rangle \\
&=\; \Big\langle \big[J_{12}\;(\lambda\,J_{A-2})\,I_\lambda\big]J_A\,|\big[J_{A-2}\;(\lambda'\,J_{12})\,I'_\lambda\big]J_A\Big\rangle \\
&=\; (-1)^{J_{12}+\lambda+J_{A-2}+J_A} \\
&\quad\times \hat{I}_\lambda\,\hat{I''_\lambda}\,\left\{\begin{array}{ccc} J_{12} & \lambda & I''_\lambda \\ J_{A-2} & J_A & I_\lambda \end{array}\right\}
\end{aligned}
$$

$$
\begin{aligned}
&\times\Big\langle \big[\,(J_{12}\,\lambda)\,I''_\lambda\;J_{A-2}\big]\,J_A\,\big|\big[J_{A-2}\;\;(\lambda'\,J_{12})\,I'_\lambda\big]\,J_A\,\Big\rangle \\
= \;& (-1)^{J_{12}+\lambda+J_{A-2}+J_A+I''_\lambda-J_{12}-\lambda} \\
&\times \hat{I}_\lambda\,\hat{I''_\lambda}\,\left\{\begin{array}{ccc} J_{12} & \lambda & I''_\lambda \\ J_{A-2} & J_A & I_\lambda \end{array}\right\} \\
&\times\Big\langle \big[\,(\lambda\,J_{12})\,I''_\lambda\;J_{A-2}\big]\,J_A\,\big|\big[J_{A-2}\;\;(\lambda'\,J_{12})\,I'_\lambda\big]\,J_A\,\Big\rangle \\
= \;& (-1)^{J_{A-2}+J_A+I''_\lambda+J_A-J_{A-2}-I''_\lambda} \\
&\times \hat{I}_\lambda\,\hat{I''_\lambda}\,\left\{\begin{array}{ccc} J_{12} & \lambda & I''_\lambda \\ J_{A-2} & J_A & I_\lambda \end{array}\right\} \\
&\times\Big\langle \big[J_{A-2}\;\;(\lambda\,J_{12})\,I''_\lambda\big]\,J_A\,\big|\big[J_{A-2}\;\;(\lambda'\,J_{12})\,I'_\lambda\big]\,J_A\,\Big\rangle \\
\\
= \;& \delta_{\lambda'\,\lambda}\,\delta_{I'_\lambda\,I''_\lambda}\,(-1)^{2J_A}\;\hat{I}_\lambda\,\hat{I''_\lambda}\,\left\{\begin{array}{ccc} J_{12} & \lambda & I''_\lambda \\ J_{A-2} & J_A & I_\lambda \end{array}\right\}\,. \qquad \text{(B.4)}
\end{aligned}
$$

For the isospin matrix elements, the recoupling simply results in a phase factor:

$$
\Big\langle\,(T_{12}\,T_{A-2})\,T_A\,\big|\,(T_{A-2}\,T_{12})\,T_A\,\Big\rangle \;=\; (-1)^{T_A-T_{12}-T_{A-2}}\,. \qquad \text{(B.5)}
$$

Furthermore, another phase factor is originated from the opposite direction of λ and λ', which leads to the full expression:

$$
\begin{aligned}
\langle\tilde{\beta}^{(2)}|\beta^{(2)\star}\rangle \;=\; & (-1)^{\lambda+2J_A+T_A-T_{12}-T_{A-2}}\;\hat{I}_\lambda\,\hat{I}'_\lambda \\
& \times\left\{\begin{array}{ccc} J_{12} & \lambda & I'_\lambda \\ J_{A-2} & J_A & I_\lambda \end{array}\right\}\,\langle\,\gamma_{(A-2)\mathrm{N}}\,|\,\beta_{(A-2)\mathrm{N}}\,\rangle\,, \qquad \text{(B.6)}
\end{aligned}
$$

where now the overlap $\langle\,\gamma_{(A-2)\mathrm{N}}\,|\,\beta_{(A-2)\mathrm{N}}\,\rangle$ of the $(A-1)$-nucleon system is included.

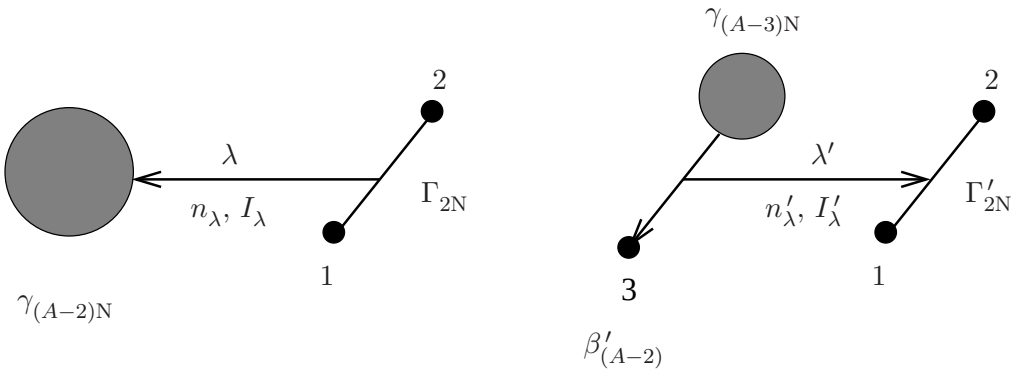

Figure B.2: Illustration of the transition $\langle\tilde{\beta}^{(2)}|\beta^{(2)\star}\rangle$.

B.2 Transition $\langle\beta^{(2)\star}|\hat{\beta}^{(2)}\rangle$

Fig. B.3 visualises the transition $\langle\beta^{(2)\star}|\hat{\beta}^{(2)}\rangle$. Since we have to evaluate the coordinate transformation here, we proceed analogously to Eqs. (2.15)- (2.19):

a) JJ**-coupling** $\rightarrow$ LS**-coupling :**

First, we disentangle the angular momentum part according to:

$$\Big\langle \Big\{ \big[J'_{A-3}\ \big(l'_{A-2}\, s_3\big)\, I'_{A-2}\big] J'_{A-2}\ (\lambda'\, J'_{12})\, I'_\lambda \Big\}\, J'_A \,|\, \Big\{ \big[J_{12}\ (l_3\, s_3)\, I_3\big] J_3\ (\lambda\, J_{A-3})\, I_\lambda \Big\}\, J_A \Big\rangle$$

$$= \Big\langle \Big\{ \big[J_{A-3}\ \big(l'_{A-2}\, s_3\big)\, I'_{A-2}\big] J_{A-2}\ (\lambda'\, J_{12})\, I'_\lambda \Big\}\, J_A \,|\, \Big\{ \big[J_{12}\ (l_3\, s_3)\, I_3\big] J_3\ (\lambda\, J_{A-3})\, I_\lambda \Big\}\, J_A \Big\rangle$$

$$= (-1)^{I'_{A-2}-l'_{A-2}-s_3+I_3-l_3-s_3}$$

$$\times \Big\langle \Big\{ \big[J_{A-3}\ \big(s_3\, l'_{A-2}\big)\, I'_{A-2}\big] J_{A-2}\ (\lambda'\, J_{12})\, I'_\lambda \Big\}\, J_A \,|\, \Big\{ \big[J_{12}\ (s_3\, l_3)\, I_3\big] J_3\ (\lambda\, J_{A-3})\, I_\lambda \Big\}\, J_A \Big\rangle$$

$$= (-1)^{I'_{A-2}-l'_{A-2}-s_3+I_3-l_3-s_3}$$
$$\times\ (-1)^{J_{A-3}+s_3+l'_{A-2}+J'_{A-2}+J_{12}+s_3+l_3+J_3}$$

$$\times \sum_{S'_{A-1}S_3} \hat{S}'_{A-2}\,\hat{I}'_{A-2} \begin{Bmatrix} J_{A-3} & s_3 & S'_{A-2} \\ l'_{A-2} & J'_{A-2} & I'_{A-2} \end{Bmatrix} \hat{S}_3\,\hat{I}_3 \begin{Bmatrix} J_{12} & s_3 & S_3 \\ l_3 & J_3 & I_3 \end{Bmatrix}$$

$$\times \Big\langle \Big\{ \big[\ \big(J_{A-3}\, s_3\big)\, S'_{A-2}\, l'_{A-2}\big] J'_{A-2}\, (\lambda'\, J_{12})\, I'_\lambda \Big\}\, J_A \,|\, \Big\{ \big[\ (J_{12}\, s_3)\, S_3\, l_3\big] J_3\ (\lambda\, J_{A-3})\, I_\lambda \Big\}\, J_A \Big\rangle$$

$$= (-1)^{I'_{A-2}+I_3+J_{A-3}+J'_{A-2}+J_{12}+J_3}$$
$$\times\ (-1)^{-J'_{A-2}+l'_{A-2}+S'_{A-2}-J_3+S_3+l_3}$$

$$
\begin{aligned}
&\times \sum_{S'_{A-1}S_3} \hat{S}'_{A-2}\,\hat{I}'_{A-2} \left\{ \begin{array}{ccc} J_{A-3} & s_3 & S'_{A-2} \\ l'_{A-2} & J'_{A-2} & I'_{A-2} \end{array} \right\} \hat{S}_3\,\hat{I}_3 \left\{ \begin{array}{ccc} J_{12} & s_3 & S_3 \\ l_3 & J_3 & I_3 \end{array} \right\} \\
&\times \Big\langle \Big\{ \big[\, l'_{A-2} \;\; (J_{A-3}\, s_3)\, S'_{A-2} \big] J'_{A-2}\, (\lambda'\, J_{12})\, I'_\lambda \Big\}\, J_A \,|\, \Big\{ \big[\, l_3 \;\; (J_{12}\, s_3)\, S_3 \big] J_3 \;\; (\lambda\, J_{A-3})\, I_\lambda \Big\}\, J_A \Big\rangle \\
&= (-1)^{I'_{A-2}+I_3+J_{A-3}+J_{12}+l'_{A-2}+S'_{A-2}+S_3+l_3} \\
&\times\; (-1)^{-S'_{A-2}+s_3+J_{A-3}-S_3+J_{12}+s_3} \\
&\times \sum_{S'_{A-1}S_3} \hat{S}'_{A-2}\,\hat{I}'_{A-2} \left\{ \begin{array}{ccc} J_{A-3} & s_3 & S'_{A-2} \\ l'_{A-2} & J'_{A-2} & I'_{A-2} \end{array} \right\} \hat{S}_3\,\hat{I}_3 \left\{ \begin{array}{ccc} J_{12} & s_3 & S_3 \\ l_3 & J_3 & I_3 \end{array} \right\} \\
&\times \Big\langle \Big\{ \big[\, l'_{A-2} \;\; (s_3\, J_{A-3})\, S'_{A-2} \big] J'_{A-2}\, (\lambda'\, J_{12})\, I'_\lambda \Big\}\, J_A \,|\, \Big\{ \big[\, l_3 \;\; (s_3\, J_{12})\, S_3 \big] J_3 \;\; (\lambda\, J_{A-3})\, I_\lambda \Big\}\, J_A \Big\rangle \\
&= (-1)^{I'_{A-2}+I_3+2J_{A-3}+l'_{A-2}+l_3+2s_3} \\
&\times \sum_{S'_{A-1}S_3} \hat{S}'_{A-2}\,\hat{I}'_{A-2} \left\{ \begin{array}{ccc} J_{A-3} & s_3 & S'_{A-2} \\ l'_{A-2} & J'_{A-2} & I'_{A-2} \end{array} \right\} \hat{S}_3\,\hat{I}_3 \left\{ \begin{array}{ccc} J_{12} & s_3 & S_3 \\ l_3 & J_3 & I_3 \end{array} \right\} \\
&\times \Big\langle \Big\{ \big[\, l'_{A-2} \;\; (s_3\, J_{A-3})\, S'_{A-2} \big] J'_{A-2}\, (\lambda'\, J_{12})\, I'_\lambda \Big\}\, J_A \,|\, \Big\{ \big[\, l_3 \;\; (s_3\, J_{12})\, S_3 \big] J_3 \;\; (\lambda\, J_{A-3})\, I_\lambda \Big\}\, J_A \Big\rangle
\end{aligned}
\tag{B.7}
$$

b) <u>isospin T matrix elements:</u>

Step a) already recouples the spins. For the isospin T we get:

$$
\begin{aligned}
&\big\langle \big[(T_{A-3}\, t_3)\, T'_{A-2}\; T_{12} \big]\, T_A | \, \big[(T_{12}\, t_3)\, T_3\; T_{A-3} \big]\, T_A \big\rangle \\
&\qquad = (-1)^{T'_{A-2}-T_{A-3}-t_3-T_3+T_{12}+t_3} \\
&\qquad\quad \times \big\langle \big[(t_3\, T_{A-3})\, T'_{A-2}\; T_{12} \big]\, T_A | \, \big[(t_3\, T_{12})\, T_3\; T_{A-3} \big]\, T_A \big\rangle \\
&\qquad = (-1)^{T'_{A-2}-T_{A-3}-T_3+T_{12}} \\
&\qquad\quad \times \big\langle \big[(t_3\, T_{A-3})\, T'_{A-2}\; T_{12} \big]\, T_A | \, \big[(t_3\, T_{12})\, T_3\; T_{A-3} \big]\, T_A \,. \big\rangle
\end{aligned}
\tag{B.8}
$$

Using the HO bracket for the corresponding transformation space and considering that this transformation implies $\delta_{\Gamma'_{2N}\Gamma_{2N}}$ and $\delta_{\Gamma'_{(A-3)N}\Gamma_{(A-3)N}}$, one obtains:

$$
\begin{aligned}
&\langle \beta^{(2)\star} | \hat{\beta}^{(2)} \rangle \\
&\quad = \delta_{\Gamma'_{2N}\Gamma_{2N}}\, \delta_{\Gamma'_{(A-3)N}\Gamma_{(A-3)N}}
\end{aligned}
$$

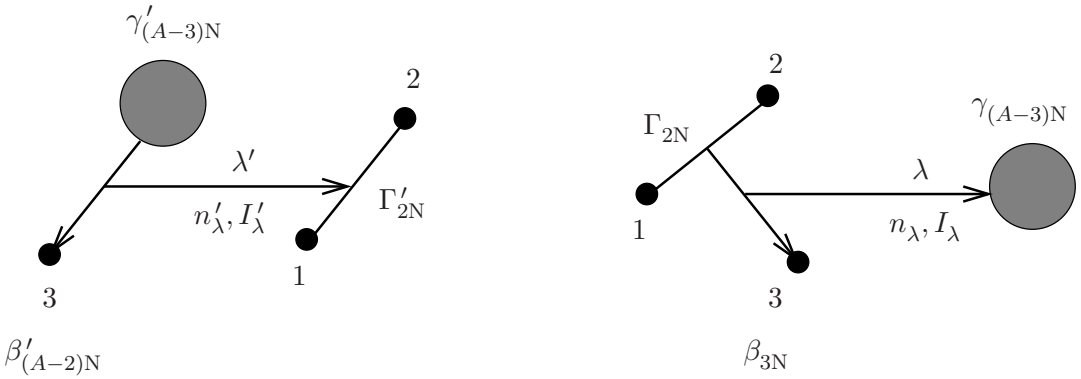

Figure B.3: Illustration of the transition $\langle\beta^{(2)\star}|\hat{\beta}^{(2)}\rangle$.

$$
\begin{aligned}
&\times (-1)^{I'_{A-2}+I_3+2J_{A-3}+l'_{A-2}+l_3+2s_3} \\
&\times (-1)^{J_{12}+J_{A-3}+2T'_{A-2}+2T_{12}+\lambda'+\lambda} \\
&\times \hat{I}'_{A-2}\,\hat{I}_3\,\hat{J}'_{A-2}\,\hat{I}'_\lambda\,\hat{J}_3\,\hat{I}_\lambda\,\hat{T}'_{A-2}\,\hat{T}_3 \\
&\times \sum_{S'_{A-1}S_3} (-1)^{S'_{A-2}+S_3}\,\hat{S}'^2_{A-2}\,\hat{S}^2_3 \left\{ \begin{array}{ccc} J_{A-3} & s_3 & S'_{A-2} \\ l'_{A-2} & J'_{A-2} & I'_{A-2} \end{array} \right\} \left\{ \begin{array}{ccc} J_{12} & s_3 & S_3 \\ l_3 & J_3 & I_3 \end{array} \right\} \\
&\times \sum_{LS} \hat{L}^2\,\hat{S}^2 \left\{ \begin{array}{ccc} J_{12} & s_3 & S_3 \\ J_{A-3} & S & S'_{A-2} \end{array} \right\} \left\{ \begin{array}{ccc} T_{12} & t_3 & T_3 \\ T_{A-3} & T_A & T'_{A-2} \end{array} \right\} \\
&\quad \times \left\{ \begin{array}{ccc} l'_{A-2} & S'_{A-2} & J'_{A-2} \\ \lambda' & J_{12} & I'_\lambda \\ L & S & J_A \end{array} \right\} \left\{ \begin{array}{ccc} l_3 & S_3 & J_3 \\ \lambda & J_{A-3} & I_\lambda \\ L & S & J_A \end{array} \right\} \\
&\quad \times \langle n'_{A-2}\,l'_{A-2}\,,\; n'_\lambda\,\lambda' : L|\, n_3\,l_3,\; n_\lambda\,\lambda : L\rangle_{d=\frac{2(A-3)}{A}}\ . \qquad \text{(B.9)}
\end{aligned}
$$

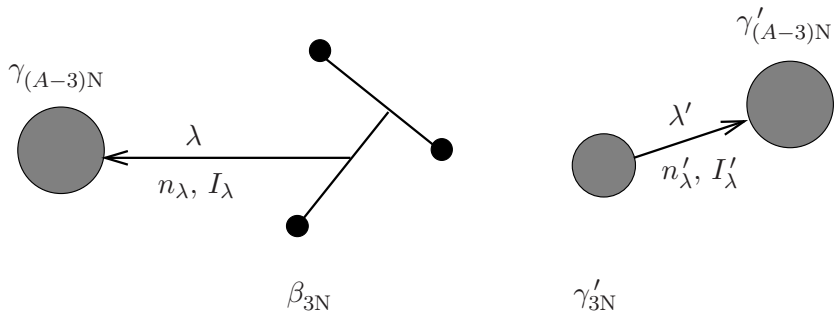

Figure B.4: Illustration of the transition $\langle\hat{\beta}^{(2)}|\tilde{\beta}^{(3)}\rangle$

B.3 Transition $\langle\,\hat{\beta}^{(2)}|\,\tilde{\beta}^{(3)}\rangle$

This overlap is a rather simple one, see Fig. B.4: since the $\gamma_{(A-3)\mathrm{N}}$–state remains unchanged for this transition, this reduces to the antisymmetrisation of the 3N-subsystem of the $\hat{\beta}^{(2)}$–states, which is given by the $\langle\,\beta\,|\,\gamma\,\rangle$–coefficients of the 3N-system. Therefore, this projection yields:

$$\langle\hat{\beta}^{(2)}|\tilde{\beta}^{(3)}\rangle \;=\; \delta_{\Gamma'_{A-3}\Gamma_{A-3}}\;\delta_{\lambda'\lambda}\,\delta_{n'_\lambda n_\lambda}\,\delta_{I'_\lambda I_\lambda}\langle\,\beta_{3\mathrm{N}}|\,\gamma_{3\mathrm{N}}\rangle\,. \tag{B.10}$$

Based on this three-step procedure, we were able to implement a code that calculates $\langle\,\gamma\,|\,\tilde{\beta}^{(3)}\,\rangle$-overlaps. First sets of coefficients have been generated and orthogonality relations checked.

Bibliography

[1] H. D. Politzer, "Reliable Perturbative Results for Strong Interactions?," *Phys.Rev.Lett.* **30** (1973) 1346–1349.

[2] D. Gross and F. Wilczek, "Ultraviolet Behavior of Nonabelian Gauge Theories," *Phys.Rev.Lett.* **30** (1973) 1343–1346.

[3] S. Dürr, Z. Fodor, J. Frison, C. Hoelbling, R. Hoffmann, *et al.*, "Ab-Initio Determination of Light Hadron Masses," *Science* **322** (2008) 1224–1227, `arXiv:0906.3599 [hep-lat]`.

[4] S. R. Beane, W. Detmold, K. Orginos, and M. J. Savage, "Nuclear Physics from Lattice QCD," *Prog. Part. Nucl. Phys.* **66** (2011) 1–40, `arXiv:1004.2935 [hep-lat]`.

[5] V. G. J. Stoks, R. A. M. Klomp, C. P. F. Terheggen, and J. J. de Swart, "Construction of high quality NN potential models," *Phys. Rev.* **C 49** (1994) 2950–2962, `arXiv:nucl-th/9406039`.

[6] R. Machleidt, "The high-precision, charge-dependent Bonn nucleon-nucleon potential (CD-Bonn)," *Phys. Rev.* **C 63** (2001) 024001, `arXiv:nucl-th/0006014`.

[7] R. B. Wiringa, V. G. J. Stoks, and R. Schiavilla, "An accurate nucleon-nucleon potential with charge independence breaking," *Phys. Rev.* **C 51** (1995) 38–51, `arXiv:nucl-th/9408016`.

[8] N. Kalantar-Nayestanaki, E. Epelbaum, J. G. Messchendorp, and A. Nogga, "Signatures of three-nucleon interactions in few-nucleon systems," *Rept. Prog. Phys.* **75** (2012) 016301, `arXiv:1108.1227 [nucl-th]`.

[9] W. N. Polyzou and W. Glöckle, "Three-body interactions and on-shell equivalent two-body interactions," *Few Body Syst.* **9** (1990) 97–121.

[10] A. Amghar and B. Desplanques, "Are all models of the N N interaction independent of each other?," *Nucl. Phys.* **A585** (1995) 657–692.

[11] S. A. Coon, M. D. Scadron, P. C. McNamee, B. R. Barrett, D. W. E. Blatt, and B. H. J. McKellar, "The two pion exchange, three nucleon potential and nuclear matter," *Nucl. Phys.* **A317** (1979) 242–278.

[12] B. S. Pudliner, V. R. Pandharipande, J. Carlson, and R. B. Wiringa, "Quantum Monte Carlo calculations of $A \leq 6$ nuclei," *Phys. Rev. Lett.* **74** (1995) 4396–4399.

[13] S. C. Pieper, V. R. Pandharipande, R. B. Wiringa, and J. Carlson, "Realistic models of pion-exchange three-nucleon interactions," *Phys. Rev.* **C 64** (2001) 014001, arXiv:nucl-th/0102004.

[14] **Particle Data Group** Collaboration, C. Amsler *et al.*, "Review of particle physics," *Phys. Lett.* **B667** (2008) 1.

[15] J. Goldstone, A. Salam, and S. Weinberg, "Broken Symmetries," *Phys. Rev.* **127** (1962) 965–970.

[16] V. Bernard, N. Kaiser, and U.-G. Meißner, "Chiral dynamics in nucleons and nuclei," *Int. J. Mod. Phys.* **E4** (1995) 193–346, arXiv:hep-ph/9501384.

[17] S. Weinberg, "Nuclear forces from chiral Lagrangians," *Phys. Lett.* **B251** (1990) 288–292.

[18] S. Weinberg, "Effective chiral Lagrangians for nucleon - pion interactions and nuclear forces," *Nucl. Phys.* **B363** (1991) 3–18.

[19] S. Weinberg, "Three body interactions among nucleons and pions," *Phys. Lett.* **B295** (1992) 114–121, arXiv:hep-ph/9209257.

[20] E. Epelbaum, "Few-nucleon forces and systems in chiral effective field theory," *Prog. Part. Nucl. Phys.* **57** (2006) 654–741, arXiv:nucl-th/0509032.

[21] E. Epelbaum, "Few-nucleon forces and systems in chiral effective field theory," *Few Body Syst.* **43** (2008) 57–62.

[22] E. Epelbaum, A. Nogga, W. Glöckle, H. Kamada, U.-G. Meißner, and H. Witała, "Three-nucleon forces from chiral effective field theory," *Phys. Rev.* **C 66** (2002) 064001, arXiv:nucl-th/0208023.

[23] A. Nogga, P. Navrátil, B. R. Barrett, and J. P. Vary, "Spectra and binding energy predictions of chiral interactions for ^{7}Li," *Phys. Rev.* **C 73** (2006) 064002, arXiv:nucl-th/0511082.

[24] P. Navrátil, V. G. Gueorguiev, J. P. Vary, W. E. Ormand, and A. Nogga, "Structure of $A = 10 - 13$ nuclei with two- plus three-nucleon interactions from chiral effective field theory," *Phys. Rev. Lett.* **99** (2007) 042501, arXiv:nucl-th/0701038.

[25] D. Gazit, S. Quaglioni, and P. Navrátil, "Three-Nucleon Low-Energy Constants from the Consistency of Interactions and Currents in Chiral Effective Field Theory," *Phys. Rev. Lett.* **103** (2009) 102502, arXiv:0812.4444 [nucl-th].

[26] D. R. Entem and R. Machleidt, "Accurate Charge-Dependent Nucleon-Nucleon Potential at Fourth Order of Chiral Perturbation Theory," *Phys. Rev.* **C 68** (2003) 041001, arXiv:nucl-th/0304018.

[27] E. Epelbaum, W. Glöckle, and U.-G. Meißner, "The two-nucleon system at next-to-next-to-next-to-leading order," *Nucl. Phys.* **A747** (2005) 362–424, arXiv:nucl-th/0405048.

[28] V. Bernard, E. Epelbaum, H. Krebs, and U.-G. Meißner, "Subleading contributions to the chiral three-nucleon force I: long-range terms," *Phys. Rev.* **C 77** (2008) 064004, arXiv:0712.1967 [nucl-th].

[29] V. Bernard, E. Epelbaum, H. Krebs, and U.-G. Meißner, "Subleading contributions to the chiral three-nucleon force II: Short-range terms and relativistic corrections," *Phys. Rev.* **C 84** (2011) 054001, arXiv:1108.3816 [nucl-th].

[30] E. Epelbaum, "Four-nucleon force in chiral effective field theory," *Phys. Lett.* **B639** (2006) 456–461, arXiv:nucl-th/0511025.

[31] E. Epelbaum, "Four-nucleon force using the method of unitary transformation," *Eur. Phys. J.* **A 34** (2007) 197–214, arXiv:0710.4250 [nucl-th].

[32] R. Skibiński, J. Golak, K. Topolnicki, H. Witała, E. Epelbaum, W. Glöckle, H. Krebs, A. Nogga, and H. Kamada, "The triton with long-range chiral N^3LO three nucleon forces," *Phys.Rev.* **C84** (2011) 054005, arXiv:1107.5163 [nucl-th].

[33] A. Nogga, E. Epelbaum, J. Golak, H. Kamada, H. Witała, D. Rozpędzik, R. Skibiński, and W. Glöckle, "Four-nucleon force contribution to the binding energy of ^{4}He," in *19th International IUPAP Conference on Few-Body Problems in Physics*, vol. 3 of *EPJ Web of Conferences*, p. 05006. 2010. August 31 - September 5, 2009.

[34] E. Epelbaum, W. Glöckle, and U.-G. Meißner, "Low-momentum effective theory for nucleons," *Phys. Lett.* **B439** (1998) 1–5, arXiv:nucl-th/9804005.

[35] S. Bogner, R. Furnstahl, and A. Schwenk, "From low-momentum interactions to nuclear structure," 0912.3688. http://arxiv.org/abs/0912.3688.

[36] S. K. Bogner, R. J. Furnstahl, and R. J. Perry, "Similarity renormalization group for nucleon-nucleon interactions," *Phys. Rev.* **C 75** (2007) 061001, arXiv:nucl-th/0611045.

[37] M. Viviani, A. Deltuva, R. Lazauskas, J. Carbonell, A. Fonseca, *et al.*, "Benchmark calculation of n-^3H and p-^3He scattering," *Phys.Rev.* **C84** (2011) 054010, arXiv:1109.3625 [nucl-th].

[38] R. Lazauskas *et al.*, "Low energy $n -^3$ H scattering : a novel testground for nuclear interaction," *Phys. Rev.* **C 71** (2005) 034004, arXiv:nucl-th/0412089.

[39] A. Kievsky, M. Viviani, and S. Rosati, "Polarization observables in p-d scattering below 30 MeV," *Phys. Rev.* **C 64** (2001) 024002, arXiv:nucl-th/0103058.

[40] W. Glöckle, H. Witała, D. Hüber, H. Kamada, and J. Golak, "The Three nucleon continuum: Achievements, challenges and applications," *Phys. Rept.* **274** (1996) 107–285.

[41] A. Nogga, H. Kamada, and W. Glöckle, "Solution of the Faddeev-Yakubovsky equations using realistic NN and 3N interaction," *Nucl. Phys.* **A689** (2001) 357–360, arXiv:nucl-th/0010005. Proceedings of the "17th European Conference on Few-Body Problems in Physics", Évora, 2000.

[42] H. Witała, J. Golak, R. Skibiński, W. Glöckle, H. Kamada, and W. N. Polyzou, "Three-nucleon force in relativistic three-nucleon Faddeev calculations," *Phys. Rev.* **C 83** (2011) 044001, arXiv:1101.4053 [nucl-th].

[43] A. Deltuva, A. Fonseca, and R. Lazauskas, "Faddeev equation approach for three-cluster nuclear reactions," arXiv:1201.4979 [nucl-th].

[44] A. Nogga, H. Kamada, W. Glöckle, and B. R. Barrett, "The α-particle based on modern nuclear forces," *Phys. Rev.* **C 65** (2002) 054003, arXiv:nucl-th/0112026.

[45] M. Viviani, A. Kievsky, and S. Rosati, "Calculation of the Alpha–Particle Ground State within the Hyperspherical Harmonic Basis," *Phys. Rev.* **C 71** (2005) 024006, arXiv:nucl-th/0408019.

[46] M. Gattobigio, A. Kievsky, M. Viviani, and P. Barletta, "The Harmonic hyperspherical basis for identical particles without permutational symmetry," *Phys.Rev.* **A79** (2009) 032513, arXiv:0811.4259 [physics.comp-ph].

[47] M. Gattobigio, A. Kievsky, and M. Viviani, "Non-symmetrized hyperspherical harmonic basis for A-bodies," *Phys.Rev.* **C83** (2011) 024001, arXiv:1009.3426 [nucl-th].

[48] W. Leidemann, G. Orlandini, S. Bacca, and N. Barnea, "Effective interaction method for hyperspherical harmonics," *Nucl. Phys.* **A737** (2004) 231–235.

[49] G. Orlandini, N. Barnea, and W. Leidemann, "The Effective interaction hyperspherical harmonics method for non-local potentials," arXiv:1008.4492 [nucl-th].

[50] S. Bacca, N. Barnea, and A. Schwenk, "Matter and charge radius of ^{6}He in the hyperspherical-harmonics approach," *Phys. Rev. C* **86** (2012) 034321, arXiv:1202.0516 [nucl-th].

[51] N. Barnea, V. D. Efros, W. Leidemann, and G. Orlandini, "Incorporation of three-nucleon force in the effective interaction hyperspherical harmonic approach," *Few Body Syst.* **35** (2004) 155–167, arXiv:nucl-th/0404086.

[52] H. Kamada, A. Nogga, W. Glöckle, E. Hiyama, M. Kamimura, K. Varga, Y. Suzuki, M. Viviani, A. Kievsky, S. Rosati, J. Carlson, S. C. Pieper, R. B. Wiringa, P. Navrátil, B. R. Barrett, N. Barnea, W. Leidemann, and G. Orlandini, "Benchmark Test Calculation of a Four-Nucleon Bound State," *Phys. Rev.* **C 64** (2001) 044001, arXiv:nucl-th/0104057.

[53] Y. Suzuki and K. Varga, "Stochastic variational approach to quantum-mechanical few body problems," *Lect. Notes Phys.* **M54** (1998) 1–310.

[54] R. B. Wiringa, S. C. Pieper, J. Carlson, and V. R. Pandharipande, "Quantum Monte Carlo calculations of A=8 nuclei," *Phys. Rev.* **C 62** (2000) 014001, arXiv:nucl-th/0002022.

[55] S. C. Pieper, R. B. Wiringa, and J. Carlson, "Quantum Monte Carlo calculations of excited states in A = 6–8 nuclei," *Phys. Rev.* **C 70** (2004) 054325, arXiv:nucl-th/0409012.

[56] S. C. Pieper and R. B. Wiringa, "Quantum Monte Carlo Calculations of Light Nuclei," *Ann. Rev. Nucl. Part. Sci.* **51** (2001) 53–90, arXiv:nucl-th/0103005.

[57] S. C. Pieper, K. Varga, and R. B. Wiringa, "Quantum Monte Carlo calculations of $A = 9, 10$ nuclei," *Phys. Rev.* **C 66** (2002) 044310, arXiv:nucl-th/0206061.

[58] E. Epelbaum, H. Krebs, D. Lee, and U.-G. Meißner, "Lattice effective field theory calculations for A = 3,4,6,12 nuclei," *Phys. Rev. Lett.* **104** (2010) 142501, arXiv:0912.4195 [nucl-th].

[59] E. Epelbaum, H. Krebs, T. A. Lähde, D. Lee, and U.-G. Meißner, "The fate of carbon-based life as a function of the light quark mass," arXiv:1212.4181 [nucl-th].

[60] D. Lee, "Lattice simulations for few- and many-body systems," *Prog. Part. Nucl. Phys.* **63** (2009) 117–154, arXiv:0804.3501 [nucl-th].

[61] F. Hoyle, "On Nuclear Reactions Occuring in Very Hot Stars. I the Synthesis of Elements from Carbon to Nickel," *Astrophys. J. Suppl. Ser.* **1** (1954) 121.

[62] C. Cook, W. Fowler, C. Lauritsen, and T. Lauritsen, "B-12, C-12, and the Red Giants," *Phys.Rev.* **107** (1957) 508–515.

[63] E. Epelbaum, H. Krebs, D. Lee, and U.-G. Meißner, "Ab initio calculation of the Hoyle state," *Phys. Rev. Lett.* **106** (2011) 192501, arXiv:1101.2547 [nucl-th].

[64] E. Epelbaum, H. Krebs, T. Lahde, D. Lee, and U.-G. Meißner, "Structure and rotations of the Hoyle state," *Phys. Rev. Lett.* **109** (2012) 252501, arXiv:1208.1328 [nucl-th].

[65] Collaborative Research Centre (CRC) 110, "Symmetries and the Emergence of Structure in QCD." Funded by dfg and nsfc.

[66] R. Roth and P. Navrátil, "Ab Initio Study of ^{40}Ca with an Importance Truncated No-Core Shell Model," *Phys. Rev. Lett.* **99** (2007) 092501, arXiv:0705.4069 [nucl-th].

[67] D. J. Dean, G. Hagen, M. Hjorth-Jensen, T. Papenbrock, and A. Schwenk, "Comment on 'Ab Initio study of ^{40}Ca with an importance- truncated no-core shell model'," *Phys. Rev. Lett.* **101** (2008) 119201, arXiv:0709.0449 [nucl-th].

[68] S. Bogner, R. Furnstahl, P. Maris, R. Perry, A. Schwenk, and J. P. Vary, "Convergence in the no-core shell model with low-momentum two-nucleon interactions," *Nucl.Phys.* **A801** (2008) 21–42, arXiv:0708.3754 [nucl-th].

[69] P. Navrátil, G. P. Kamuntavicius, and B. R. Barrett, "Few-nucleon systems in translationally invariant harmonic oscillator basis," *Phys. Rev.* **C 61** (2000) 044001, arXiv:nucl-th/9907054.

[70] P. Navrátil and B. R. Barrett, "Shell-model calculations for the three-nucleon system," *Phys. Rev.* **C 57** (1998) 562–568, arXiv:nucl-th/9711027.

[71] P. Navrátil and B. R. Barrett, "Four-nucleon shell-model calculations in a Faddeev-like approach," *Phys. Rev.* **C 59** (1999) 1906–1918, arXiv:nucl-th/9812062.

[72] G. Hagen, T. Papenbrock, D. J. Dean, and M. Hjorth-Jensen, "Ab initio coupled-cluster approach to nuclear structure with modern nucleon-nucleon interactions," *Phys. Rev.* **C 82** (2010) 034330, arXiv:1005.2627 [nucl-th].

[73] G. Jansen, M. Hjorth-Jensen, G. Hagen, and T. Papenbrock, "Toward open-shell nuclei with coupled-cluster theory," *Phys.Rev.* **C83** (2011) 054306, arXiv:1102.1293 [nucl-th].

[74] G. R. Jansen, "Spherical coupled-cluster theory for open-shell nuclei," arXiv:1207.7099 [nucl-th].

[75] F. Coester, "Bound states of a many-particle system," *Nuclear Physics* **7** (1958) no. 0, 421 – 424. http://www.sciencedirect.com/science/article/pii/0029558258902803.

[76] F. Coester and H. KÃmmel, "Short-range correlations in nuclear wave functions," *Nuclear Physics* **17** (1960) no. 0, 477 – 485. http://www.sciencedirect.com/science/article/pii/0029558260901401.

[77] R. J. Bartlett, "Coupled-cluster approach to molecular structure and spectra: a step toward predictive quantum chemistry," *The Journal of Physical Chemistry* **93** (1989) no. 5, 1697–1708, http://pubs.acs.org/doi/pdf/10.1021/j100342a008. http://pubs.acs.org/doi/abs/10.1021/j100342a008.

[78] G. Hagen, T. Papenbrock, D. J. Dean, A. Schwenk, A. Nogga, M. Włoch, and P. Piecuch, "Coupled-cluster theory for three-body Hamiltonians," *Phys. Rev.* **C 76** (2007) 034302, arXiv:0704.2854 [nucl-th].

[79] B. Gebremariam, S. K. Bogner, and T. Duguet, "Microscopically-constrained Fock energy density functionals from chiral effective field theory. I. Two- nucleon interactions," *Nucl. Phys.* **A851** (2010) no. 1, 17–43, arXiv:1003.5210 [nucl-th].

[80] M. Stoitsov, M. Kortelainen, S. Bogner, T. Duguet, R. Furnstahl, B. Gebremariam, and N. Schunck, "Microscopically-based energy density functionals for nuclei using the density matrix expansion: Implementation and pre-optimization," *Phys. Rev.* **C 82** (2010) 054307, arXiv:1009.3452 [nucl-th].

[81] N. Kaiser and W. Weise, "Nuclear energy density functional from chiral pion-nucleon dynamics revisited," *Nucl. Phys.* **A836** (2010) 256–274, arXiv:0912.3207 [nucl-th].

[82] N. Kaiser, "Nuclear energy density functional from chiral pion-nucleon dynamics: Isovector terms," *Eur.Phys.J.* **A45** (2010) 61–68, arXiv:1003.1143 [nucl-th].

[83] N. Kaiser, "Isovector part of nuclear energy density functional from chiral two- and three-nucleon forces," *Eur.Phys.J.* **A48** (2012) 36, arXiv:1203.6284 [nucl-th].

[84] P. Navrátil, S. Quaglioni, I. Stetcu, and B. R. Barrett, "Recent developments in no-core shell-model calculations," *J. Phys.* **G 36** (2009) 083101, arXiv:0904.0463 [nucl-th].

[85] G. P. Kamuntavicius, R. K. Kalinauskas, B. R. Barrett, S. Mickevicius, and D. Germanas, "The general harmonic-oscillator brackets: compact expression, symmetries, sums and Fortran code," *Nucl. Phys.* **A695** (2001) 191–201, arXiv:nucl-th/0105009.

[86] G. P. Kamuntavicius, P. Navrátil, B. R. Barrett, G. Sapragonaite, and R. K. Kalinauskas, "Isoscalar Hamiltonians for light atomic nuclei," *Phys. Rev.* **C 60** (1999) 044304, arXiv:nucl-th/9907047.

[87] D. Hüber, H. Witała, A. Nogga, W. Glöckle, and H. Kamada, "A new look into the partial-wave decomposition of three- nucleon forces," *Few Body Syst.* **22** (1997) 107–134, arXiv:nucl-th/9611021.

[88] A. Nogga. private communication.

[89] D. R. Tilley *et al.*, "Energy levels of light nuclei A=5, A=6, A=7," *Nucl. Phys.* **A708** (2002) 3–163.

[90] M. Abramowitz and I. A. Stegun, *Handbook of Mathematical Functions with Formulas, Graphs, and Mathematical Tables*, vol. 55 of *Applied Mathematics Series*. National Bureau of Standards, 1972.

Danksagung

Zuerst möchte ich mich bei Dr. Andreas Nogga bedanken für die fantastische Betreuung während der letzten fünf Jahre. Von Anfang an war er immer gerne bereit meine Fragen zu beantworten, vom grundsätzlichen bis hin zur optimalen Implementierung des Codes. Seine Geduld, sein Humor und seine Kompetenz waren immer großartige Unterstützung und Motivation. Ich habe mich jederzeit gut aufgehoben gefühlt und kann mir keine bessere Betreuung vorstellen. Vielen herzlichen Dank dafür!
Bedanken möchte ich mich auch bei Prof. Dr. Ulf-G. Meißner sowie bei Prof. Dr. Hans-Werner Hammer für die weitere Betreuung und die Übernahme der Begutachtung dieser Arbeit.
Meinen Kollegen David Minossi und Stefan Kölling möchte ich für die gute Atmosphäre im Büro danken und die Bereitschaft der beiden mir jederzeit mit Tipps, Tricks, Rat und Tat zur Seite zu stehen. Besonders Stefan hat mich mit Fragen und Anregungen vor allem bei der Fertigstellung dieser Arbeit erheblich unterstützt.
Bei PD Dr. Christoph Hanhart bedanke ich mich für seine große Unterstützung, gerade zu Beginn der Arbeit. Ich danke auch Prof. Dr. Evgeny Epelbaum für die freundliche Kooperation in mehreren Gebieten.

Besonderer Dank gebührt auch dem Forschungszentrum Jülich, wo diese Arbeit angefertigt wurde, und insbesondere dem ganzen IKP-III. Die fünf Jahre, die ich hier während meiner Diplomarbeit und meiner Promotion verbracht habe, werden mir immer in guter Erinnerung bleiben und geben mir Vorfreude auf die nächsten zwei Jahre. Ein weiterer Dank gilt den Mitarbeitern des JSC und Michael Rambadt für die gute Zusammenarbeit und die Hilfe bei allen Fragen zu den Supercomputern und UNICORE.

Zum Schluss möchte ich mich noch insbesondere bei Doris für ihre persönliche Anteilnahme, beständiges Interesse in allen Belangen und die herausragend liebenswerte Unterstützung bedanken und bei Frau Dr. Irina Meltser–Chafran für ihre unbeschreibliche Herzlichkeit und Momente der Ruhe. Des weiteren danke ich Angelo, HD, Julia, Stefan, den Beastern Gitte und Olli, Anna–Katharina, Katharina, Dana und Frank, Jan, Dirk, Moritz und Chuck Lorre und allen, die sich an dieser Stelle vermissen.